August 2019

INSIGHTS FROM COMBINED DETRITAL MONAZITE GEOCHRONOLOGY AND ND ISOTOPIC COMPOSITION ON SEDIMENTARY RECYCLING AND PROVENANCE RECONSTRUCTION

Sarah Wade Kittross
Syracuse University

Abstract

Minerals chosen for provenance studies are typically those that are resistant to resetting during low-moderate temperature metamorphic events and thus preserve information about their source region. However, minerals that are extremely resistant to weathering (e.g. quartz, zircon) can be recycled, often multiple times, and thus can cause confusion about the amount of material derived from immediate sources versus those from the original source region. Resistant minerals, such as zircon, that generally only form under very high temperature events (i.e. magmatic events) often miss recording orogenic events that are dominated by moderate temperature, magma-poor, metamorphic events. To overcome some of these difficulties, detrital monazite from Modern alluvium, potential bedrock sources, and Pennsylvanian-Permian sandstones from the southern Appalachian Mountains have been analyzed via Laser Ablation Split Stream Inductively Coupled Mass Spectrometry (LASS-ICP-MS) for U-Th-Pb age and Nd isotopic composition. Previous studies have investigated these units, and related ones, using U-Pb dating of detrital zircon. Because monazite can form at temperatures much lower than that of zircon crystallization, it is able to record lower grade metamorphic events in addition to original source signals, thus a more complete provenance analysis can be acquired. The results from our modern alluvium detrital monazite U-Th-Pb analysis show a bimodal signature of Paleozoic ages and Grenville ages (~1250-950 Ma), with the majority of the ages coinciding with the Taconic Orogeny ~450 Ma. Age peaks matching the multiple distinct Paleozoic orogenies are much more clearly captured in the detrital monazite record than the zircon record that sees almost no ages overlapping the Acadian (~420-380 Ma) and Alleghanian (~330 – 280 Ma) orogenies. The Grenville-aged peak in the detrital monazite record is additionally more representative of the area of Grenville-aged bedrock actually eroding in the watershed compared to the overpowering Grenville signal recorded by detrital zircon. The Nd data offer composition information about the original source of the monazite (i.e. predominantly metamorphic rocks) but also sedimentary characteristics for diagenetic monazite. The ranges in ϵNdi values from Neoproterozoic low-grade metasediments (~ -7 – +4), Paleozoic bedrocks (~ -9.5 – +0.5), and modern alluvium (~ -14.5 – +3.5) support an argument for crustal recycling of Grenvillian crust as the primary juvenile component during the Taconic Orogeny. Utilizing combined U-Th-Pb and Nd isotopes as a dual detrital monazite characterization method provides a high throughput workflow for detailed provenance analysis. Information gathered with this method is critical to a more comprehensive understanding of sedimentary systems.

INSIGHTS FROM COMBINED DETRITAL MONAZITE GEOCHRONOLOGY AND ND ISOTOPIC COMPOSITION ON SEDIMENTARY RECYCLING AND PROVENANCE RECONSTRUCTION

By

Sarah W. Kittross

B.S. Union College, Schenectady, NY, 2016

Thesis

Submitted in partial fulfillment of the requirements for the degree of

Master of Science in Earth Sciences

Syracuse University

August 2019

Acknowledgements

Funding for this project came from generous grants awarded to Dr. Samson and Dr. Moecher by the National Science Foundation and from the support of a Sigma Xi Grants-in-Aid-of-Research award. Thank you to my advisor, Dr. Scott Samson, for your guidance over the past 2+ years. Thank you to the other members of my committee, Dr. Dave Moecher and Dr. Jay Thomas for your invaluable help on crucial aspects of my project. Thank you to Jack Hietpas and Evan Kelly for paving the way for this project and providing samples for my research. Andrew Kylander-Clark and Bruce Wilkinson provided vital data reduction help and Jeremy Inglis worked magic on the TIMS in Los Alamos. Thank you to Kyle Makovsky for being the most helpful and supportive lab mate. And to all the family and friends that supported me throughout, thank you!

Table of Contents

List of Figures

List of Tables

List of Supplementary Data Figures and Tables

1. Introduction

Single-mineral provenance studies have proven to be a tremendous tool in understanding paleo-sedimentary transport, collisional histories, and continental-scale reconstruction. For decades, zircon has been well-established as the most prominently used detrital mineral for provenance studies and other geochronological investigations (e.g. Gehrels et al., 2008). Because zircon contains high amounts of U and minimal initial Pb, is common in many rock types, and is extremely resistant to chemical and physical weathering, it is a particularly suitable candidate for detrital mineral studies. Micro-analytical techniques have advanced in the last few decades to make the extraction of ages from populations of zircon grains via the measurement of $^{207}Pb/^{235}U$ and $^{206}Pb/^{238}U$ ratios an inexpensive, widely available, and fast method for geochronology studies (Jackson et al., 2004).

More recently, however, studies have revealed limitations of detrital zircon in provenance studies (Moecher and Samson, 2006; Hietpas et al., 2010, O'Sullivan et al., 2016). Zircon crystallization is very limited during nonmagmatic to marginally magmatic thermotectonic events, rendering zircon insensitive to orogenic events that have experienced primarily low-medium grade metamorphism (below upper amphibolite-eclogite facies conditions) (O'Sullivan et al., 2016). If a tectonic event *does* reach sufficiently high metamorphic temperatures to form new zircon crystals and/or metamorphic rims, substantially different age information can be gathered from the same zircon grain depending on if a xenocrystic zircon core or a new metamorphic overgrowth is being measured (Hietpas et al., 2010). Additionally, zircon's extreme resilience to weathering allows the mineral to be recycled through multiple orogenic events over time, primarily recording the original crystallization event in the detrital record for hundreds of millions of years. This recycling leads to a natural bias in the detrital record

(Moecher and Samson, 2006) that overrepresents old inherited zircon ages compared to crystallization ages of the proximal crust that is providing the bulk of the detritus (Hietpas et al., 2010).

Monazite [$(La,Nd,Ce)PO_4$] is a REE-bearing phosphate mineral that is a common accessory mineral in igneous, metamorphic, and sedimentary rocks. Monazite partitions U and Th into its structure with insignificant initial uptake of Pb, making it a good candidate for U-Th-Pb geochronology. Crystallization of monazite can occur at temperatures lower than zircon and is possible over a large range of metamorphic conditions ranging from diagenesis and low-pressure contact aureoles to granulitic facies and ultrahigh-pressure conditions (Spear and Pyle, 2002). Monazite is a moderately resistant mineral but, importantly, is less durable than zircon during sedimentary transport. This makes it less likely to survive multiple occurrences of sediment recycling.

Monazite is still underutilized in single mineral geochronological studies, though analysis of monazite has become more common in the last 30 years since the recognition of monazite's superb capabilities to date the crystallization of igneous rocks, metamorphism of metamorphic rocks, and determine characteristics of source materials for igneous and sedimentary rocks (Parrish, 1990; Evans et al., 2001). This is partially because there is a lithological bias towards metapelites, making monazite less ubiquitous than other minerals and it is partially due to the significantly more difficult identification and separation processes compared to other heavy minerals (Hering and Zimmerle, 1963; O'Sullivan et al., 2016). Though there has been considerable modern advancement of microanalytical methods for both selection (scanning electron microscopes [SEM]) and data collection (i.e. improved laser ablation inductively coupled plasma mass spectrometry [LA-ICP-MS]), monazite only represents 1.6% (11,522) of

all single mineral U-Pb ages collected globally while 97.5% (682,909) are zircon ages (Woodhead et al., 2016, Puetz, 2018). The number of studies utilizing *detrital* monazite is even more extraordinarily low considering the well understood benefits of using it as a geochronometer and provenance tool (e.g. Pe-Piper et al., 2014). While few in number, previous detrital monazite studies have explored the distinctly different information gathered in detrital monazite verses detrital zircon studies (Hietpas et al., 2010; Hietpas et al., 2011; Moecher et al., 2011), investigated the mechanisms by which detrital monazite grains provide the source components for metamorphic monazite (Rasmussen and Muhling, 2009; Fisher et al., 2017), and combined detrital monazite age dating with textural analysis to prove the occurrence of sediment recycling in large orogenic basins (Moecher et al., 2019). Importantly for this study, monazite has been established as a promising candidate to act as a first-cycle provenance proxy that will provide a more accurate assessment of proximal sources than zircon, a mineral more likely to reflect the ultimate original source (Hietpas et al., 2010, Moecher et al., 2019).

In addition to geochronological information, geochemical data have also been incorporated into detrital mineral provenance studies to enhance source analysis for decades (Morton, 1991). While, some have even used combined U-Pb and Nd isotopic data to characterize sedimentary provenance, these studies focused on a low number of samples due to the analytical techniques used or due to focusing on detailed variations within single grains (Ross et al., 2005; Williams et al., 2007; Fisher et al., 2017). With the advent and development of simultaneous U-Th-Pb and trace element isotope data collection using laser ablation split stream inductively coupled plasma mass spectrometry (LASS-ICP-MS), it is now possible to ensure that age and geochemical data are not only being collected from the same mineral grain, but from the identical region of each analyzed crystal (Kylander-Clark et al., 2013). This eliminates the

concern of collecting skewed data if two analyses are completed on a grain with chemical or age heterogeneity. This is especially helpful when analyzing the petrochronology of monazite, a mineral that is notorious for often exhibiting chemical complexity (e.g. Figure 1). Compositional heterogeneity in monazite grains is common due to slow diffusion rates that allow for multiple generation events to be recorded in separate domains within single grains (Williams, 2007). The use of LASS-ICP-MS insures that detrital monazite can be analyzed in a high-throughput fashion, in the same way that most detrital zircon studies are conducted. Improved techniques, analytical instrumentation, and the utility of the data have allowed the benefits of detrital monazite dual characterization to far outweigh the costs of the more laborious process of identifying and separating it from a whole rock sample when it is unidentifiable under a standard petrographic microscope.

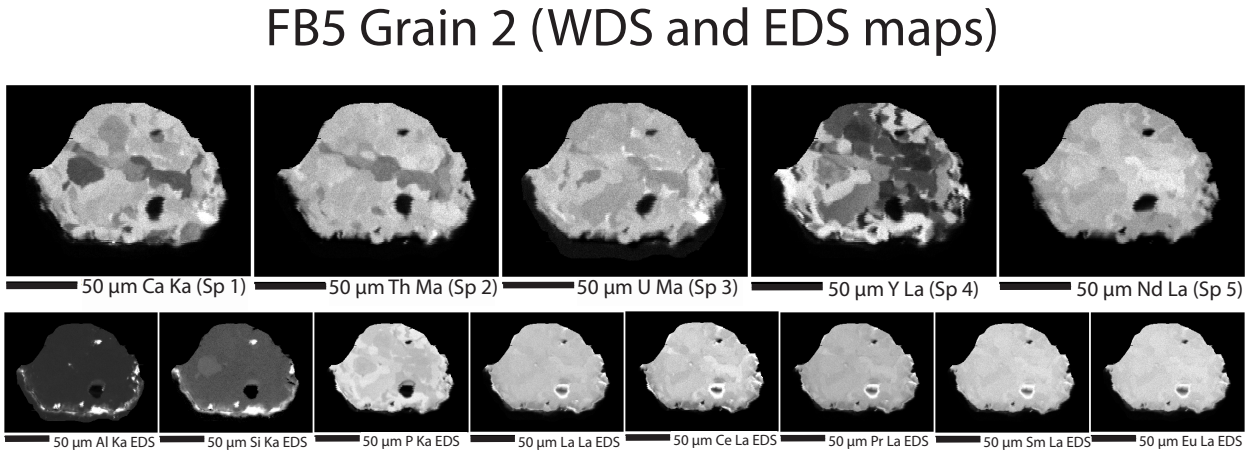

Figure 1. WDS and EDS maps of a monazite crystal (452 Ma) collected on a Cameca SXFive Electron Microprobe. Chemical heterogeneity is prominent in many of the x-ray maps. X-ray analysis was run at 15 kV and 203 nA.

In this study we analyzed detrital monazite grains from modern alluvium in the French Broad River in the Southern Appalachian Mountains and potential sources using LASS-ICP-MS in order to explore further the utility of collecting simultaneous age data and isotopic data allowing for a more detailed dual-characterization provenance analysis method. Five potential bedrock sediment sources were sampled in an attempt to match a portion of the detrital monazite

ages from the modern alluvium to local bedrock units through *both* U-Th-Pb ages and Nd isotopes – allowing for a more confident assessment of provenance than when utilizing only detrital age data. The Ashe gneiss, Ashe schist, Fines Creek schist, Looking Glass granite, and Six Mile schist (described below) had all been previously identified by Hietpas et al. (2012) as likely sources of detritus to the French Broad (Figure 2). Detrital zircon ages for the modern alluvium samples have been previously collected (Hietpas et al., 2010; Moecher et al., 2011) and this current data set thus augments the previous work and discusses the benefits of detrital monazite verses detrital zircon in sedimentary basin provenance studies. These data in combination with the many previous studies make the French Broad River one of the most intensely studied river systems globally for multiproxy single-grain U-Pb analysis, highlighting the dependence of provenance information on mineral proxy choice (Hietpas et al., 2010; Moecher et al., 2011; O'Sullivan et al., 2016). The modern alluvium samples are also used in this study as a proxy to explore nearby Neoproterozoic sandstones, analyzed via the same methodology, to better understand the processes that occurred prior to deposition, lithification, and exhumation of these ancient rocks.

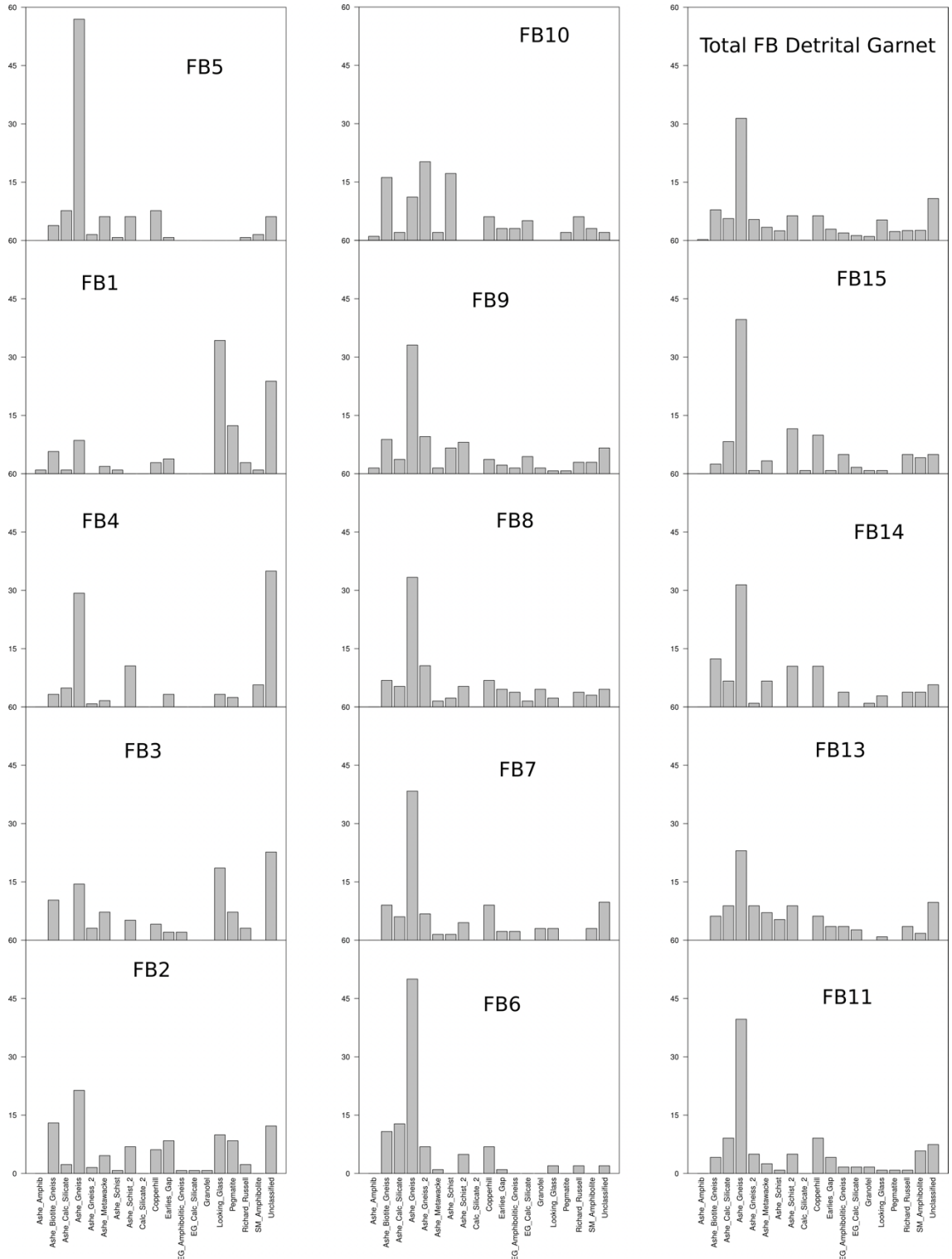

Figure 2. Percent abundance bar charts summarizing the datasets linking the alluvium in the French Broad River to potential source rocks. This was done by calculating the canonical discriminant functions for ~2,300 detrital garnet compositions and classifying them according to their Mahalanobis distance. This method produced only ~10% of grains as "unclassified", robustly linking the rest of the detrital garnet grains in the French Broad River to potential garnet donor lithologies (Hietpas et al., 2012).

2. Geologic setting

The Appalachian Mountains extend from Alabama to Maine in the USA and continue through Newfoundland and Labrador in Canada. The geologic features of the Appalachians have been intensely studied since the early 1800's (Maclure, 1809) and these studies laid the foundation for many major concepts related to the building of mountain chains (e.g. Hatcher, 1989). Although the crystalline southern Appalachians have a less extensive documented history than the northern segments of the mountain belt, the area has been well documented to have experienced multiple orogenies, and by proxy, multiple potential sediment generation and recycling events. Much of the Appalachians were built on Grenville-aged (~1250 – 950 Ma) basement rocks of eastern Laurentia through a series of overprinting Paleozoic collisional events. The basement rock was deformed during the volcanic arc accretion of the Taconic Orogeny (~470 – 440 Ma), the microcontinent collision of the Acadian Orogeny (~420 – 380 Ma), and the supercontinent amalgamation of Laurentia and western Gondwana to create Pangea during the Alleghanian Orogeny (~330 – 280 Ma) (Hatcher, 1989).

2.1 Geologic setting of the French Broad watershed

Modern alluvium samples from which detrital monazite was extracted were collected from the French Broad River in North Carolina and Tennessee (samples FB1-15). The trunk river of a large drainage basin, it flows generally northward with sediment transport relatively undisturbed since the Cenozoic formation of the drainage basin (Hietpas et al., 2011). It crosses lithologies of multiple ages, gathering alluvium from the tectonically complex and lithologically diverse southern Appalachian Orogen (Hietpas et al., 2011). The main tributary, the Pigeon River, contributes alluvium from the Great Smoky Mountains and sillimanite grade to chlorite grade metamorphic rock in the area (Carpenter, 1970; Hadley and Nelson, 1971). Known

regional tectonometamorphism and magmatic events in the drainage basin include Mesoproterozoic magmatism and granulite facies metamorphism, Neoproterozoic continental rift magmatism and potential metamorphism, and Paleozoic plutonism and regional metamorphism (Su et al., 1994; Tollo et al., 2004; Moecher et al., 2011). The relevant units that the French Broad River drains are described in the following pages (Figure 3).

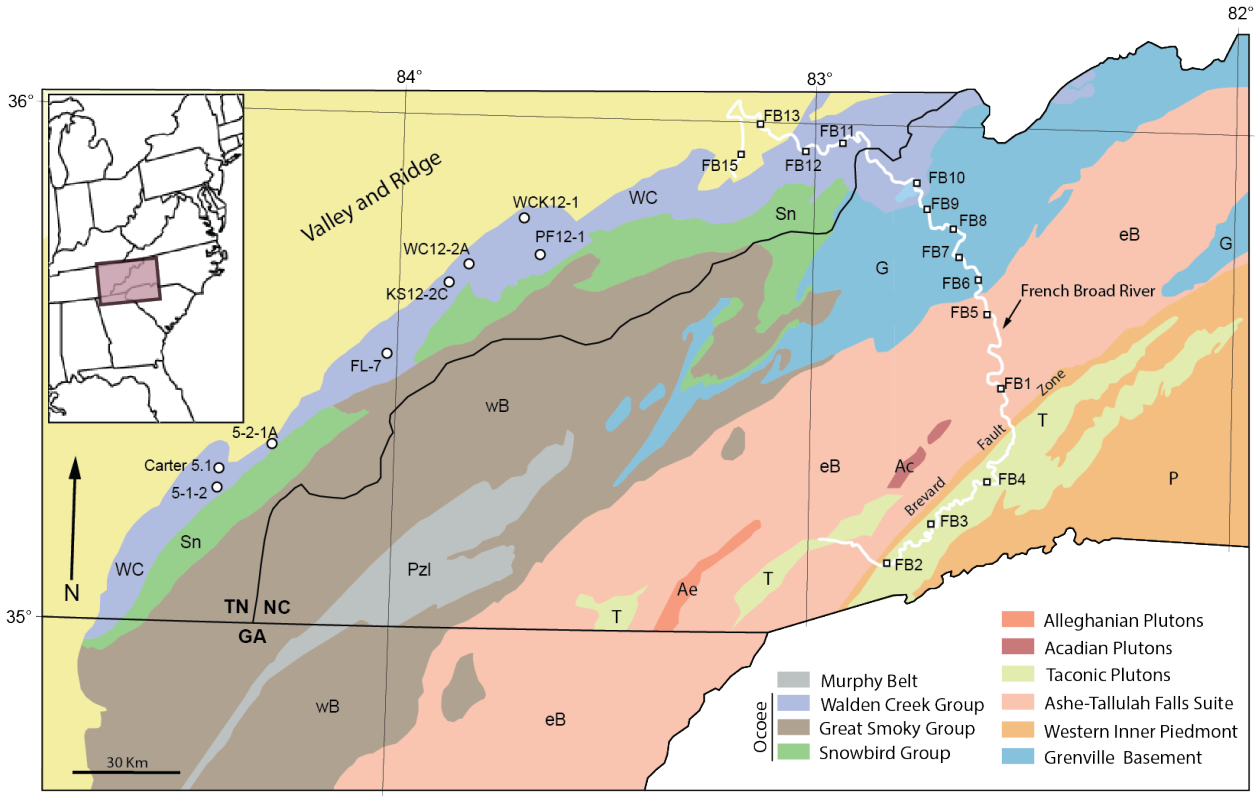

Figure 3. Simplified geologic map of the study area (modified from Moecher et al., 2011and Moecher et al., 2019) (Digital cartography data (Open-File Report OF-2005-1323) available from US Geological Survey, EROS Data Center, Sioux Falls, SD.). Locations of samples used from the Walden Creek Group (Kelly, 2014) and French Broad River (Hietpas et al., 2010) are denoted. Inset shows the location of the study area in the eastern USA. Pzl – Murphy Belt; WC – Walden Creek Group; wB – Great Smoky Group; Sn – Snowbird Group; Ae – Alleghanian Plutons; Ac – Acadian Plutons; T – Taconic Plutons; eB – Ashe-Tallulah Falls Suite; P – Western Inner Piedmont; G – Grenville Basement.

The Ashe-Tallulah Falls Metamorphic Suite (ATFS) accounts for a large portion of the bedrock that the French Broad cuts through. The suite is located in the Eastern Blue Ridge and western Inner Piedmont, existing on both sides of the northeastern-striking Brevard fault zone (Figure 3). Designated the Ashe Formation in NW North Carolina and the Tallulah Falls formation in NE Georgia and South Carolina, the two units are inferred to be time equivalent based on regional bedrock mapping (Hatcher, 2002; Bream et al., 2004). The ATFS is a mixed assemblage of late Neoproterozoic metapelites and mafic volcanic rocks metamorphosed to upper amphibolite facies during Paleozoic orogenesis (Abbott and Raymond, 1984). Migmatitic paragneisses in the suite have inferred Neoproterozoic clastic protoliths and have experienced metamorphism ranging from biotite-grade to migmatitic sillimanite-grade. Isotopic ages demonstrate the ATFS rocks were metamorphosed during both Taconic and Acadian orogenesis (Butler, 1991; Goldberg and Dallmeyer, 1997; Miller et al., 2000; Bream et al., 2004; Moecher et al., 2004, 2011; Corrie and Kohn, 2007). Samples of migmatitic Ashe paragneiss (Ashe Gneiss) and Ashe pelitic schist (Ashe Schist) were provided from Hietpas et al. (2011) for additional analysis in this study.

The western Inner Piedmont, on the southeast side of the Brevard fault zone, is correlated with the Tallulah Falls Formation of the Eastern Blue Ridge, though the metamorphic age peak differs with regional metamorphism in the western Inner Piedmont occurring in Late Devonian to Mississippian (i.e., “Neo-Acadian”: Hatcher, 2002; Dennis, 2007). The Six Mile Schist (SC) and Fines Creek Schist (NC, of the Great Smoky Group, Copper Hill Formation) analyzed in this study both refer to geologic mapping quadrangles in which the schists are located.

Numerous Paleozoic metaplutonic gneisses were emplaced during the Taconic, Acadian, and Alleghanian orogenies (Figure 3). These Appalachian plutons, emplaced throughout the

Paleozoic into a compressional setting, were variably deformed by each phase of orogenesis (Hietpas et al., 2011). One of the largest plutons, at the French Broad headwaters in the Southern Blue Ridge, is the early Paleozoic Henderson orthogneiss that was probably emplaced during a period of abundant granitic magmatism (447.6 ± 5.4 Ma; Hietpas et al., 2011). Others include the Mesoproterozoic Toxaway Gneiss (Carrigan et al., 2003), the Ordovician Whiteside Pluton, and Devonian Looking Glass and Pink Beds plutons (Miller et al., 2000). The Looking Glass pluton, analyzed in this study, has one of the strongest metamorphic fabrics and intruded the ATFS. The host rocks of the Paleozoic intrusions are primarily metasedimentary schists and quartzofeldspathic paragneisses, both with varying amounts of interlayered amphibolite (Miller et al., 2000).

Basement massifs of the Appalachian Orogen expose Mesoproterozoic (Grenville, ~1250 – 950 Ma) granitoid plutons and orthogneissic equivalents that are the dominant component of eastern Laurentian crust (Figure 3; Hatcher, 1987). The Grenville orogenic cycle is broadly characterized by three compressional phases, the Shawinigan (~1190 – 1140 Ma), Ottawa (1080 – 1020 Ma), and Rigolet (1000 – 980 Ma) orogenies (McLelland et al., 2001; Rivers et al., 2002). All of these basement units were variably deformed during the subsequent metamorphic events in the Paleozoic.

2.2 Geologic Setting of Walden Creek Group

The Ocoee Supergroup in the western Great Smoky Mountains, USA covers a 24,000 km^2 area in eastern Tennessee, western North Carolina, and northern Georgia (King et al., 1958). The ~10,000 m thick sequence of dominantly clastic metasediments is interpreted to have been deposited in a localized rift basin developed in Grenvillian continental crust between ca. 750 and 550 Ma (Rankin, 1975). The Ocoee Supergroup is thought to be correlative to the Ashe suite

(ATFS). The Walden Creek Group (WCG), the upper unit of the Ocoee Supergroup, consists of clastic metasediments deposited in the Neoproterozoic that have been subsequently deformed to sub-greenschist to greenschist facies (biotite grade) (Figure 4; King et al., 1958; Kelly, 2014). Lithologies in the WCG include siltstone, shale, interbedded sandstone and quartz conglomerate, course sandstone, sandy siltstones, conglomerates, and some carbonates (King et al., 1958).

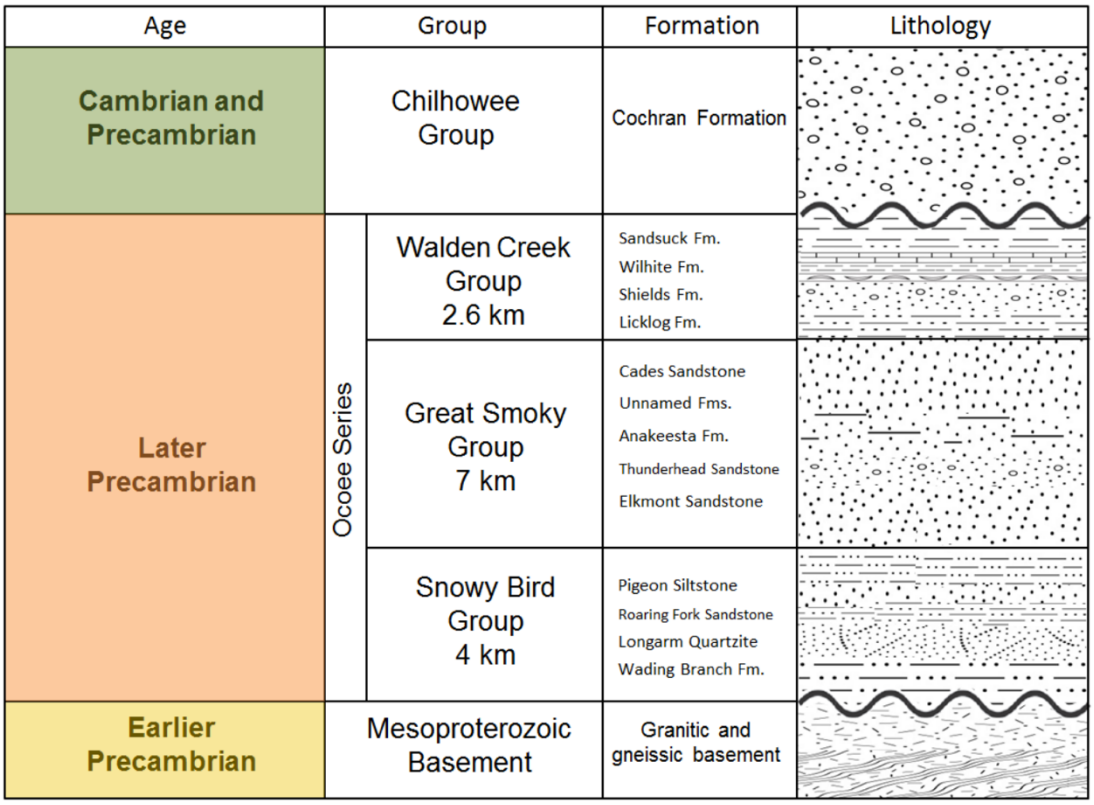

Figure 4. Stratigraphic section for the Ocoee Series which contains the Walden Creek Group from Kelly, 2014.

2. Methods

2.1 Mineral Separation

Monazite was separated from five samples (for analysis of the Walden Creek Group and area bedrock). The rest of the samples discussed in this paper were previously collected and

processed by Hietpas (2010) and Kelly (2014) (Locations shown in Figure 3). Conventional mineral separation methods (e.g. crushing, sieving, density separation) were used to purify the monazite separates initially. The samples were first reduced to single-grain size by jaw crushing and disc mill grinding. The sample was wet and dry sieved to produce a size fraction of 28- to 400-micron grains. This was done by first decanting the sample small portions at a time in a 1000 ml beaker to concentrate dense minerals, including monazite, and to remove dust, metal shavings, and glass with low density. Once the remaining denser material was dried, magnetite and other highly magnetic material like metal shavings from the disc mill were removed from the sample using a hand magnet.

The samples were then separated by magnetic susceptibility using a Frantz magnetic separator. The sample was first run through the Frantz at 0.1Å, 15° side slope, to eliminate the most magnetic minerals and any remaining metal shavings from the disc mill. It was then run through at 0.25Å, 0.50Å, 0.8Å, and 1.0Å with a side slope of 15° to determine which magnetic separate has the highest concentration of monazite grains. According to the literature, monazite is most abundant in the 0.3Å to 0.8Å fraction, though in our experience it was also highly abundant in the 1.0Å magnetic fraction (Rosenblum and Brownfield, 1999). The monazite-bearing portion of sample was then processed with heavy liquids (2.9 g/cm^3 Bromoform and 3.3 g/cm^3 Methyl Iodide) before being passed through the magnetic separator again. Unlike separating common heavy minerals such as zircon, one is not able to directly handpick monazite crystals under a petrographic microscope at this stage because of the extreme variability in morphology, size, and color of detrital monazite. It is thus necessary to utilize back-scattered electron (BSE) imaging to identify monazite grains. Hundreds of grains were scatter mounted on adhesive carbon tape, carbon coated, and analyzed using a CAMECA SXFive electron

microprobe. Because of their extremely high REE content, the monazite grains have the highest backscattered electron intensity, followed by zircon, apatite and other minerals. The contrast and brightness settings for the electron images were adjusted to accentuate only the monazite crystals. The "bright" grains were confirmed to be monazite with energy-dispersive spectroscopy by quantitatively evaluating their phosphorous and REE concentrations. Secondary electron (SE) images were taken at the same magnification (2000 x 2400 μm) and location as the BSE images to provide information on the surface morphological details to aid in identifying grains for handpicking and subsequent analysis. The identified monazite grains were hand-picked under a binocular stereo microscope, cast in epoxy, and polished. The monazite crystals used in this study are predominately anhedral to subuhedral, vary in size, shape, and color and were sometimes composite grains containing monazite and other minerals. Crystal colors under plain light include gray, tan, orange, and brown of varying opaqueness. They range in size from ~30 μm to ~300 μm in diameter. The monazite crystals also exhibit a variety of textural properties. While some have distinct grain boundaries, others are intergrown with other minerals. There is a wide variety in the internal physical properties of these crystals including number, size, and type of inclusions, shape, cracks, zoning, etc. (Figure 5).

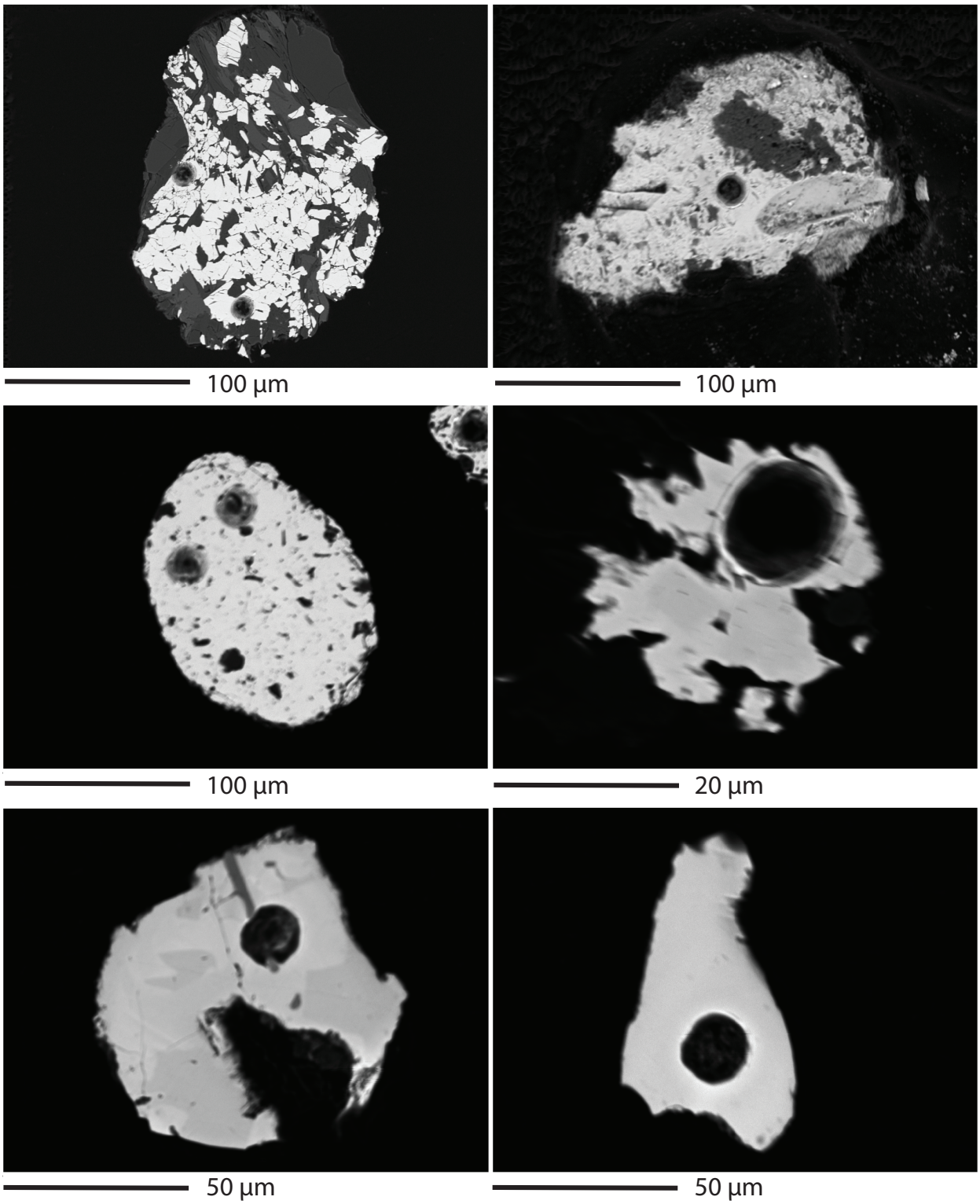

Figure 5. BSE images of six typical monazite crystals that were analyzed in this study, shown to exemplify the wide variety of shapes, sizes, inclusion density, and chemical heterogeneity. Dark round circles are 15 µm laser ablation spots post-analysis.

2.2 Laser Ablation Split Stream Analysis (LASS-ICP-MS)

Two new mounts and four additional mounts analyzed by other methods in previous studies (from Hietpas 2010; Kelly 2014) were analyzed at the University of California, Santa Barbara for U-Th-Pb and Nd isotopic composition using laser ablation split stream inductively coupled plasma mass spectrometry (LASS-ICP-MS). The split stream allowed for the simultaneous measurement of U-Th-Pb isotopes on an Agilent 7700x quadrupole ICP-MS and several REE isotopes including the measurement of $^{143}Nd/^{144}Nd$ ratios on a Nu instruments Plasma HR-ES multi-collector ICP from the same laser spot analysis (spot size 15 μm) (Cottle et al., 2012; Cottle et al., 2013). A Photon Machines 193 nm excimer laser ablation system used the combined Nu Instruments Plasma HR-ES multi-collector ICP with twelve Faraday cups and four low-mass ion counters and the Agilent 7700x quadrupole inductively coupled plasma mass spectrometer for analysis. Spot size for the laser shots was 15 μm, laser duration was 29 seconds, and there was one minute of background and washout between each sample.

U-Th-Pb isotopic ratios and their uncertainties are calculated by interspersing matrix-matched reference materials among samples and then reducing the data using the Iolite software (Paton et al., 2010; Kylander-Clark et al., 2013). For monazite, a typical ablation of ~1-3 ng of material yields $^{208}Pb/^{232}Th$, $^{206}Pb/^{238}U$, and $^{207}Pb/^{206}Pb$ ratios with 0.5-2.5%, 0.6-1.5%, and 0.3-1.5% precision (2SE), respectively, and the general absence of measurable ^{204}Pb in monazite in a large collection of standards and unknowns means that there is no need for a common Pb correction (Kylander-Clark et al., 2013). Standard reference materials used in this study included: MaeKlang (27 Ma, Dunning et al., 1995), Manangotry (555 Ma, Horstwood et al., 2003; Hacker et al., 2015), Moacyr (515 Ma, Palin et al., 2013), Stern (512 Ma, Palin et al., 2013), Trebilcock (272 Ma, Tomascak et al., 1996), and JNdi glass REE standard. Ages

presented in this study are 'Best Ages' based on reduction of U-Pb data in Isoplot 3.75 (Ludwig, 2012). The dates are representative of the best estimate of the crystallization age of the monazite. Preliminary studies suggest that even grains with similar ages could have very different Nd isotopic composition depending on whether they are primary (metamorphic or igneous) grains or recycled (originally authigenic) grains (Fisher et al., 2017).

2.3 Cameca SXFive Electron Microprobe

The Cameca SXFive electron probe microanalyzer at Syracuse University was used for BSE imaging and to produce x-ray maps. The microprobe is equipped with a LaB6 electron gun with five wavelength dispersive spectrometers that contain large area diffraction crystals and complementary counters.

In addition to using the back scattered electron (BSE) imaging capabilities on the electron microprobe to facilitate identification of grains during mineral separation, BSE imaging was done prior to LASS-ICP-MS analysis to use as a guide for selecting the most appropriate regions of the grains for lasing. By collecting BSE images one can avoid inclusions and areas of strong chemical zonation during laser analysis.

The Cameca SXFive electron probe microanalyzer was used to construct x-ray compositional domains within monazite grains analyzed for U-Th-Pb and Nd. A representative set of detrital monazite grains was selected based on shapes, sizes, ages, occurrence of inclusions, and compositional zoning (e.g. Figure 1). Five elements were mapped using wavelength dispersive spectrometry (WDS) and eight elements were mapped using energy dispersive spectrometry (EDS), all simultaneously. WDS maps were collected for U, Th, and Y using a large PET crystal, Ca using a small PET crystal, and Nd using an LIF crystal. EDS maps were collected for Al, Si, P, La, Ce, Sm, Eu, and Pr. Each grain was added to a batch run with

the same parameters and run over multiple days depending on the size of the batch run. The instrument was run at 200 nA with a 200 ms dwell time at 15 kV with a <1.0 nm spot size. The step size was 0.5 nm except for grain FB14_24 that was run with a step size of 1.0 nm due to the large size of the crystal.

Table 1. Grains selected for x-ray mapping. Images of each grain can be found in supplementary data.

Sample Grain	**Age (U-Th-Pb)**	**BSE observations**	
FB3_30	335 Ma	Zoning patterns	
01-TN-02A_49	1163 Ma	Quartz inclusions	
FB5_2	452 Ma	Zoning patterns	
01-TN-02A_2	1037 Ma	Zoning patterns	
FB4_7	326 Ma	Homogeneous	
01-TN-02A_44	1070 Ma	Homogeneous	Previously dated twice
01-TN-02A_51	468 Ma	Inclusions	Previously dated twice
FB14_24	360 Ma	Inclusions	

3. Results

3.1 U-Th-Pb Geochronology

U-Pb age data for all detrital monazite samples discussed in this paper are given in Table S1. The composite detrital monazite age spectrum (n = 404) of the Modern alluvium from all French Broad River samples is dominated by an age peak at 510 – 410 Ma, centered at ~455 Ma (Figure 6). A large number of analyses are discordant, most likely due to radiogenic Pb loss in the monazite over time, especially prevalent in monazite grains because of their fragile and often diagenetic nature (Figures 7 & 8). Of the French Broad samples, almost 18% were >10% discordant, more so in the Paleozoic grains than Mesozoic grains (Figure 9). While the discordance of the monazite population is important on its own, the ages discussed in this remainder of this study are crystals with U-Pb dates with <10% discordance (Figure 8). 26 of

404 (6.4%) of the concordant grains are younger than 360 Ma, and overlap with the duration of the Alleghanian Orogeny (~330-280 Ma). Nine of 404 (2.2%) of grains are Devonian, consistent with crystallization during the Acadian Orogeny. Over 87% of the grains are Ordovician, overlapping in time with the Taconic Orogeny (~470-440 Ma). Fourteen of 404 (3.5%) of the detrital monazite from the Modern alluvium range in age from 1321-939 Ma (Figure 6). Some French Broad River alluvium samples only contain grains of Ordovician age (FB-5, FB-6, FB-8). Samples FB-1-4 and FB-15 record primarily Ordovician grains in addition to Permian and/or Devonian grains. FB-2 also records one grain at 653 Ma. Four samples (FB-9-11 and FB-13) record primarily Ordovician grains with small Mesoproterozoic age peaks. FB-14 records Devonian, Ordovician, and Mesoproterozoic ages.

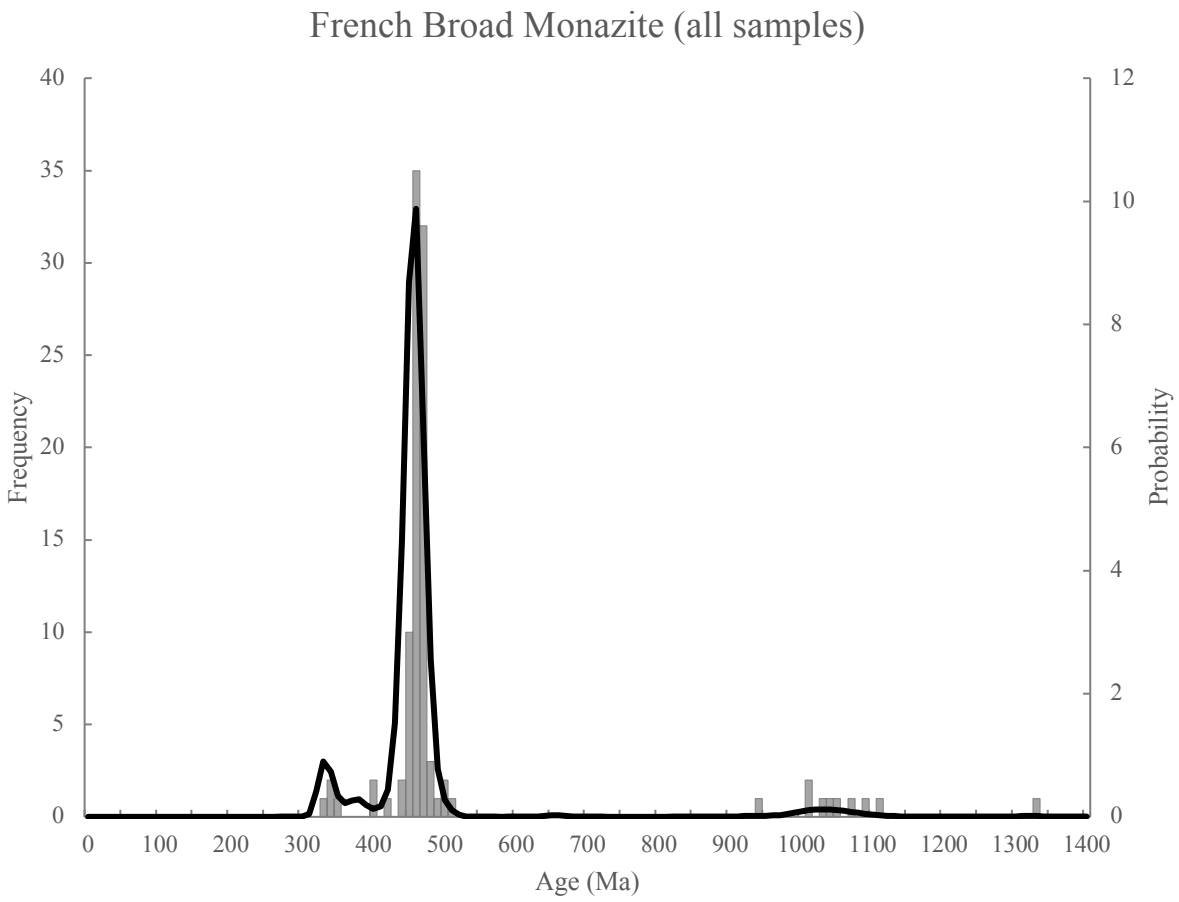

Figure 6. Histogram and probability density plot of French Broad detrital monazite samples 1-6, 8-11, 13-15 (n = 404).

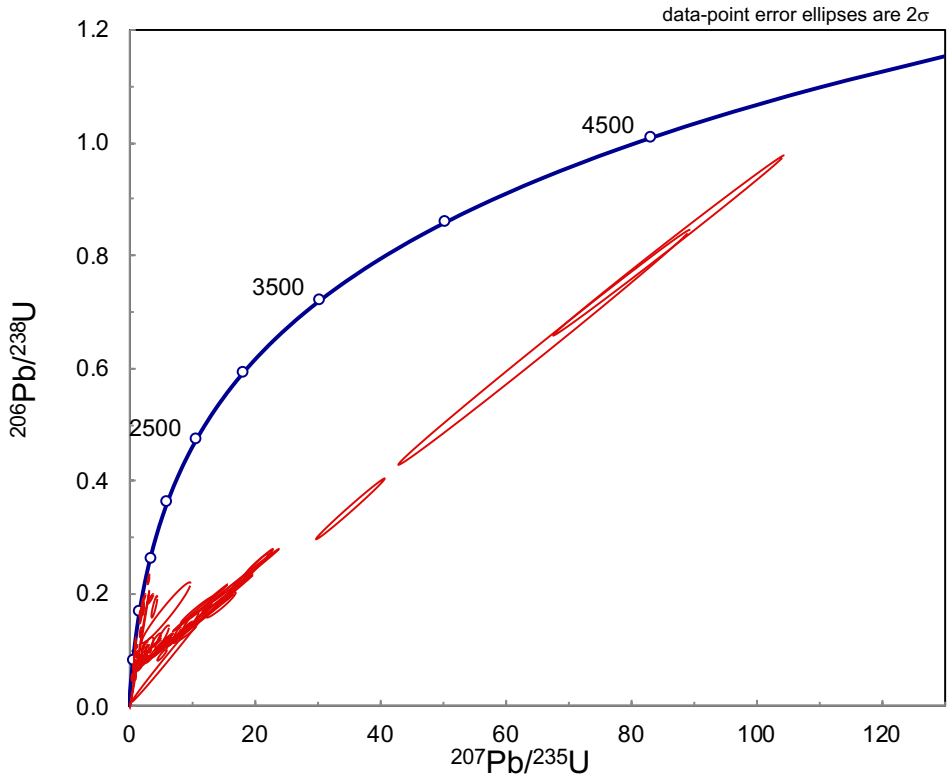

Figure 7. Concordia diagram of French Broad U-Pb data showing all ages including ~18% of total data that are discordant grains.

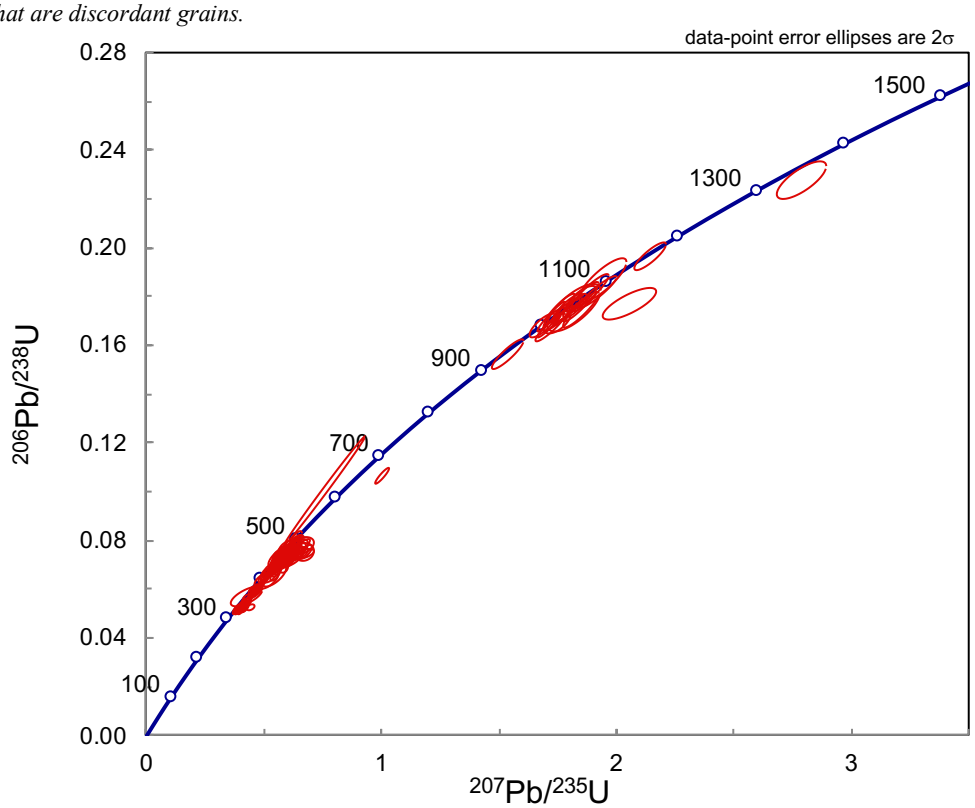

Figure 8. Concordia diagram of French Broad U-Pb data showing only French Broad grains that are <10% discordant.

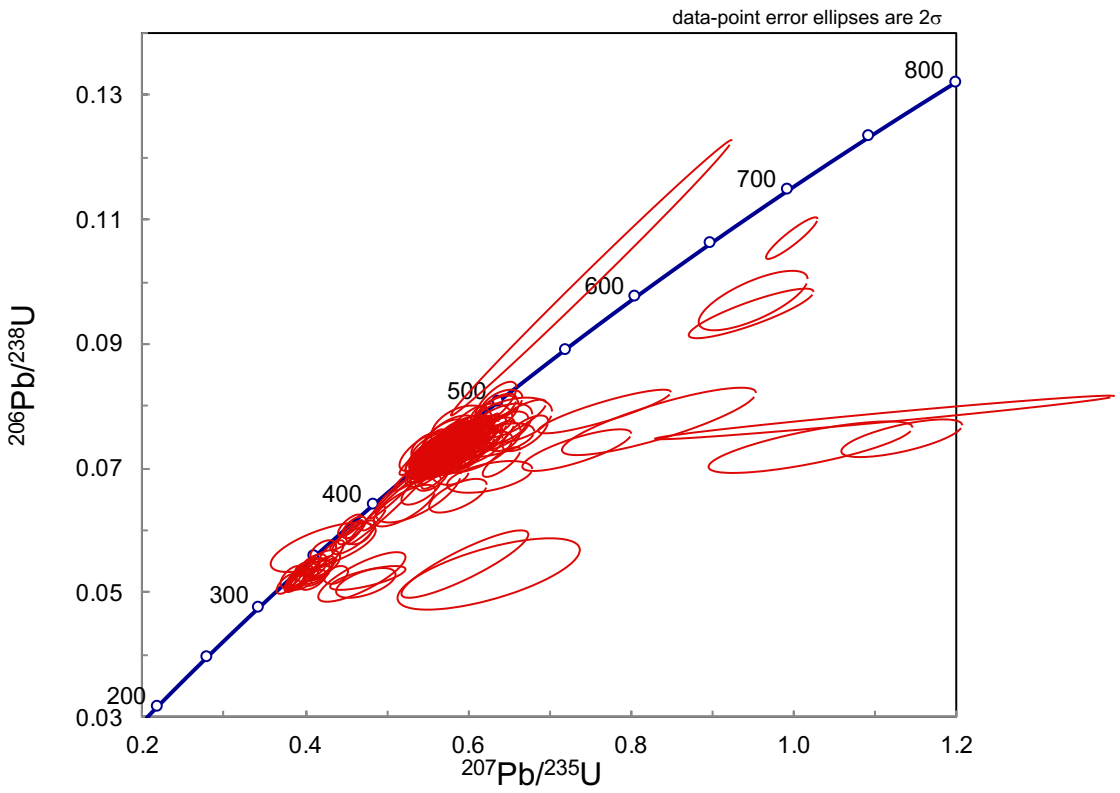

Figure 9. Concordia diagram of all French Broad detrital monazite analyses of Paleozoic age.

The monazite age spectrum (n = 98) of the bedrock samples (gneisses, schists, and a granite) collected in the French Broad River watershed only record Paleozoic ages ranging from 474 – 321 Ma, with the strongest peak at 450 Ma, second highest peak at 340 Ma, and a third distinct peak at 370 Ma (Figure 10). 87.5% of all analyzed grains were >10 % concordant, with all discordant grains exhibiting U-Pb dates between 330 and 345 Ma (Figure 11).

The Neoproterozoic Walden Creek Group of the Ocoee Series detrital monazite age spectrum (n = 105) is dominated by ~1 Ga ages (93%). The remaining seven percent of grains include one Neoproterozoic grain, three Cambrian grains, and three late Devonian ages (Figure 12). A very large proportion of the grains from the Walden Creek Group are discordant, with just under 50% of the analyzed grains being >10% discordant (Figure 13 & 14).

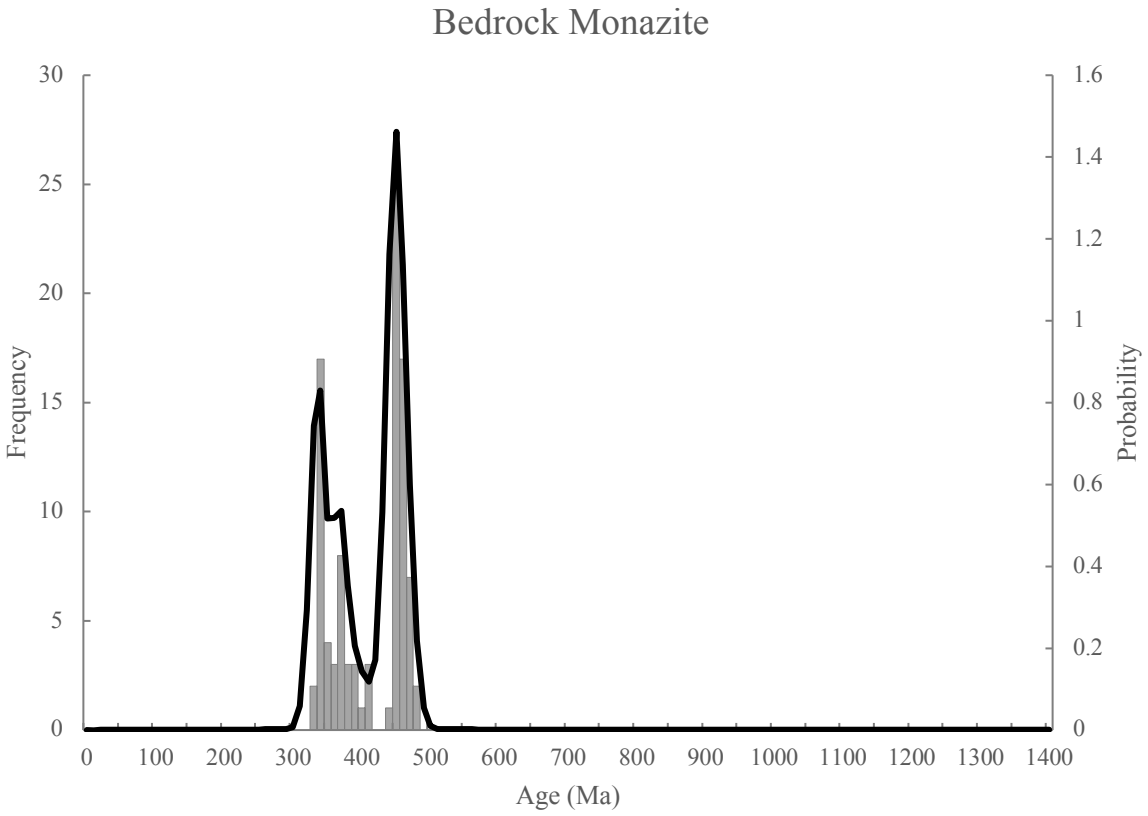

Figure 10. Histogram and probability density plot of bedrock monazite in the French Broad River monazite samples FB1SR Ashe Schist, Ashe Gneiss, Ashe Schist, Fines Creek Schist, Six Mile Schist, Looking Glass Granite.

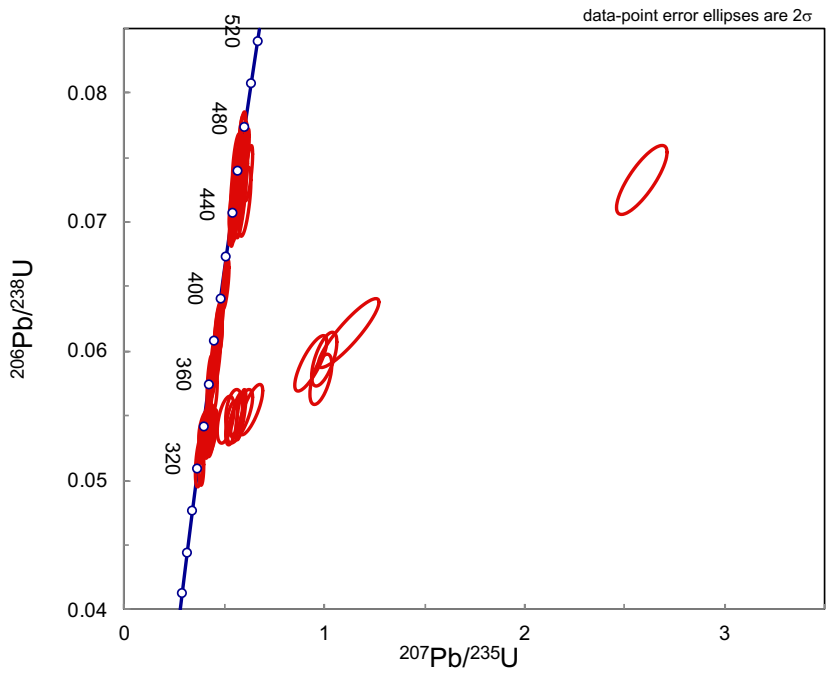

Figure 11. Concordia diagram of all bedrock monazite analyses including the ~12.5% of discordant grains that are not used in the rest of the discussion.

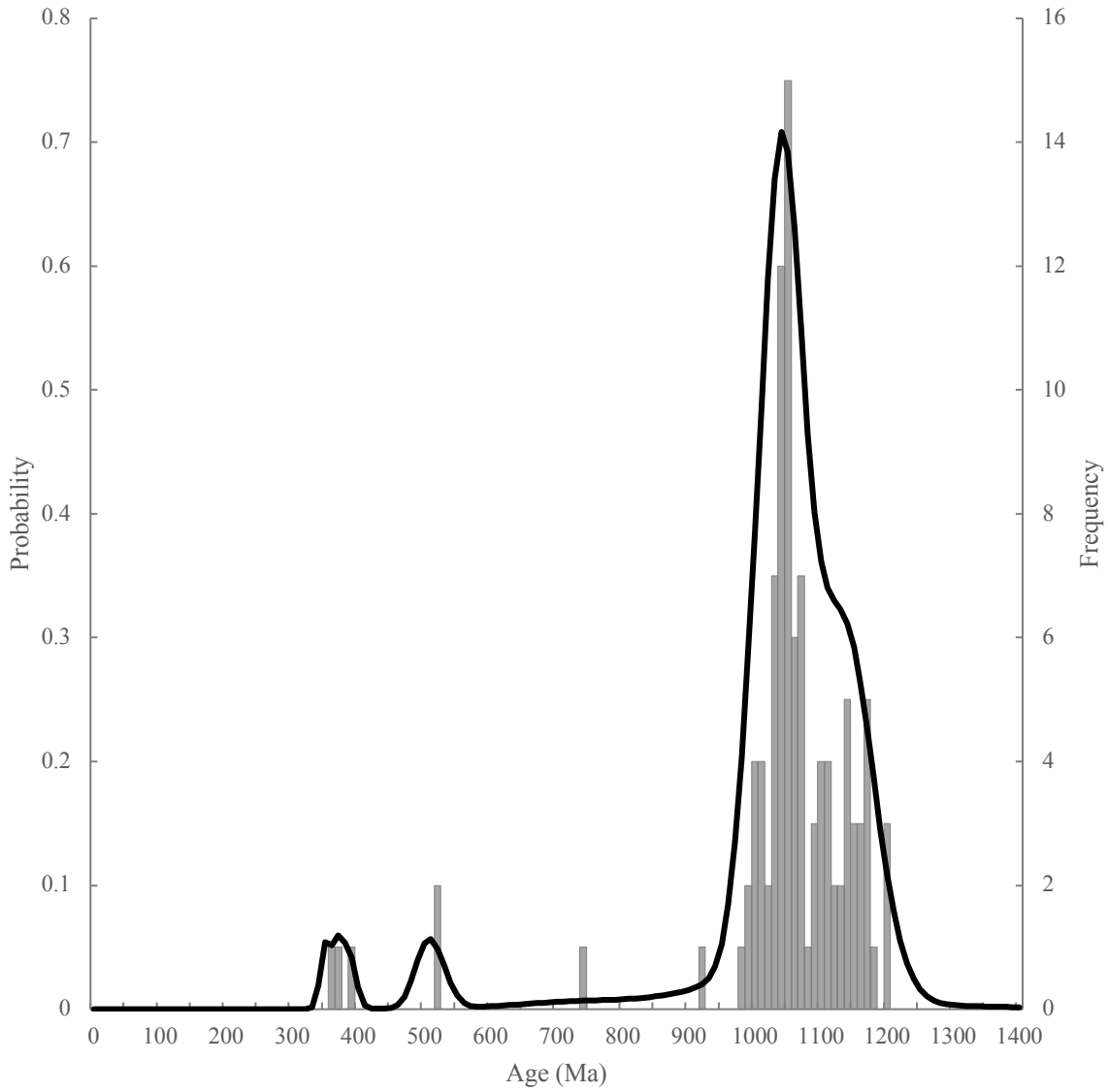

Figure 12. Histogram and probability density plot of Neoproterozoic Walden Creek Group detrital monazite samples Carter 5-1-2, 5-2-1, FL7, KS12-2C, PF12-1-Shields, WCK12-1-Sands.

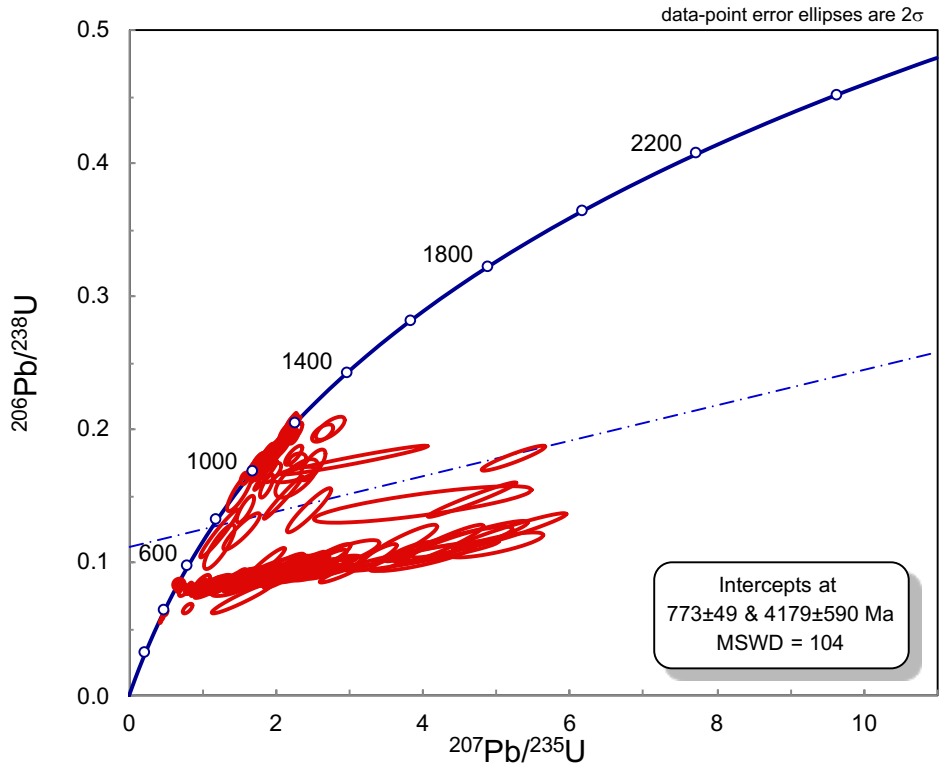

Figure 13. Concordia diagram of all detrital monazite from the Walden Creek Group samples. Almost 50% of the total analyzed grains were >10% discordant, and 15% are >50% discordant.

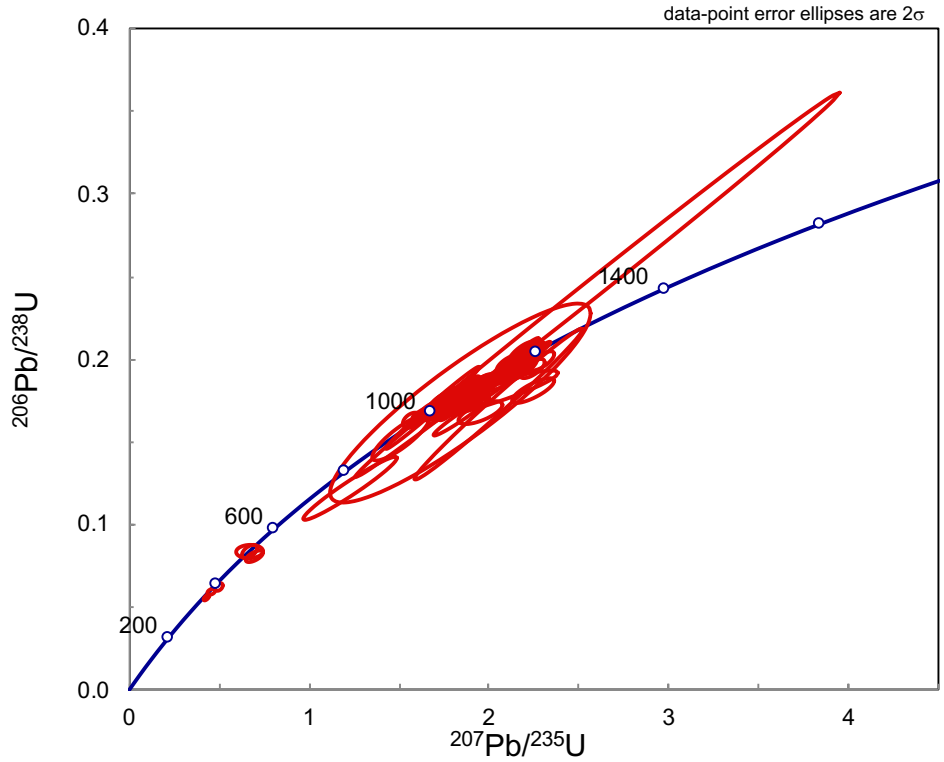

Figure 14. Concordia diagram of all concordant grains from the Walden Creek Group.

3.2 Nd Isotope Geochemistry (LASS-ICP-MS)

Sm-Nd isotope results are given in Table S2 and other REE concentrations are given in Table S3. Initial $^{143}Nd/^{144}Nd$ ratios and ϵNd values for each grain are calculated based on the U-Pb 'Best Age' date determined for that grain. The Nd composition of each monazite grain reflects the Nd isotopic composition of the detrital grain's sedimentary protolith in which it formed during subsequent metamorphism. The bulk chemical composition of the sedimentary protolith reflects contributions from juvenile vs. evolved crust in the Nd values. The monazite is a proxy for the whole rock sedimentary protolith, in the same way that Hf isotope composition in zircon grains is commonly used as a proxy for the composition of the magma from which they crystallized. All Nd values shown are designated as "initial ϵNd" (or ϵNdi), meaning ϵNd at the time of monazite crystallization given by the U-Th-Pb age. Positive ϵNdi values indicate contributions from a more juvenile source while negative ϵNdi values represent crystallization in a rock with more evolved source material, indicating more crustal contamination. Nd data were collected for monazite in modern alluvium, bedrock within the French Broad watershed, and the Neoproterozoic Walden Creek Group.

The ϵNdi values for many of the bedrock samples cluster together as seen in Figure 15. The Looking Glass Granite monazite grains (the only igneous bedrock source collected) came from the most juvenile source material of the collected bedrock (with ϵNdi of -3.0 to +1.0), also exhibiting the youngest monazite ages (between 320 and 340 Ma). The Six Mile Schist, consisting of Devonian-aged grains, appears to contain sediment derived from much more evolved source material (ϵNdi ~-10.0 to -6.0). The Ashe Gneiss, Ashe Schist, and Fines Creek Schist, originally of late Neoproterozoic depositional age but metamorphosed in the Ordovician, cluster together very closely between -8.0 and -4.0 ϵNdi. The error bars were omitted from these

three samples on Figure 15 because they made it difficult to see the points, but they are comparable to the error bars on the other two bedrock samples. While each of these samples are of the same age and have ϵNdi values within error of each other, it could be postulated that the Ashe Schist contains a greater contribution of sediment derived from a more juvenile source (less negative ϵNdi) than the Ashe Gneiss grains (Figure 15). However, these grains needed to be analyzed with a higher precision technique to separate the two populations with any confidence. Figure 16 also presents the modern alluvium detrital monazite ϵNdi values with the bedrock overlain to illustrate some of the alluvium's potential sources. Only five bedrock samples have been analyzed for Nd data thus far, meaning there are many potential sources represented in the Modern alluvium that we have neither age or Nd data for.

There is a large range of ϵNdi values for monazite from the Modern alluvium (Figure 17). The Permian- and Devonian-aged monazite grains range from -8.0 to 0.0 ϵNdi. The Taconic-aged grains come from an even wider variety of sources with ϵNdi values ranging from -14.5 to +2.4, although still primarily showing contributions from more evolved sources for most of these grains. The majority of the Taconic-aged grains range in ϵNdi -8.5 to -4.0. The ~1 Ga detrital monazite crystals range in ϵNdi from -6.0 to +4.0.

The Neoproterozoic Walden Creek Group detrital monazite grains also exhibit a wide range of ϵNdi values (Figure 18). The majority of the grains are ~1 Ga in age but have ϵNdi that range from -6.8 to +3.8 ϵNdi. The grains that are younger than the 1 Ga majority, discussed above, all have negative ϵNdi values between -5.0 and -2.0 (Figure 18).

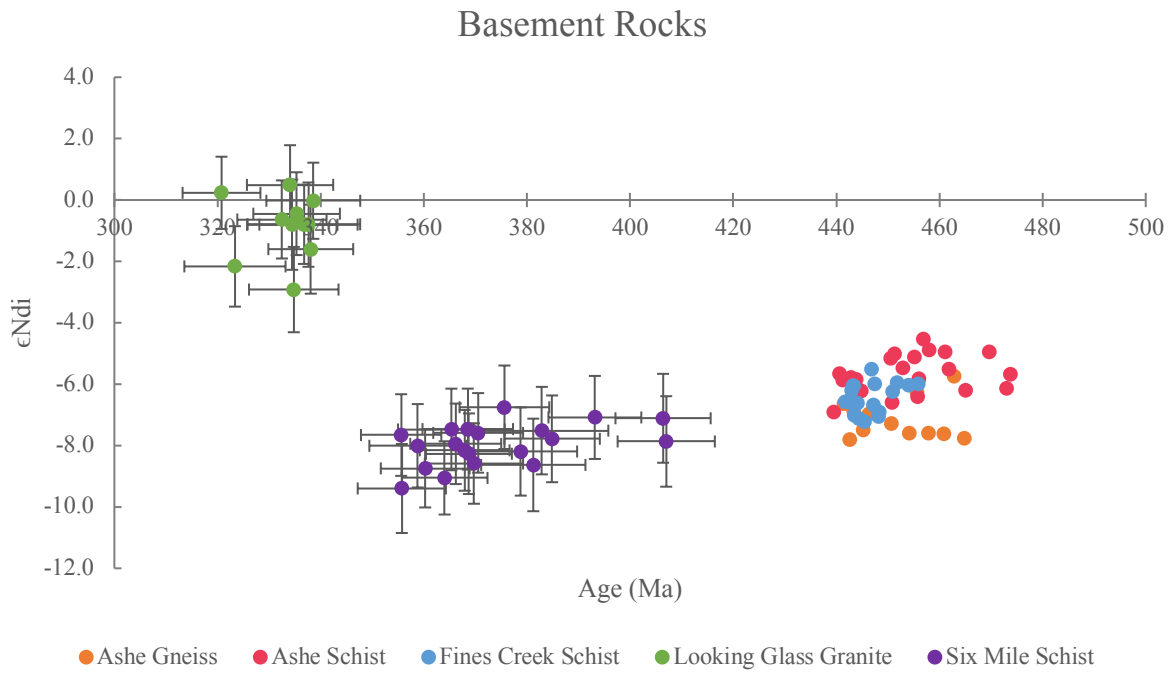

Figure 15. Age and εNdi values for monazite grains in five bedrock samples from the French Broad River watershed. Error bars are comparable to the other two samples on Ashe Schist, Ashe Gneiss, and Fines Creek Schist samples but are omitted for ease of viewing.

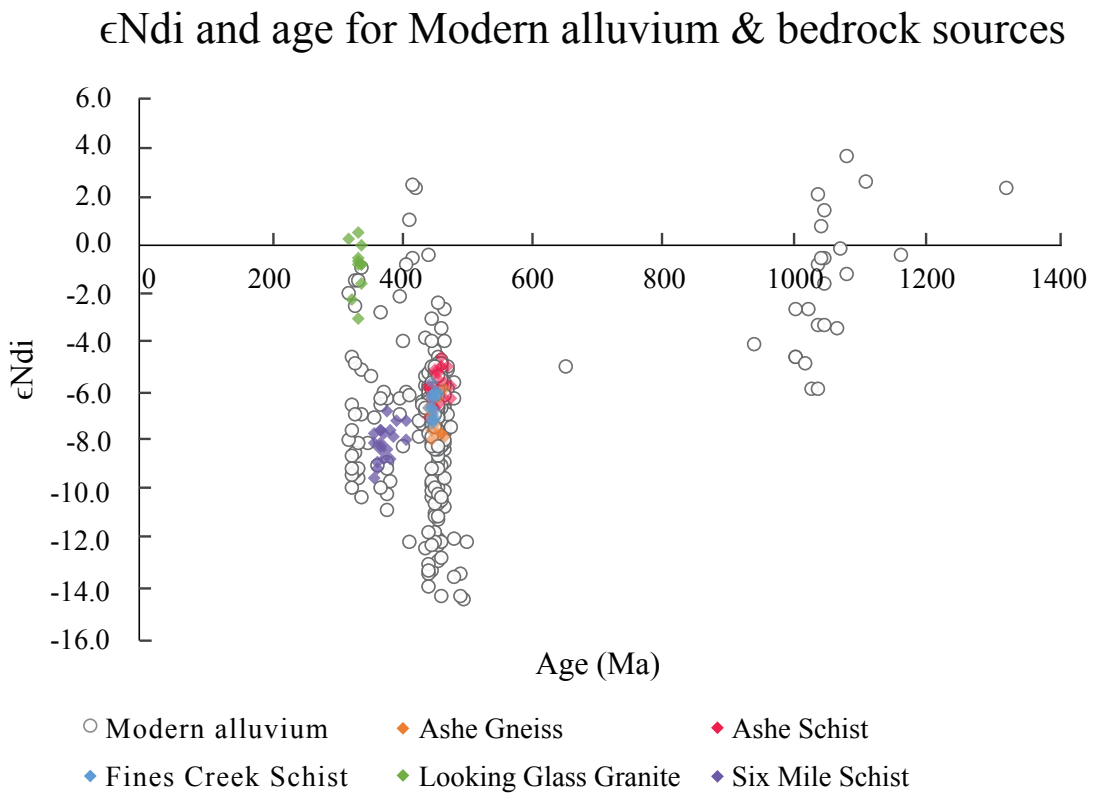

Figure 16. Age and εNdi values for five bedrock samples with all detrital monazite from the Modern alluvium of the French Broad River overlain in gray. Colored circles help distinguish separate bedrock populations.

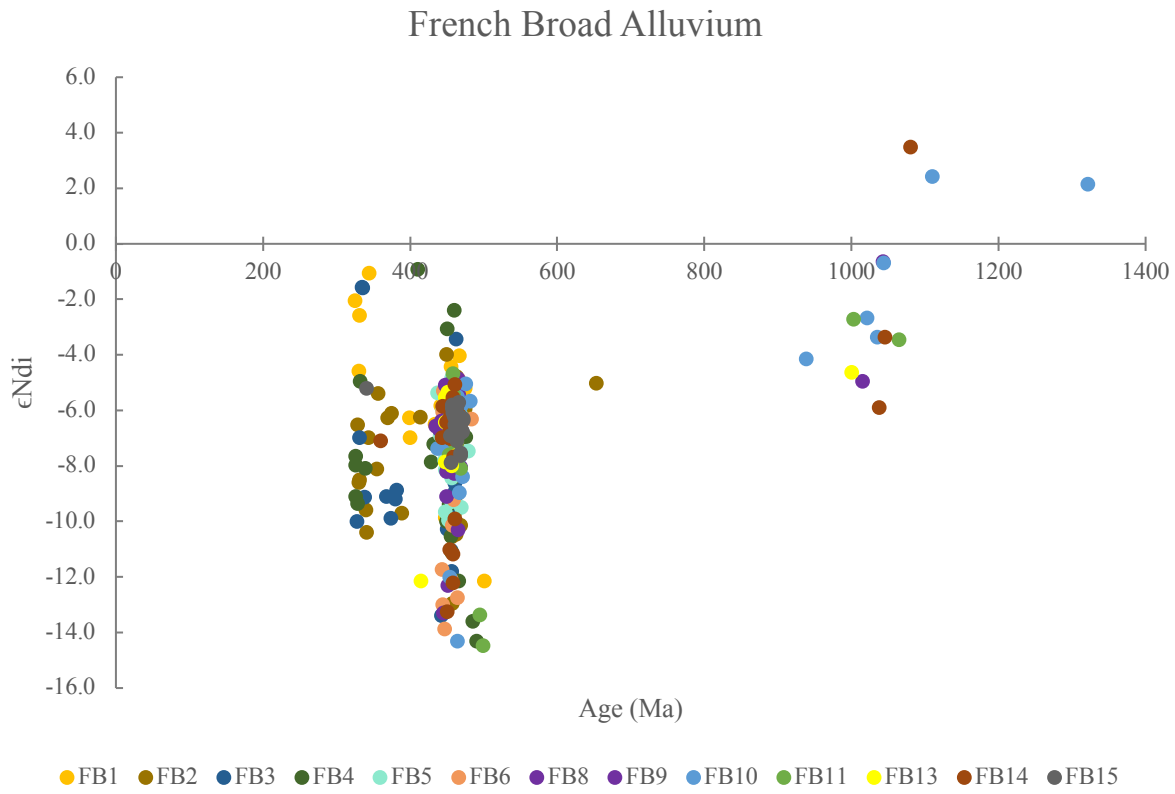

Figure 17. French Broad River alluvium detrital monazite age and εNdi values separated by French Broad sample.

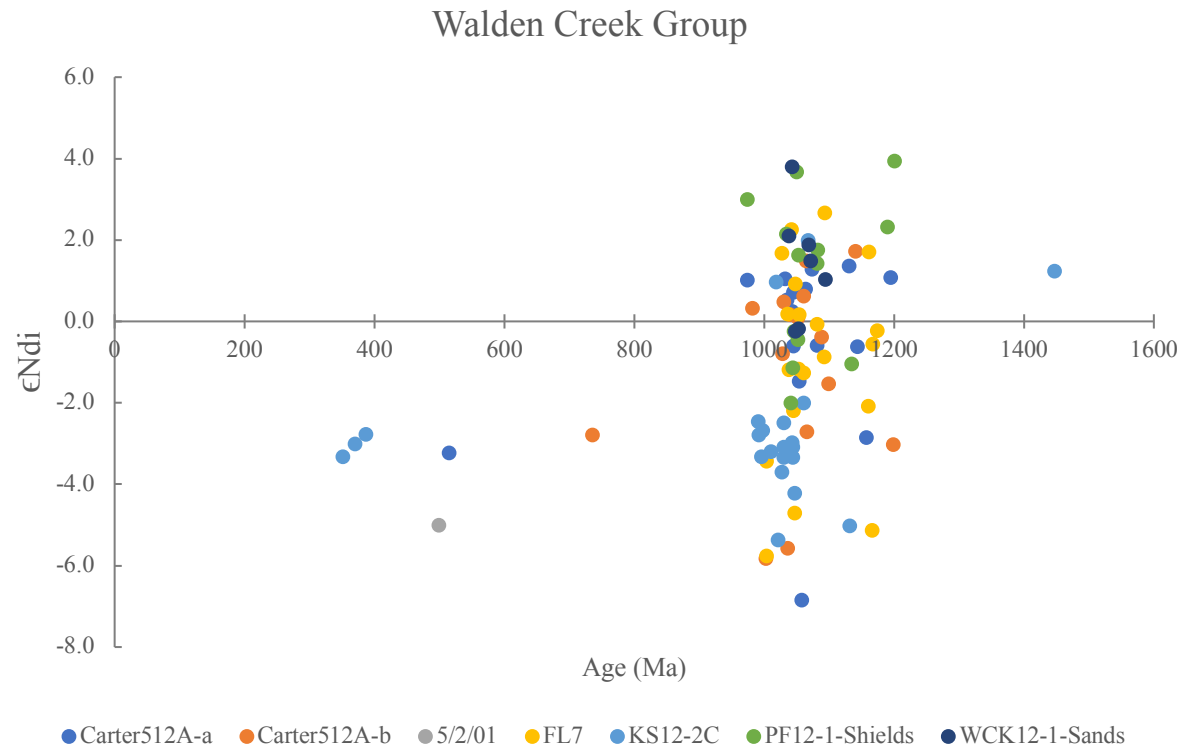

Figure 18. Detrital monazite age and εNdi values from the Neoproterozoic Walden Creek Group separated by sample.

3.3 Nd Isotope Geochemistry (TIMS)

In order to assess the utility and the precision of the LASS-ICP-MS method for measuring the Nd isotopes, we evaluated five of the same grains via the well-established, high precision method of Thermal Ionization Mass Spectrometry (TIMS) to verify the measurements of the LASS. Grains were hand plucked from the mount that was previously analyzed via laser and dissolved on a hot plate in 10 molar ultra-clean hydrochloric acid to be analyzed via TIMS at Los Alamos National Laboratory. Grains were chosen from two bedrock samples (Ashe Schist and Ashe Gneiss) of the same age and similar ϵNdi values (Figure 15). Samples of the Ashe Schist, Fines Creek Schist, and Ashe Gneiss are all ~450 Ma (Taconic Orogeny-aged) and range in ϵNdi values from -8.0 to -4.0 (Figure 19). Within the error bars of the LASS-ICP-MS ϵNdi data, these samples cannot be distinguished from one another (Figure 19). However, if the error bars are omitted, it would appear that the Ashe Schist and Ashe Gneiss are distinct populations (Figure 15). In order to test the hypothesis that the two samples are in fact discernable from one another, and additionally test the accuracy of the LASS-ICP-MS measurements, grains from each sample (FB1SR-Ashe Schist grains 3, 9, 10 and Ashe Gneiss grains 8 and 11) were analyzed via TIMS after they were analyzed via laser ablation (Figure 19).

Figure 20 shows the results of the TIMS analysis. The ϵNdi values measured via TIMS fall within the error bars of the laser data for each of the five samples and significantly reduces the size of the error bars. These data coinciding confirms the accuracy of the LASS data as well as more conclusively showing that the Ashe Schist and Ashe Gneiss populations do not overlap in ϵNdi values.

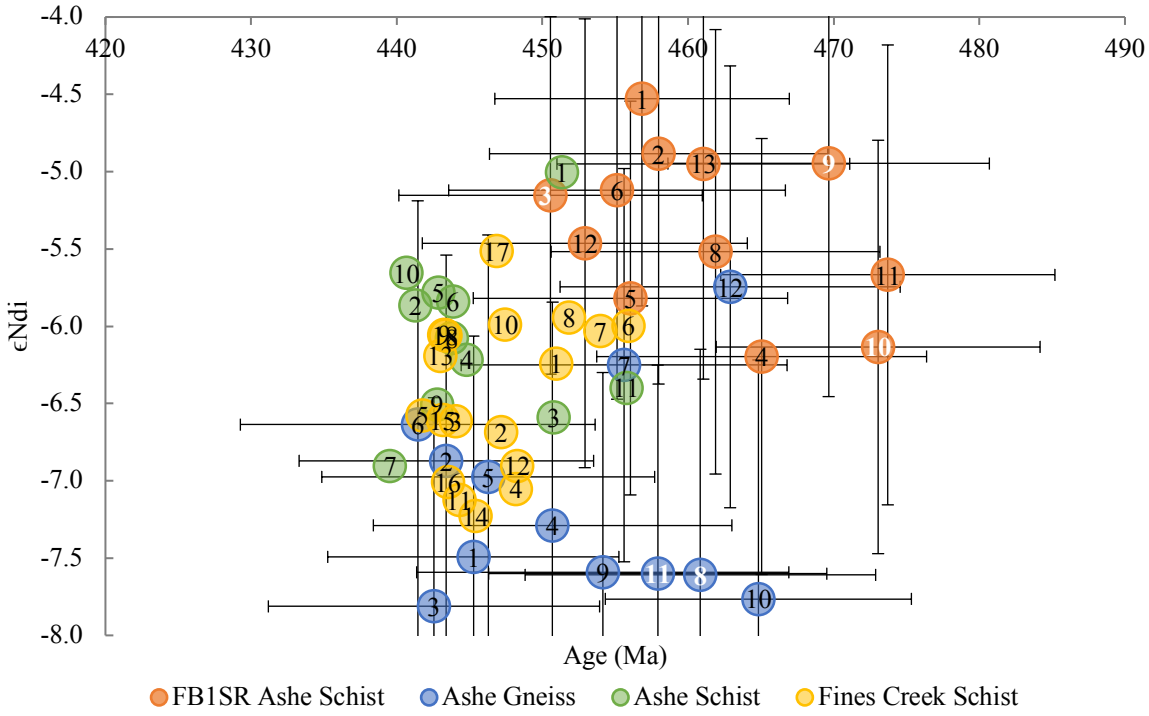

Figure 19. εNdi values and U-Pb ages of Taconic-aged bedrock samples with error bars.

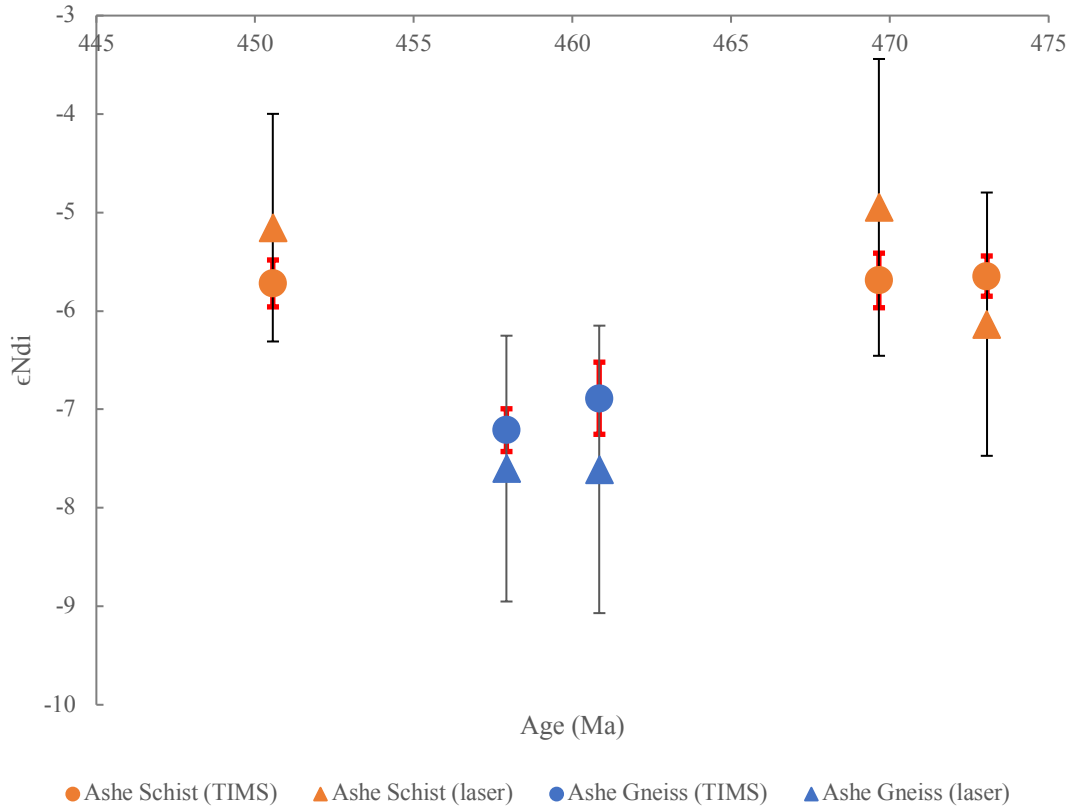

Figure 20. Laser analyzed εNdi values for five samples shown as triangles with black error bars. TIMS analysis of the same samples show εNdi values as circles with red error bars. The U-Pb age from the LASS analysis is used for each point.

4. Discussion

4.1 Comparison of detrital monazite and detrital zircon as provenance indicators

As discussed above, the potential for monazite to be a more accurate provenance mineral than zircon when investigating immediate vs. ultimate sources of detritus had been proposed by previous studies (e.g. Hietpas et al., 2010; Hietpas et al., 2011). Both detrital zircon and monazite studies have shown that the age spectrum of French Broad River alluvium is diverse, more so than that of smaller scale tributaries, reflecting the river's regional sampling scale, and leading to significant heterogeneity in the alluvium samples (Hietpas et al., 2010). According to detrital garnet data from Hietpas (2013), there are two broad groups of French Broad samples linked to potential sources (Figure 2). According to the detrital garnet data, samples 1-4 are very similar to one another, with sediment contributions sourced from metapelites, the Looking Glass pluton, and granitic pegmatite. Sample groups FB5-9 and FB11-15 are similar to one another and dominated by sediment input by the Ashe-Tallulah Falls Metamorphic Suite and the Ashe Gneiss. FB10 shows a weaker Ashe Gneiss source contribution, with additional contributions from other pelites and the Ashe schist as potential sources (Figures 2 & 3). While this study is important to understanding potential provenances for the modern alluvium, it is important to discuss the different information that can be gathered by different detrital minerals. Because we have detrital zircon *and* monazite data from the "French Broad samples" (Figure 3), and zircon is the most commonly used detrital mineral for provenance studies, it is imperative that the differences are carefully evaluated. This study adds a large number of detrital monazite ages to the data set discussed in Hietpas et al. (2010). Comparison of detrital zircon U-Pb age data from Hietpas et al. (2010) and newly acquired LASS-ICP-MS detrital monazite U-Th-Pb ages from

the same samples demonstrate the unique utility of monazite as a first-cycle provenance investigation tool (Figure 21).

Detrital zircon dates from French Broad Alluvium in the southern Appalachians are dominated by a large Mesoproterozoic peak that overlaps the timing of the Grenville orogenic events (Hietpas et al., 2010). This age peak greatly overrepresents the abundance of Grenville basement rock exposed in the watershed of the French Broad River. Bedrock of this age is mapped as 12% of the area's exposed bedrock (Moecher and Samson, 2006). About 63% of detrital zircon ages collected from Modern alluvium from the French Broad River (n = 836) are 'Grenville' in age (i.e. ~1200 – 980 Ga). This vast overrepresentation of these older zircon grains is due to a number of factors, including the high zirconium nature of Grenville magmatism created extremely abundant zircon during this orogeny (Moecher and Samson, 2006), the physical durability of zircon during sediment transport and metamorphic events allows them to preserve original crystallization ages through multiple large orogenic events, and a high crystallization temperature makes zircon unable to record lower P/T metamorphic events (Samson et al., 2018; Hietpas et al., 2011).

In contrast, the Mesoproterozoic age peak in the French Broad River detrital monazite record (n = 404) accounts for only about 3.5% of the ages (Figure 6), reflecting monazite infertility of exposed Grenville granitoids in the French Broad drainage basin.

While capable of surviving some metamorphic events and weathering from erosion, monazite is more susceptible to chemical breakdown than zircon and therefore less likely to be recycled multiple times (Rasmussen and Muhling, 2009; Hietpas et al., 2010). In addition to a more accurate representation of the proportion of monazite-fertile bedrock sources in the detrital record, monazite is able to record metamorphic events that the zircon record misses. Rocks

metamorphosed during the Acadian Orogeny in the Devonian are only represented by 1% of zircon ages verses 3% of monazite ages. Rocks metamorphosed during the Alleghanian Orogeny (~300 Ma) are only represented by one rim of one zircon grain (~0.1%) versus over 6% of monazite ages. Without the one metamorphic zircon rim, this supercontinent collision event would be entirely missed in the detrital zircon record. Detrital monazite clearly provides a superior record of these metamorphic events while detrital zircon overrepresents magmatic events in potential source rocks (Hietpas et al., 2010, 2011).

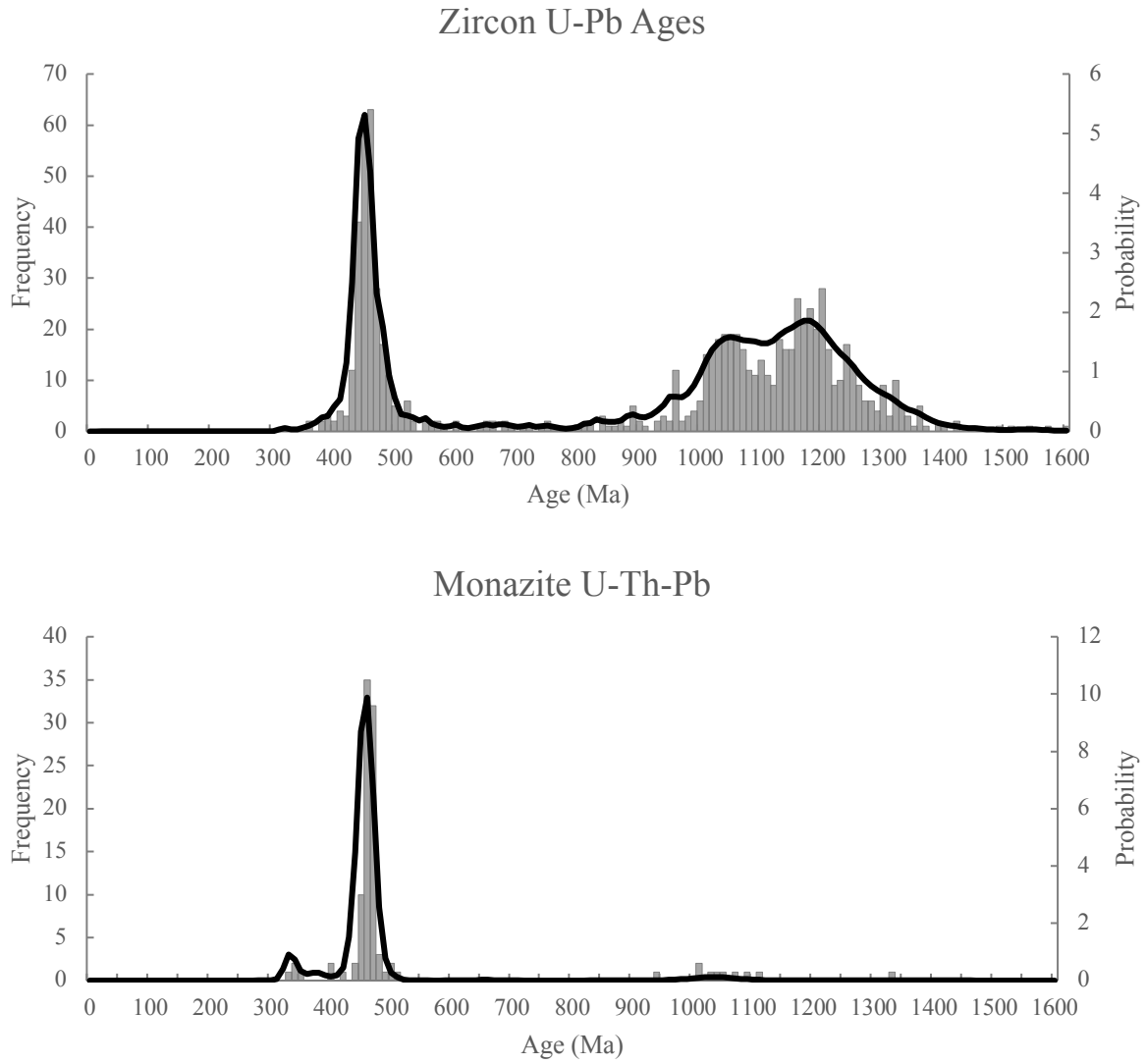

Figure 21. Comparison of detrital zircon ages (Hietpas et al., 2010) and detrital monazite ages from the same 13 samples in the French Broad River in the southern Appalachians.

It is worth noting that Hietpas et al. (2011) analyzed detrital monazite from the same French Broad alluvium samples as this study (FB1-4, 6, 8, 10, 11, 13-15) with the exceptions of FB5 and FB9. The full data set of their monazite and zircon results can be found in GSA Data Repository item 2010033. They analyzed a total of 86 monazite crystals while we analyzed 404, and disparities in the abundance of certain age populations can almost certainly be explained by random sampling of a small sample size. Hietpas et al. (2010) recorded that 14% of the analyzed detrital monazite grains were Mesoproterozoic in age, while this study's analysis reduces that number to 3.5%. Even with removing the two samples for which data were collected for this study and not for Hietpas et al. (2010) (FB5 and FB9), that percentage is only raised to 3.7% of our now 323-grain population being Mesoproterozoic in age. This may seem like a huge discrepancy in what would be expected to be comparable data, but our total number of analyses being over four times that of Hietpas et al. (2010) mostly adds to the more abundant ~450 Ma population of monazite grains that overlaps with the timing of the Taconic Orogeny. All FB samples that Hietpas et al. (2010) reported containing Mesoproterozoic monazite grains, also contained ~1 Ga grains in this study's analysis. For example, FB samples 1-4, 6, and 8 consist of an entirely Paleozoic population of monazite grains in both Hietpas et al. (2010), and in this study. These samples contain 37 analyses in their study and 191 in this study, skewing the total French Broad data much more towards a Paleozoic majority in this study compared to Hietpas et al. (2010). FB samples 9, 10, 11, 13, and 14 all contained some Mesoproterozoic-aged grains in both studies. However, due to sampling size, the differences in percentage of grains per sample that are Mesoproterozoic can seem quite drastic. The most striking example of this is sample FB14. Hietpas et al. (2010) reported five Mesoproterozoic ages of the 13 analyzed grains (38.5%) from that sample while we report three Mesoproterozoic ages of 28 analyzed grains

(10.7%). The dominance of the Taconic-aged ~450 Ma signature and the larger sampling size of our study explain the differences in the reported age data of the Modern alluvium from the French Broad River, though both Hietpas et al. (2010) and this study's reports of 14% and 3.5% Mesoproterozoic monazite grains respectively are much more accurate representations of the mapped Mesoproterozoic bedrock in the watershed (12% of exposed rock) than the zircon data (63% Mesoproterozoic). These data reinforce the concept that while zircon is a great provenance indicator for the ultimate source, recording where the grain was crystallized, monazite is a superior tool to record immediate sources, i.e., first-cycle provenance.

4.2 Provenance as a predictive tool

The detrital monazite age population can be used as a predictive tool for the immediate bedrock sources in the watershed area. Some bedrock samples were collected in an attempt to illustrate this, though there are many more source rocks that have not yet been collected and analyzed. Even with only five bedrock samples analyzed for this study, the correlation of the PD plots indicate that the bedrock samples are obvious likely sources for the alluvium (Figure 22). Both the bedrock and the alluvium have highest age peaks at 450 Ma, consistent with metamorphic crystallization during the Taconic Orogeny. Both have a larger, but distinct, Alleghanian orogenic peak compared to the Acadian orogenic age peak. The differences in the plots can be attributed to the limited bedrock sampling. All of the bedrock ages are represented in the alluvium but not all of the alluvium ages were found in the bedrock samples. The most apparent disparity is the lack of a Grenville signature in the bedrock data (Figure 22)[1].

[1] One monazite-bearing Grenville-mapped basement paragneiss was collected and processed in order to fill in this gap in the dataset but time constrains precluded split stream analysis of the monazite before the publication of this thesis.

Additionally, Taconic-aged peaks differ slightly, with the alluvium having a second, 460 Ma peak in addition to the 450 Ma peak that is visible in the bedrock PD plot (Figure 23). In this way, the age data of the Modern alluvium can be used as a predictive tool for determining what other local bedrock units are the proximal sources for the detrital monazite crystals that are being eroded into the watershed.

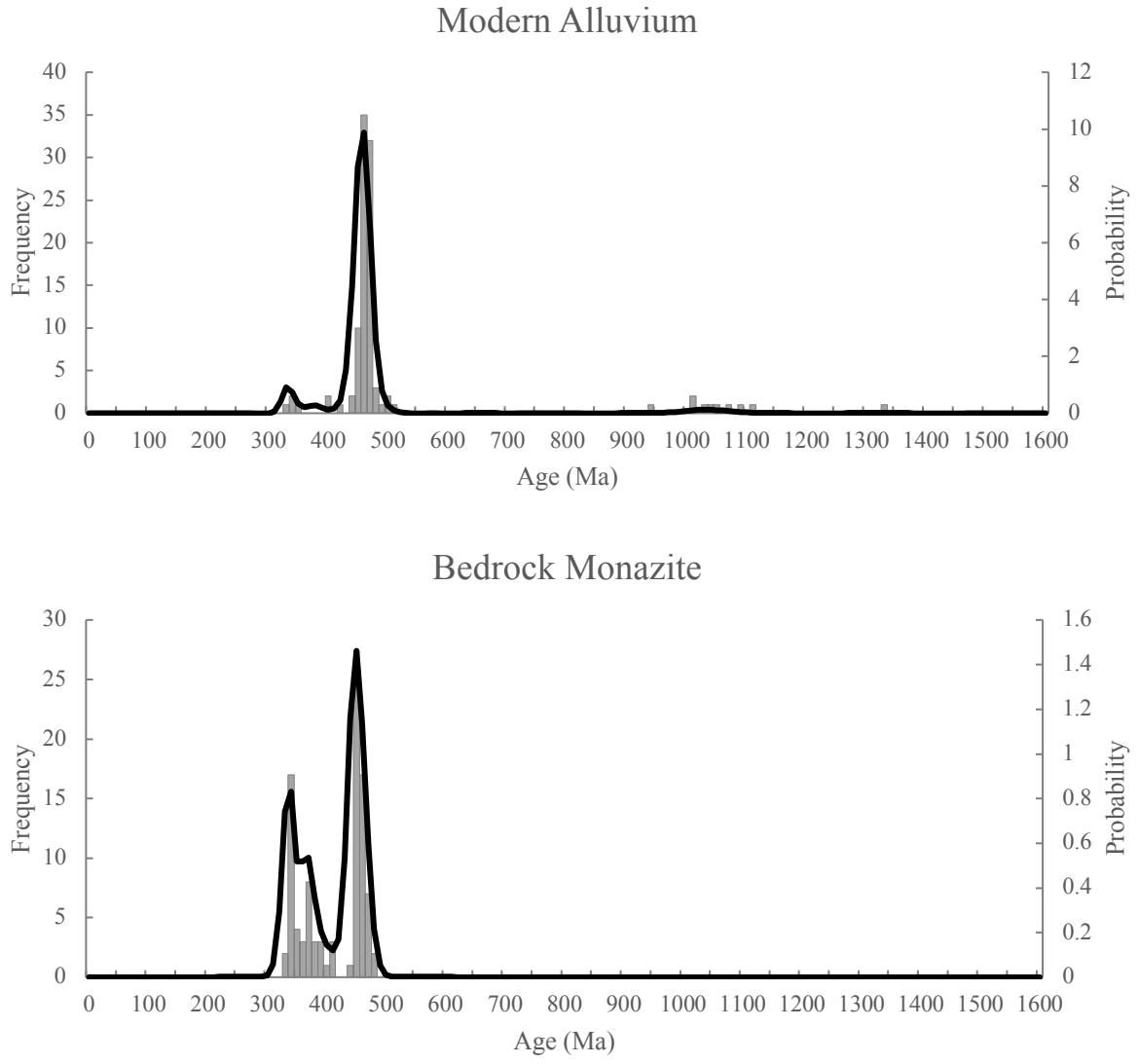

Figure 22. PD plots of detrital monazite ages from 13 Modern alluvium samples from the French Broad River (n=404) and 5 bedrock samples from the French Broad River (n=98).

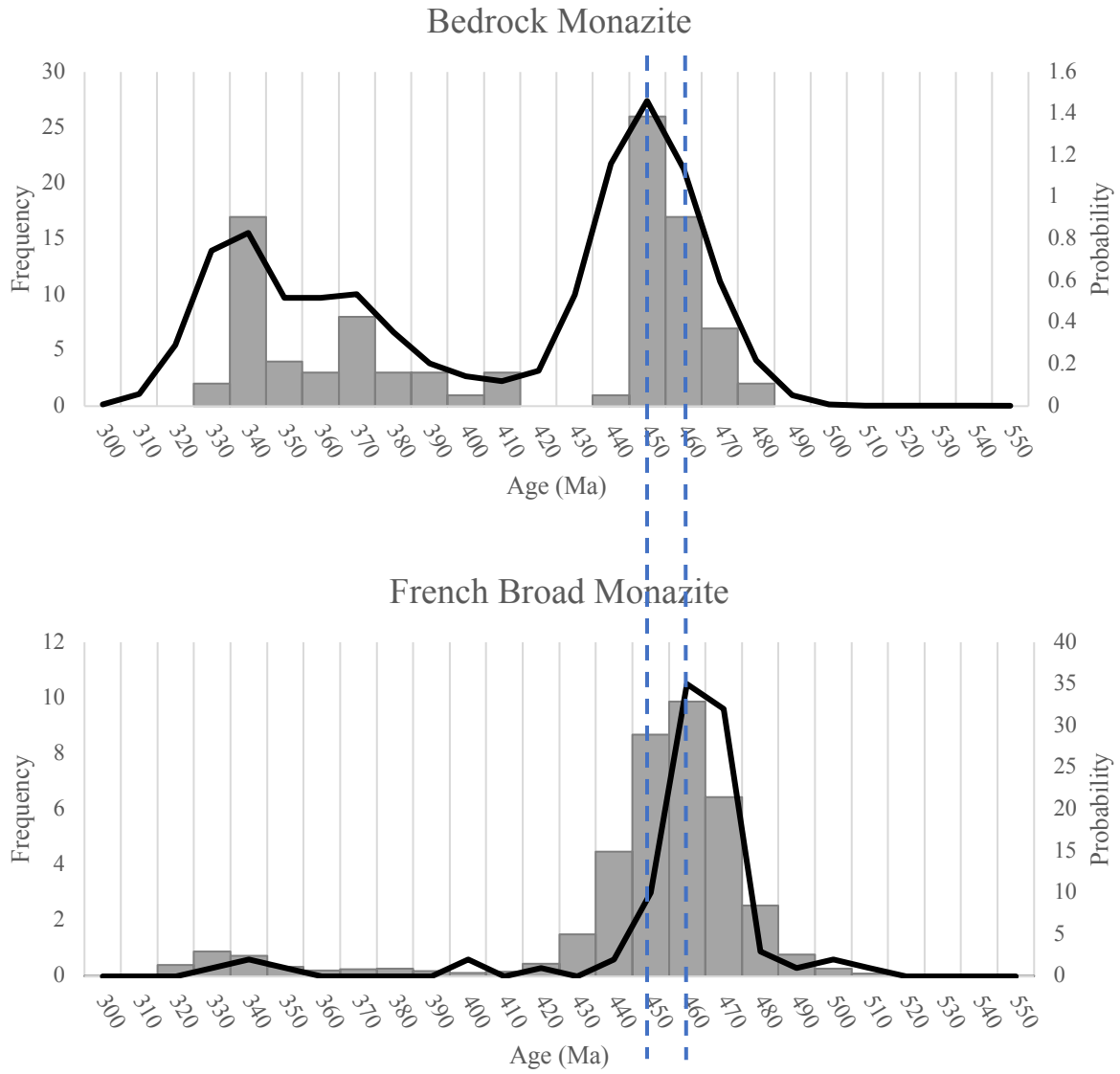

Figure 23. A closer look at the PD plots for the bedrock and Modern alluvium to illustrate the slightly different Taconic-aged peaks. Dotted lines are at 450 Ma and 460 Ma.

4.3 Spatial distribution of detrital monazite U-Th-Pb ages

Based on the spatial distribution of the monazite age data collected from Modern sediment along the length of the French Broad River, it can be inferred that detrital monazite in a Modern river system records information from very proximal bedrock sources. The combined PD plot from 13 river samples gives a representative overview of the detrital record in the watershed (Figure 6).

When looked at individually, however, each sample has a quite distinct signature (Figure 24). Figure 25 shows the spatial distribution with regards to distance downstream and there is a clear spatial pattern visible. The Taconic age peak (470-440 Ma) is present in every sample along the length of the river. The upstream samples account for the majority of both the Alleghanian (320-280 Ma) and Acadian (420-380 Ma) Orogeny signatures, with only a small number of them present in the most downstream samples. In contrast, Grenville age grains (~1300-900 Ma) are not present in any upstream samples, only those most downstream, indicating that there were no Grenville-aged bedrocks sourcing the sediment of the upstream French Broad. The increased abundance of younger monazite ages upstream is consistent with previous work demonstrating that most metamorphism is late Paleozoic in age in the inner Piedmont (Merschat et al., 2006).

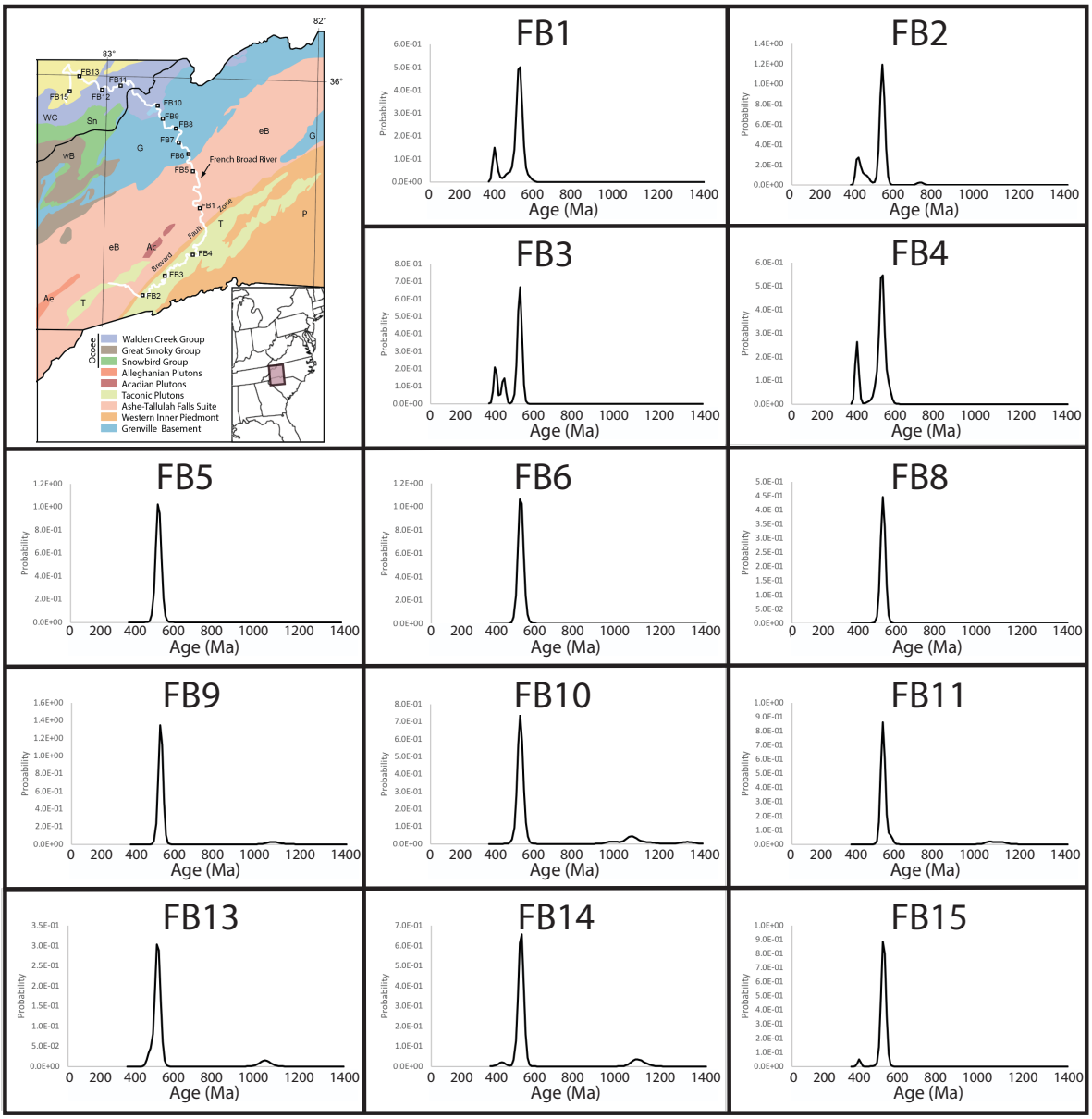

Figure 24. PD plots of each of the Modern alluvium samples from the French Broad River, with map for context.

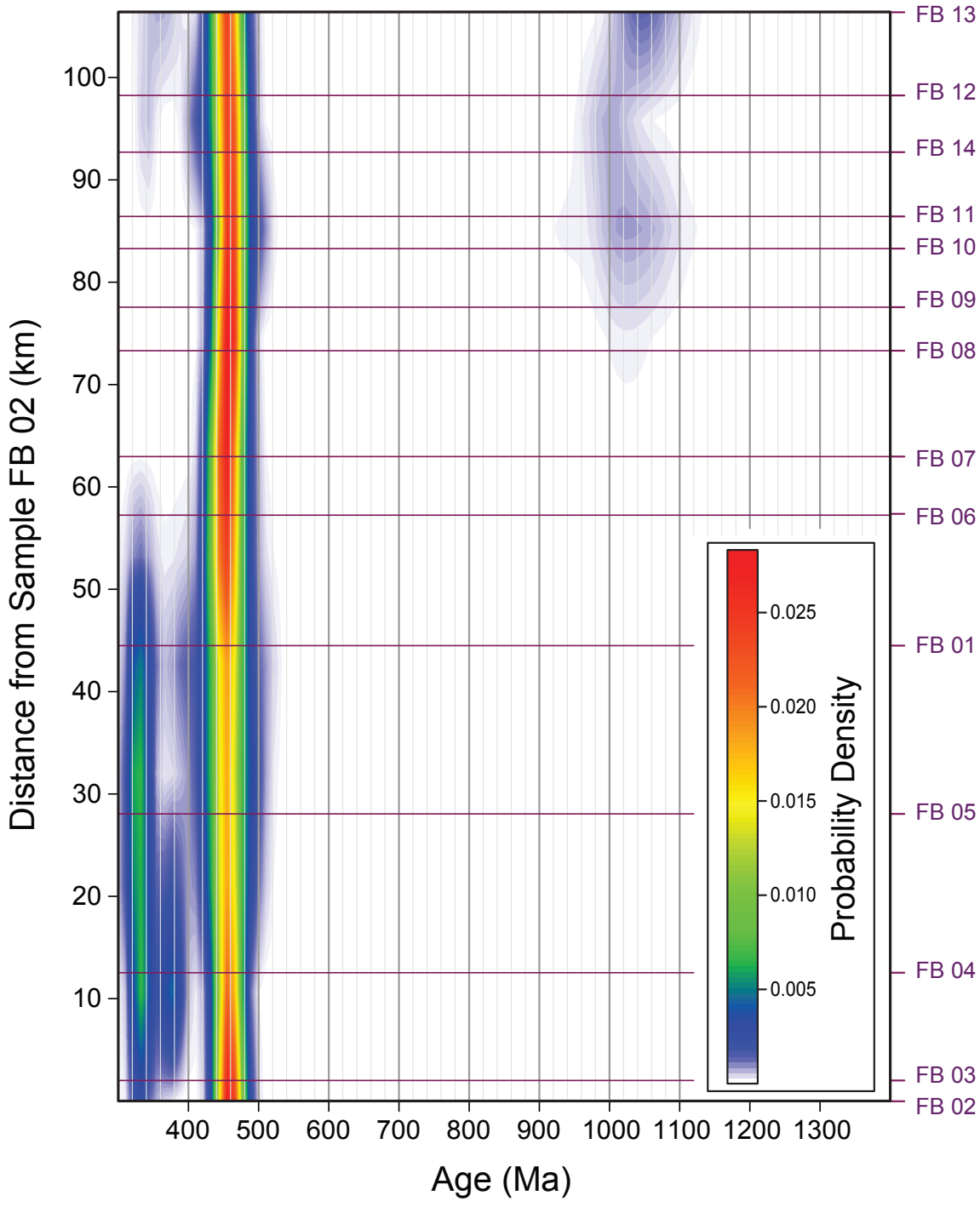

Figure 25. The y-axis is distance from the most upstream sample FB-2 and the x-axis is age. The probability density is shown as a heat map with red indicating the highest concentration of ages and blue indicating a low concentration of ages.

4.4 Utility of Nd isotopic data

Analysis of Nd isotopic data provides an important characteristic by which to identify and distinguish immediate (first-cycle) versus ultimate (recycled) sources of detrital monazite in conjunction with the U-Th-Pb age data. The LASS-ICP-MS is imperative to this method because it uses only one laser shot to collect both the U-Th-Pb data and the Nd data from the same 15-micron portion of the monazite grain. When analyzing heterogenous detrital samples like the Modern alluvium in this study, which are originating from an unknown number of sources, it is difficult to distinguish even an estimate of the number of potential sources using just U-Th-Pb age data. Using only U-Th-Pb data, one is able to assume that more detrital grains are originating from Taconic-aged sources than any other (i.e. other Paleozoic or Mesoproterozoic sources) (Figure 6). However, there is no way to know if only one, large Taconic-aged source is providing the bulk of the sediment to the watershed or if many sources are contributing detritus.

Plotting ϵNdi values in addition to the U-Th-Pb data offers one solution to this problem (e.g. Figure 16). ϵNdi values reflect the juvenile vs. evolved characteristics of the magmatic rocks of the source terrane of the sedimentary protolith that the detrital monazite grains originated from. The detrital monazite is assumed to be a faithful proxy of the Nd isotope composition of the sedimentary protolith of the metamorphic rock in which it forms. The sediment of that protolith is interpreted to have quantitatively retained the Nd and Sm concentrations of the rocks from which it was sourced. In this case, these were usually granitic crustal rocks, as the generally negative ϵNdi values indicate the involvement of ancient continental crust in the genesis of these Appalachian granitoids (Andersen and Samson, 1995). ϵNdi values of the source magmatic rocks become more negative when the source magma incorporates continental crustal material, whether through magma mixing, crustal contamination

during magma ascent, mixing source regions, or some combination of these processes (Histler et al., 2014). Because ϵNdi values provide additional information that is unique to the crystallization source of a monazite grain, the ϵNdi values can be used in combination with the U-Th-Pb data to provide dual characterization of the source of each detrital grain.

Based on U-Th-Pb ages, we know that the main contributor of detritus to the French Broad River is Taconic in age (over 96% of analyzed grains), and specifically metasediments of the Ashe-Tallulah Falls and Ocoee sequences. Using that U-Th-Pb data in combination with the Nd isotopic data, we can begin to distinguish distinct sources within a single age domain. Three bedrock samples ~450 Ma were analyzed (Ashe Schist, Fines Creek Schist (Ocoee Group), and Ashe Gneiss), but all three have ϵNdi values between ~ -8.0 and -4.0, whereas the alluvium grains of the same age have ϵNdi values ranging all the way from ~ -14.0 to 0.0. Based on this observation, there must be more evolved crustal sources eroding to provide sediment to account for the much more negative ϵNdi values recorded in the Modern alluvium. A more juvenile source must also exist to explain the less negative ϵNdi values in the Modern alluvium detrital monazite, perhaps an igneous rock produced in a volcanic arc during the Taconic Orogeny (Figure 16).

In order to further distinguish the ϵNdi values of the three similar bedrock samples, five grains were plucked from the Ashe Schist and Ashe Gneiss to be analyzed with high precision TIMS. Within the error bars of the LASS-ICP-MS ϵNdi data, these samples are indistinguishable from one another (Figure 19). The goal of this secondary characterization of the Nd isotope values was to confirm that the LASS analyses were accurate by, in essence, verifying the values with the TIMS analysis and just shrinking the error bars on the data points in hopes that the two populations would separate beyond error bars, confirming separate sources. While the

effectiveness of using the TIMS to confirm the laser data is very important for our study and this specific bedrock example, it also it important to reinforce the utility and accuracy of the LASS dual-characterization of detrital monazite. After TIMS analysis, we can much more confidently state that the two samples have distinct ϵNdi signatures, indicating that the sedimentary protoliths of these metamorphic rocks were formed from sediments of distinguishably different bulk compositions, though from isotopically similar sources (Figure 20).

The Nd data add information to the preceding literature regarding the evolution of the Laurentian margin through time. The Taconic and Sevier foreland basins (Ordovician) were sampled by Andersen and Samson (1995) and the whole rock initial $^{143}Nd/^{144}Nd$ ratios were analyzed for the clastic sedimentary rocks. The $^{143}Nd/^{144}Nd$ ratios increase with decreasing stratigraphic age, reflecting an increased component of juvenile sediment. It has been previously hypothesized that the Ordovician Taconic orogeny did not add significant amounts of juvenile crust to the Laurentian margin, but that the Nd data reflects that most rock formed in the Taconic resulted from the recycling of uplifted Grenvillian crust, upthrust as part of the Taconic allochthons (Andersen and Samson, 1995; Bock et al., 1996). This is consistent with our data from this study. The ranges in ϵNdi values from Neoproterozoic low-grade metasediments (~ -7 – +4), Paleozoic bedrocks (~ -9.5 – +0.5), and modern alluvium (~ -14.5 – +3.5) do not show a significant trend towards input of a juvenile crustal component, supporting the argument for crustal recycling of Grenvillian crust. The juvenile Nd isotope values in the Walden Creek Group points to a juvenile source we have yet to identify (<4.0 ϵNdi) that is most likely additionally sourcing the modern alluvium today.

The same method of dual-characterization can be employed for each of the distinct age domains, distinguishing sources in a way that is not done in the vast majority of detrital mineral

provenance studies that utilize primarily age data alone. For example, while the age data in isolation could have told us that there are Mesoproterozoic sources providing the Mesoproterozoic detritus, the combined Nd data show that there is a large spread in the ϵNdi values (-6.0 to +4.0) of the Mesoproterozoic grains (Figure 17). This proves that multiple sources of different amounts of crustal contamination must be providing this sediment. In this way, the dual-characterization method is a much more powerful predictive tool than U-Th-Pb data, or any single-characterization method, alone.

4.5 Neoproterozoic Walden Creek Group

The detrital monazite from the Modern alluvium, discussed above, acts as a proxy for the nearby Neoproterozoic-deposited Walden Creek Group (WCG) (Kelly, 2014). After the sediment in the French Broad River is transported, deposited, and lithified, it will resemble the lithologies of the Walden Creek Group and the rest of the Ocoee Supergroup. Six samples from the Walden Creek Group were analyzed via LASS-ICP-MS for U-Th-Pb and Nd isotopic data. It would be expected that the detrital monazite analyzed from this sandstone would represent the source material that was providing the detritus at the time. And while the majority of ages do reflect the Grenville-aged mountains that were eroding at the time, there are seven concordant grains that

are younger than the Neoproterozoic depositional age, calling into question how they formed (Figure 26).

Monazite has been shown to be able to form overgrowths and entire new grains diagenetically (post-depositionally), and it is the only logical explanation for these younger

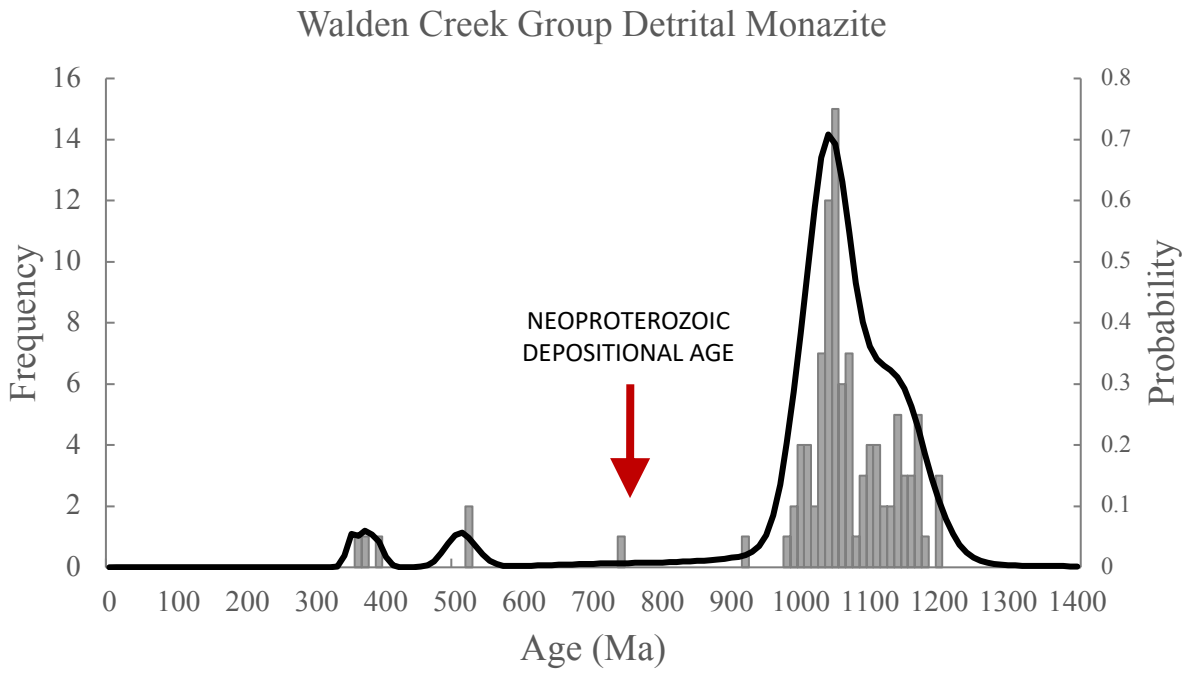

Figure 26. Probability density plot of four samples from the Walden Creek Group (n=125). Neoproterozoic depositional age established by Kelly, 2014.

grains, that are younger than the youngest of the older age population (~950 Ma) that represent the maximum age of deposition (Aleinokoff et al., 2010). One of these younger grains cannot be accounted for by Grenville-aged inheritance or post depositional diagenesis. With an age of 736±89 Ma, it has a high error, but is firmly a Neoproterozoic age. It is possible that this grain is recording the time of deposition through low temperature diagenesis of this monazite grain during burial. The three youngest diagenetic monazite grains are Devonian in age and would have needed to form in a metamorphic event that did not reach high enough temperatures to produce new zircon growth, but enough to affect some monazite grains. These events may have

been low temperature enough to not affect zircon grains in these rocks at all, meaning the zircon record would not record them even in the form of metamorphic rim growth. In the case of the Walden Creek Group (with n = 620 previously analyzed zircon), no zircon grains were analyzed with a core or a rim that were the same age as these diagenetic monazite crystals (Kelly, 2014). These diagenetic monazite grains must have formed *in situ* because their age is younger than the depositional age of the rock, but the exact mechanics of their formation are not entirely known. It has been stated that the precipitation of secondary monazite probably results from changes in fluids or metamorphic conditions during low-grade conditions and involves fluid-rock interaction, dissolution of detrital grains, transportation, and precipitation of REEs (Allaz et al., 2013). Likely, these secondary diagenetic monazite form from the breakdown of older, preexisting, detrital monazite. This method would provide the REE budget needed to form the very REE-rich mineral, but would reset the age of the secondary monazite to post depositional times. Fluid percolation, driven by orogenic loading, may induce dissolution of detrital monazite and the subsequent precipitation of new monazite that probably results from changes in fluids and/or metamorphic conditions (Allaz et al., 2013).

As an alternative method, the diagenetic mineral could form from the REE budget present in the entire sandstone that is consolidated through fluid movement during the metamorphic event. Because the most common minerals in a sandstone are quartz and feldspar, both of which have low REE contents, it is more likely that these diagenetic monazite grains are coming from the breakdown of a primary monazite in a low-grade metamorphic event verses consolidating the REE budget in the entire rock. This would also eliminate the need to explain REE transportation through metamorphic fluids. If this WCG sandstone were to erode in the future, these diagenetically-formed monazite crystals will be released into the detrital monazite population,

recording lower temperature events that are potentially not recorded by any other detrital mineral. These monazite grains are thus referred to as detrital diagenetic monazite (DDM) (Moecher et al., 2015, 2019). It is some of these DDM that we hope we are analyzing in the Modern alluvium, recording otherwise elusive information from the detrital record about minor metamorphic events and sediment recycling.

Using the below equations, the ϵNdi values of these DDM in the WCG samples can be projected back to any age based on the assumption that a diagenetic monazite recrystallized and reset the U-Th-Pb age but used the same original source material to form.

1) $$\epsilon\text{Ndi}_{\,today} = \frac{\frac{^{143}Nd}{^{144}Nd} - \frac{^{143}Nd}{^{144}Nd_{CHUR}}}{\frac{^{143}Nd}{^{144}Nd_{CHUR}}} \times 10^4$$

2) $$\frac{^{143}Nd}{^{144}Nd_{ini}} = \frac{^{143}Nd}{^{144}Nd_{measured}} - \frac{^{147}Sm}{^{144}Nd_{measured}} \times \left(e^{(6.54\times10^{-12})\times(\text{Age})} - 1\right)$$

Equation 1 is used to calculate ϵNdi from $^{143}Nd/^{144}Nd$ values.
Equation 2 is used to calculate $^{143}Nd/^{144}Nd_{ini}$ from measured $^{143}Nd/^{144}Nd$ values and U-Th-Pb ages *or* calculate $^{143}Nd/^{144}Nd_{ini}$ from 'projected' age.

Present-day CHUR values:
$^{143}Nd/^{144}Nd_{CHUR}$ = Bulk Earth = 0.512638
$^{147}Sm/^{144}Nd_{CHUR}$ = 0.1966

By back calculating the ϵNdi to an 'original crystallization' Grenville age (to match the majority of WCG monazite) relative to CHUR, the diagenetic monazite grains have an original source between +4.0 and +7.0 ϵNdi (Figure 27). Two of the projected lines (from grains KS122C 7 & 12) pass directly through grains from two of the more juvenile WCG samples - the Shields and Sandsuck Formations at +3.0 to +3.9 ϵNdi (Figure 27). These two grains were therefore likely originally crystallized from one of those two sources or a similar source and were later

altered by diagenesis. One of the grains projects to a slightly more juvenile source with a higher ϵNdi value than was collected from any of the WCG grains.

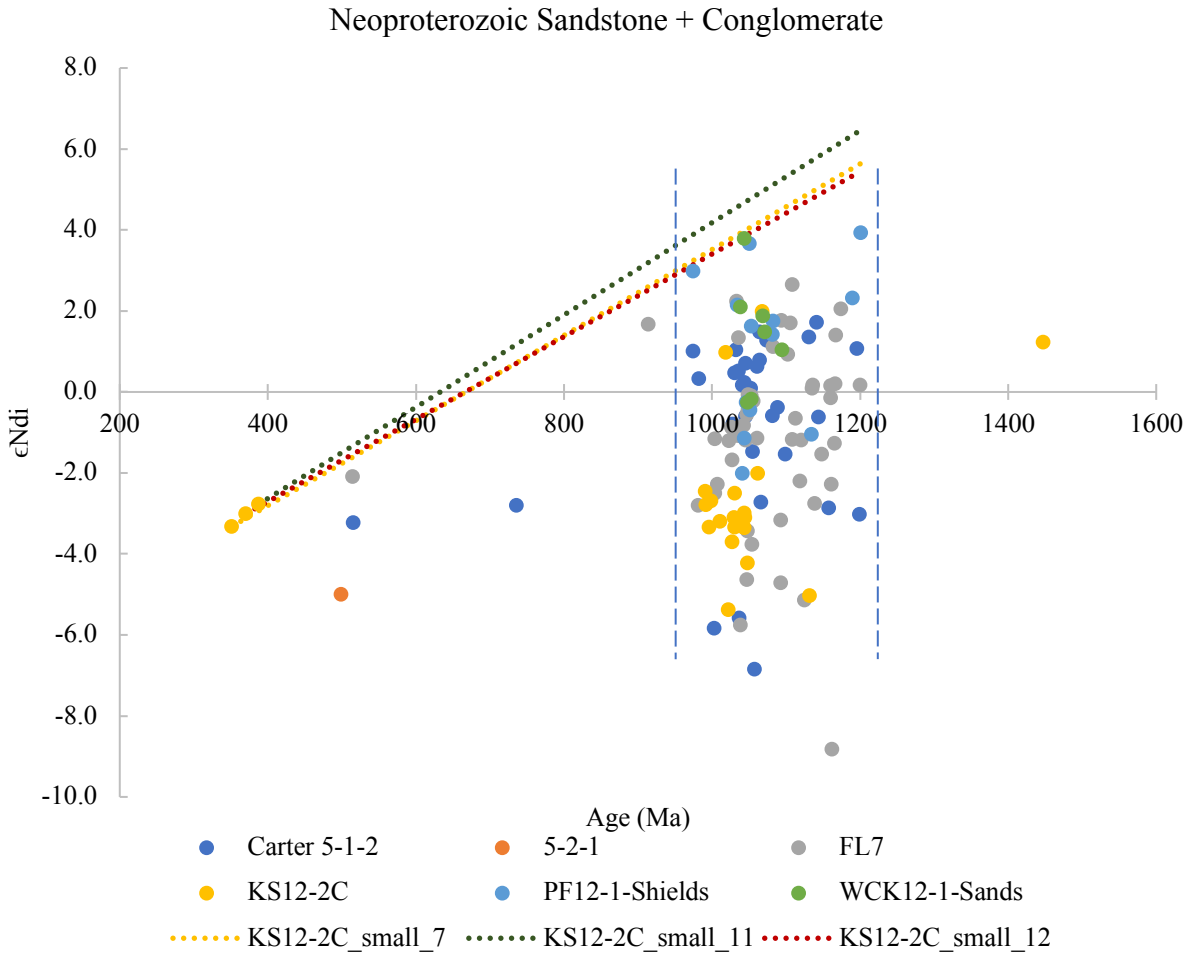

Figure 27. ϵNdi plotted against age for the detrital monazite collected from the Walden Creek Group sandstone and conglomerate. The dotted lines represent the projection of ϵNdi values relative to CHUR through time using the equations 1 and 2 above.

Future Work

Additional work is underway to strengthen some of the points of this thesis. Of the five bedrock samples analyzed in this study, none of them correlated to the Mesoproterozoic detrital monazite grains found in the Modern alluvium or in the Neoproterozoic Walden Creek Group (Figure 16). Using the ages of the alluvium as a predictive tool, we know that there are Mesoproterozoic-aged rocks contributing sediment to the river. We targeted bedrock units

mapped as Mesoproterozoic in age in order to attempt to find a monazite-bearing sample to add to our bedrock database (Merschat and Cattanach, 2008). One monazite-bearing sample (NC19-1) was processed, identified, and mounted. This sample was collected from the Sandymush felsic gneiss map unit in the Clyde (NC) 7.5-minute quadrangle. It was folded and foliated and the more muscovite-bearing portions of the sample were targeted as potentially containing more monazite due to higher phosphorous content. The plan is to analyze this sample at some future date (containing ~150 monazite grains) using LASS-ICP-MS to compare both age and Nd isotopic data to the Modern alluvium grains from the French Broad River.

Conclusions

1. Dual detrital monazite characterization (U-Th-Pb and Nd isotopic data) using split stream laser ablation (LASS-ICP-MS) is a powerful and accurate tool for high throughput provenance studies, also allowing for a more complete way to identify potential source terranes of detrital populations.
2. Detrital monazite analysis provides a more accurate representation of immediate or first-cycle sources, while the more popular zircon analysis records an original source even after being recycled multiple times.
3. Monazite must be able to crystallize during low- to moderate- temperature orogenic events that are not high enough grade to affect a zircon grain, allowing detrital monazite to more accurately record events that have transformed the sediment donor terranes during defining orogenic events.

Supplementary Data

S1-S8: *WDS and EDS maps of 8 selected monazite grains described in Table 1:*

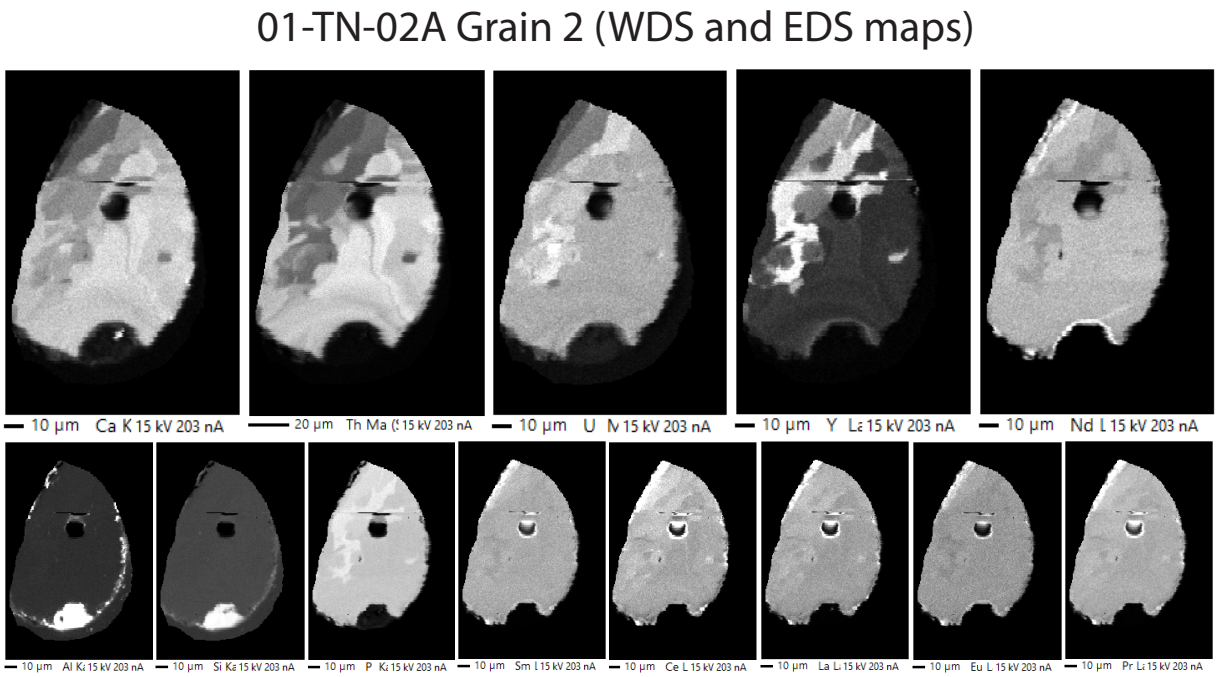

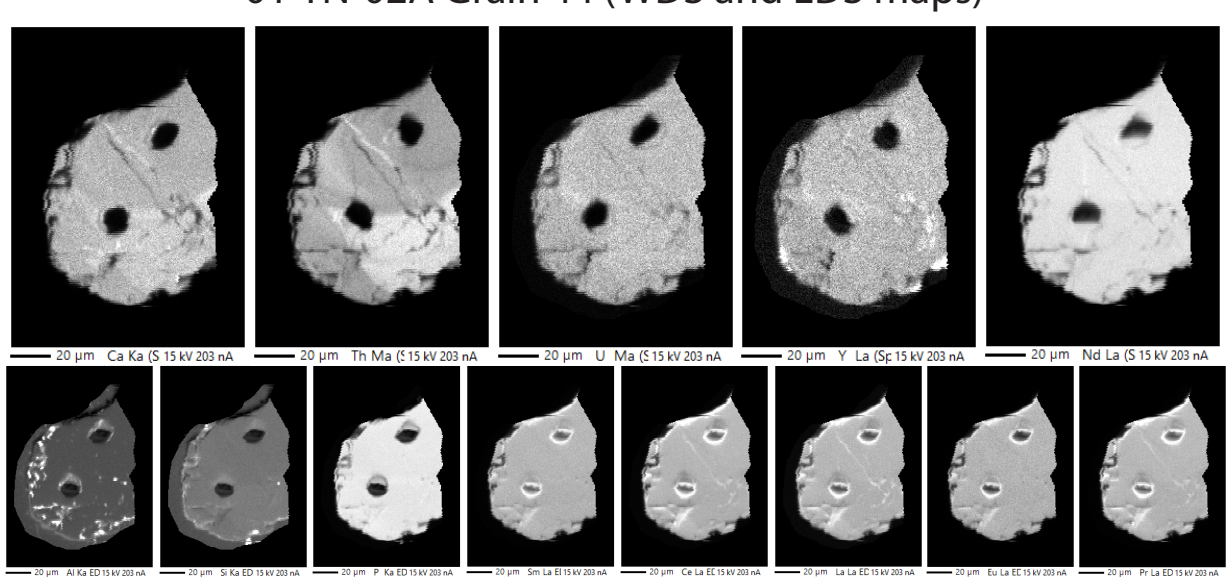

01-TN-02A Grain 49 (WDS and EDS maps)

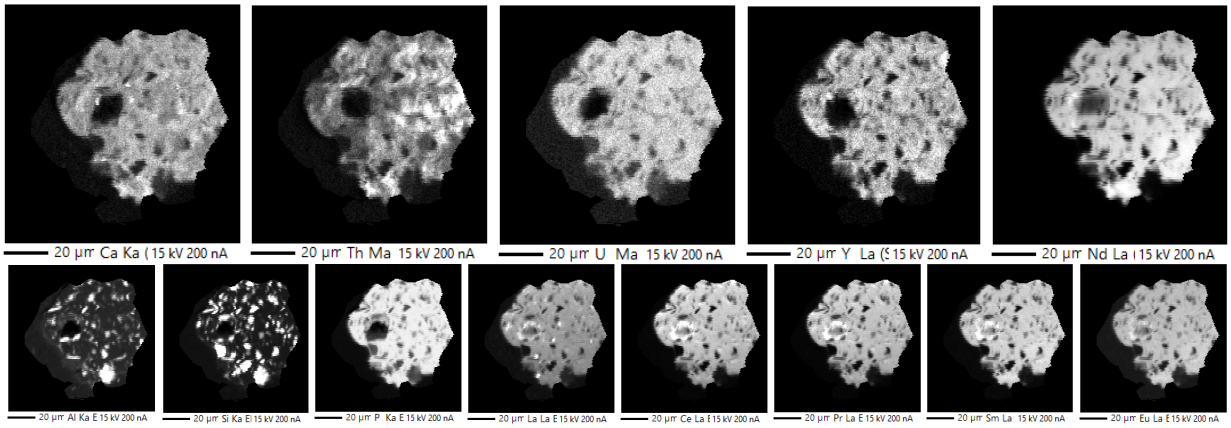

01-TN-02A Grain 51 (WDS and EDS maps)

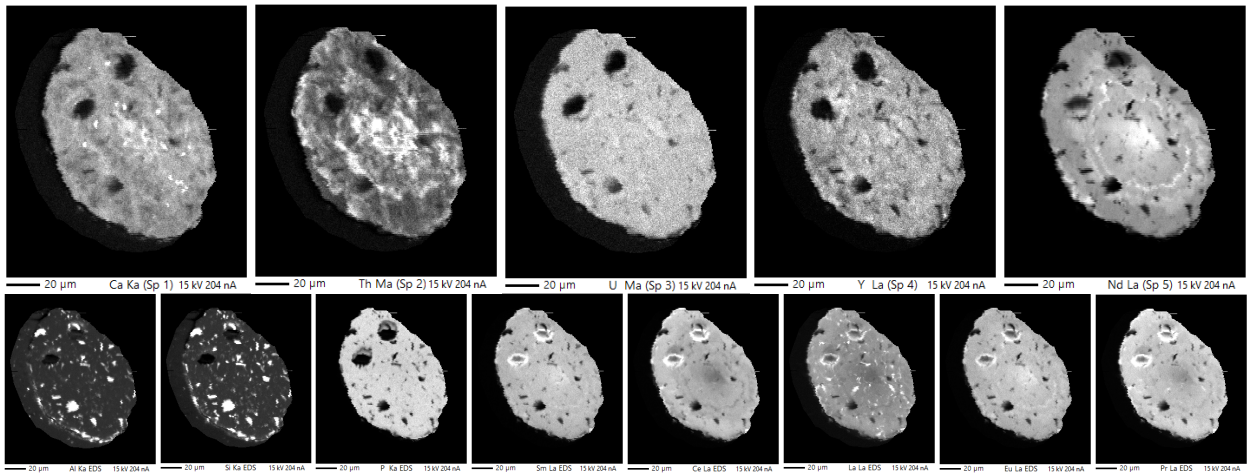

FB3 Grain 30 (WDS and EDS maps)

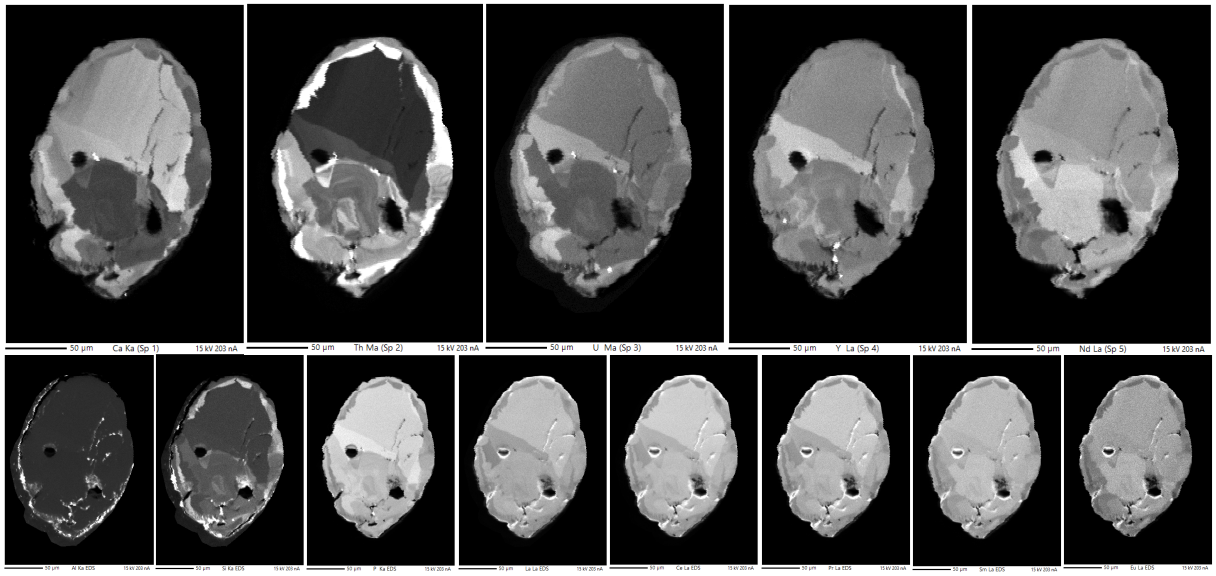

FB4 Grain 7 (WDS and EDS maps)

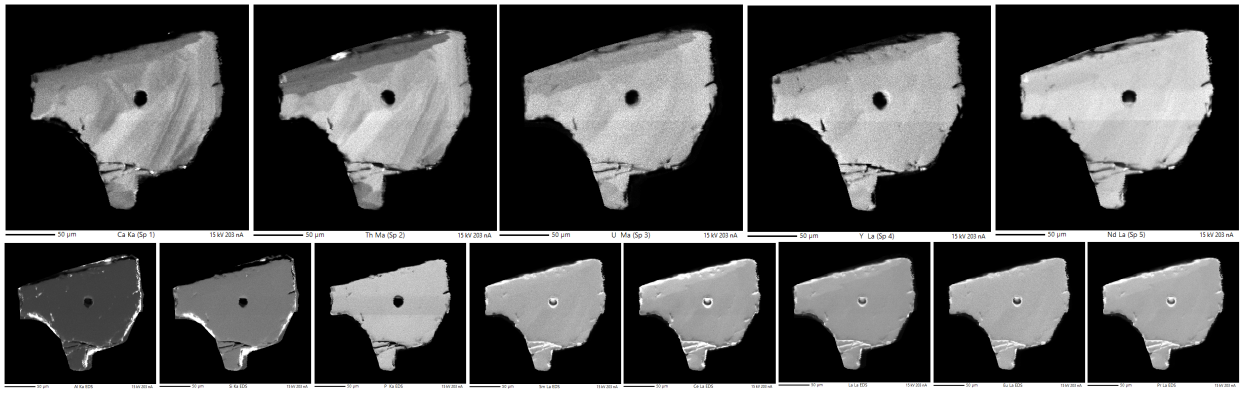

FB14 Grain 24 (WDS and EDS maps)

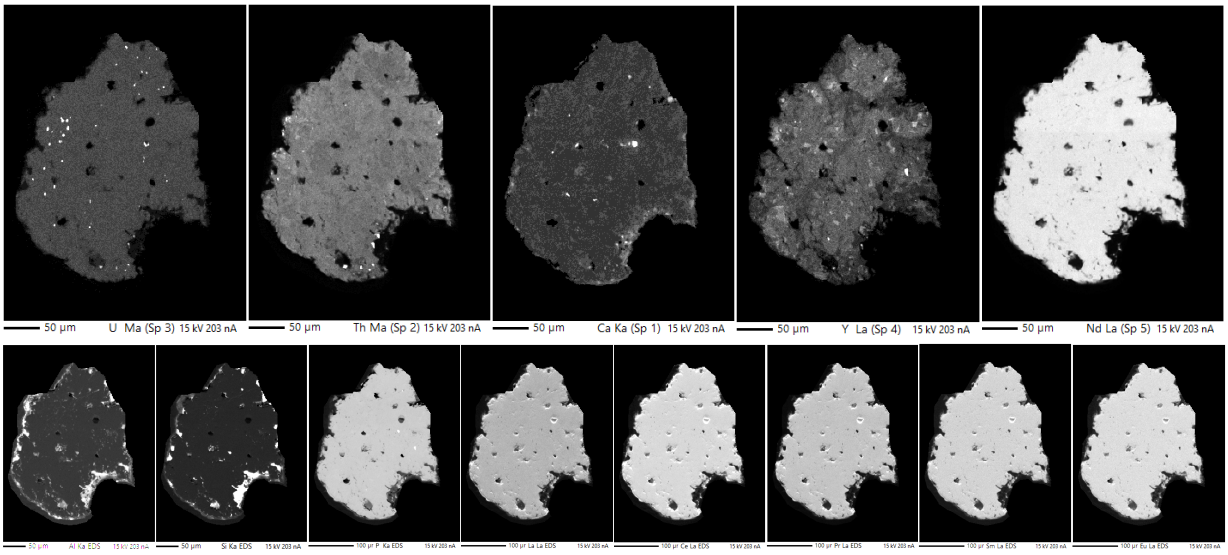

FB5 Grain 2 (WDS and EDS maps)

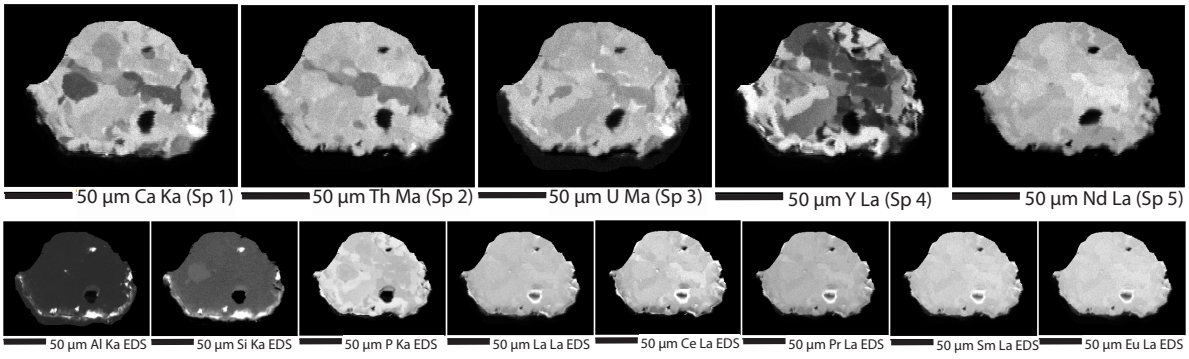

Table S1. Detrital monazite U-Th-Pb data LASS-ICP-MS
Table S2. Detrital monazite Nd isotopic data LASS-ICP-MS
Table S3. Detrital monazite REE data LASS-ICP-MS

Table S1:

Sample	U ppm	Th ppm	207Pb/235U	2s	206Pb/238U	2s	238U/206Pb	2s	207Pb/206Pb	2s	208Pb/232Th	2s	Best Age (Ma)	2s
01-TN-02A_1	2184	34000	1.882	0.07	0.182	0.01	5.485	0.18	0.075	0.00	0.057	0.00	1080.37	35.14
01-TN-02A_17	8280	27200	0.441	0.01	0.060	0.00	16.748	0.36	0.054	0.00	0.020	0.00	373.92	7.92
01-TN-02A_2	6670	23200	1.845	0.06	0.175	0.01	5.708	0.19	0.077	0.00	0.057	0.00	1036.81	33.67
01-TN-02A_21	2570	28200	0.574	0.02	0.071	0.00	14.136	0.33	0.059	0.00	0.023	0.00	438.90	9.99
01-TN-02A_25	3210	27800	0.666	0.03	0.075	0.00	13.298	0.30	0.064	0.00	0.025	0.00	463.11	10.42
01-TN-02A_29	6680	46560	0.460	0.01	0.061	0.00	16.434	0.36	0.055	0.00	0.020	0.00	380.48	8.13
01-TN-02A_3	2070	35800	0.556	0.02	0.072	0.00	13.966	0.43	0.056	0.00	0.023	0.00	445.53	13.58
01-TN-02A_30	4440	34500	0.468	0.01	0.061	0.00	16.423	0.36	0.056	0.00	0.020	0.00	380.30	8.27
01-TN-02A_31	5870	62400	1.815	0.04	0.177	0.00	5.663	0.13	0.075	0.00	0.055	0.00	1047.55	23.13
01-TN-02A_36	286	39700	1.814	0.09	0.176	0.01	5.675	0.26	0.075	0.00	0.057	0.00	1045.35	46.22
01-TN-02A_44	1186	54200	1.847	0.06	0.180	0.01	5.546	0.15	0.074	0.00	0.055	0.00	1070.20	28.97
01-TN-02A_49	2700	32780	2.140	0.05	0.198	0.00	5.063	0.12	0.078	0.00	0.062	0.00	1162.99	26.49
01-TN-02A_51	439	2630	0.662	0.03	0.076	0.00	13.175	0.51	0.063	0.00	0.026	0.00	467.80	17.79
01-TN04_1	4440	29070	0.453	0.01	0.059	0.00	16.872	0.42	0.056	0.00	0.020	0.00	370.29	9.05
01-TN04_18	6680	40500	1.718	0.05	0.172	0.00	5.807	0.16	0.072	0.00	0.055	0.00	1025.50	27.97
01-TN04_2	729	10800	0.512	0.03	0.066	0.00	15.152	0.51	0.056	0.00	0.023	0.00	411.49	13.71
01-TN05_12	2200	1648	0.487	0.02	0.065	0.00	15.352	0.36	0.054	0.00	0.023	0.00	407.01	9.37
01-TN05_19	4940	53200	0.615	0.02	0.078	0.00	12.821	0.32	0.056	0.00	0.026	0.00	484.45	11.99
01-TN05_2	1960	41900	0.481	0.02	0.064	0.00	15.601	0.46	0.054	0.00	0.021	0.00	401.02	11.69
01-TN05_28	2860	41700	0.498	0.02	0.066	0.00	15.060	0.39	0.054	0.00	0.022	0.00	414.82	10.60
01-TN05_29	2537	29550	0.578	0.02	0.075	0.00	13.280	0.35	0.056	0.00	0.025	0.00	468.10	12.14
01-TN05_3	11110	32800	0.496	0.01	0.065	0.00	15.373	0.35	0.055	0.00	0.022	0.00	406.24	9.22
01-TN05_31	1175	47500	0.523	0.02	0.068	0.00	14.706	0.42	0.056	0.00	0.022	0.00	423.61	11.99
01-TN05_32	747	22430	0.542	0.02	0.068	0.00	14.771	0.42	0.059	0.00	0.022	0.00	420.35	11.92
01-TN05_36	7860	28080	0.461	0.01	0.061	0.00	16.439	0.41	0.055	0.00	0.020	0.00	380.43	9.35
01-TN05_37	8550	27000	1.708	0.04	0.169	0.00	5.928	0.15	0.073	0.00	0.056	0.00	1004.53	24.63
01-TN05_38	5590	33640	1.770	0.05	0.175	0.00	5.731	0.13	0.073	0.00	0.056	0.00	1037.32	23.54
01-TN05_42	3560	17230	1.828	0.05	0.176	0.00	5.688	0.14	0.075	0.00	0.057	0.00	1042.33	25.19

Table S1. Detrital monazite U-Th-Pb data LASS-ICP-MS
Table S2. Detrital monazite Nd isotopic data LASS-ICP-MS
Table S3. Detrital monazite REE data LASS-ICP-MS

01-TN05_44	2782	43100	0.547	0.01	0.071	0.00	14.184	0.37	0.057	0.00	0.023	0.00	438.53	11.31
01-TN05_45	500	31460	0.593	0.03	0.076	0.00	13.210	0.54	0.056	0.00	0.025	0.00	470.79	18.88
01-TN05_5	3390	71200	0.519	0.01	0.068	0.00	14.789	0.35	0.056	0.00	0.022	0.00	421.62	9.86
01-TN05_9	10110	13810	0.579	0.02	0.074	0.00	13.477	0.35	0.057	0.00	0.025	0.00	461.06	11.63
5-1-2_small_34	756	3650	0.695	0.04	0.081	0.00	12.346	0.44	0.062	0.00	0.029	0.00	498.85	17.51
AsheGneiss_1	5680	22420	0.545	0.02	0.071	0.00	13.988	0.32	0.056	0.00	0.024	0.00	445.26	10.00
AsheGneiss_10	3430	16260	0.562	0.02	0.075	0.00	13.382	0.31	0.056	0.00	0.024	0.00	464.83	10.51
AsheGneiss_11	1730	23800	0.573	0.02	0.074	0.00	13.569	0.35	0.057	0.00	0.024	0.00	457.92	11.61
AsheGneiss_12	3830	15390	0.571	0.02	0.074	0.00	13.441	0.35	0.056	0.00	0.025	0.00	462.89	11.68
AsheGneiss_2	6760	31000	0.557	0.01	0.071	0.00	14.019	0.33	0.057	0.00	0.024	0.00	443.41	10.11
AsheGneiss_3	4130	16860	0.547	0.02	0.071	0.00	14.065	0.37	0.056	0.00	0.024	0.00	442.56	11.37
AsheGneiss_4	3500	22500	0.552	0.02	0.072	0.00	13.812	0.38	0.056	0.00	0.024	0.00	450.70	12.31
AsheGneiss_5	5170	16020	0.556	0.02	0.072	0.00	13.947	0.36	0.056	0.00	0.024	0.00	446.28	11.43
AsheGneiss_6	5020	21400	0.545	0.01	0.071	0.00	14.104	0.40	0.056	0.00	0.024	0.00	441.44	12.18
AsheGneiss_7	3270	17760	0.563	0.02	0.073	0.00	13.661	0.34	0.056	0.00	0.024	0.00	455.61	11.19
AsheGneiss_8	2310	22500	0.582	0.02	0.074	0.00	13.477	0.36	0.057	0.00	0.024	0.00	460.85	12.03
AsheGneiss_9	6360	22900	0.565	0.02	0.073	0.00	13.699	0.39	0.056	0.00	0.024	0.00	454.15	12.78
AsheSchist-newrow_1	5820	25890	0.565	0.01	0.073	0.00	13.780	0.33	0.056	0.00	0.024	0.00	451.34	10.53
AsheSchist-newrow_10	7180	26000	0.550	0.01	0.071	0.00	14.124	0.37	0.056	0.00	0.024	0.00	440.68	11.34
AsheSchist-newrow_11	4760	23600	0.571	0.02	0.073	0.00	13.643	0.38	0.057	0.00	0.024	0.00	455.76	12.37
AsheSchist-newrow_2	5350	20990	0.551	0.02	0.071	0.00	14.104	0.36	0.056	0.00	0.023	0.00	441.30	10.97
AsheSchist-newrow_3	6180	21000	0.557	0.01	0.072	0.00	13.812	0.36	0.056	0.00	0.024	0.00	450.79	11.49
AsheSchist-newrow_4	5400	21060	0.558	0.01	0.072	0.00	13.986	0.34	0.056	0.00	0.024	0.00	444.81	10.66
AsheSchist-newrow_5	6460	28100	0.560	0.02	0.071	0.00	14.045	0.38	0.057	0.00	0.024	0.00	442.85	11.77
AsheSchist-newrow_6	5480	25000	0.558	0.01	0.071	0.00	14.025	0.38	0.056	0.00	0.024	0.00	443.85	11.80
AsheSchist-newrow_7	6590	24500	0.551	0.02	0.071	0.00	14.164	0.40	0.056	0.00	0.024	0.00	439.54	12.15
AsheSchist-newrow_8	5790	25500	0.558	0.01	0.071	0.00	14.025	0.35	0.056	0.00	0.024	0.00	443.78	11.01
AsheSchist-newrow_9	6600	24740	0.560	0.02	0.071	0.00	14.047	0.34	0.057	0.00	0.024	0.00	442.76	10.46
Carter512A_a_1	4440	19720	1.814	0.04	0.176	0.00	5.679	0.13	0.075	0.00	0.058	0.00	1044.95	23.36
Carter512A_a_11	2900	11710	1.951	0.05	0.183	0.00	5.459	0.13	0.078	0.00	0.056	0.00	1081.72	24.85
Carter512A_a_12	6050	30400	2.096	0.05	0.194	0.00	5.144	0.13	0.079	0.00	0.060	0.00	1144.01	27.43

Table S1. Detrital monazite U-Th-Pb data LASS-ICP-MS
Table S2. Detrital monazite Nd isotopic data LASS-ICP-MS
Table S3. Detrital monazite REE data LASS-ICP-MS

Carter512A_a_14	2650	32900	1.897	0.05	0.180	0.00	5.559	0.15	0.077	0.00	0.058	0.00	1064.15	27.67
Carter512A_a_15	2800	32900	1.913	0.05	0.182	0.00	5.507	0.14	0.077	0.00	0.059	0.00	1073.96	26.36
Carter512A_a_2	418	49700	1.831	0.09	0.174	0.01	5.747	0.23	0.075	0.00	0.056	0.00	1032.18	39.47
Carter512A_a_5	11900	31000	1.894	0.09	0.178	0.01	5.605	0.28	0.077	0.00	0.053	0.00	1054.39	50.71
Carter512A_a_6	18400	30100	1.881	0.05	0.177	0.00	5.659	0.14	0.077	0.00	0.058	0.00	1044.88	25.21
Carter512A_a_7	18200	31300	1.868	0.04	0.176	0.00	5.669	0.13	0.077	0.00	0.058	0.00	1043.58	23.62
Carter512A_a_8	1588	43100	1.798	0.05	0.174	0.00	5.734	0.15	0.075	0.00	0.056	0.00	1035.34	26.54
Carter512A_a_9	3340	7720	1.822	0.05	0.178	0.00	5.609	0.13	0.075	0.00	0.059	0.00	1057.66	23.05
Carter512A_a_large_1	2700	36200	1.850	0.13	0.166	0.01	6.042	0.33	0.083	0.00	0.052	0.00	973.93	52.10
Carter512A_a_large_3	483	900	0.670	0.06	0.083	0.00	11.990	0.49	0.060	0.01	0.028	0.00	515.18	21.03
Carter512A_a_large_4	1433	45700	2.185	0.06	0.204	0.01	4.912	0.13	0.079	0.00	0.063	0.00	1195.27	29.97
Carter512A_a_large_5	1760	30200	2.120	0.12	0.192	0.01	5.200	0.19	0.080	0.00	0.061	0.00	1130.48	40.74
Carter512A_a_large_6	2079	28900	2.108	0.05	0.197	0.00	5.076	0.12	0.080	0.00	0.062	0.00	1157.41	25.55
Carter512A_b_1	8060	30200	2.019	0.05	0.187	0.00	5.362	0.13	0.079	0.00	0.060	0.00	1099.01	26.05
Carter512A_b_10	903	55400	1.914	0.07	0.179	0.00	5.574	0.15	0.077	0.00	0.056	0.00	1060.75	26.92
Carter512A_b_11	1103	30800	1.878	0.06	0.180	0.01	5.568	0.17	0.075	0.00	0.058	0.00	1064.62	31.80
Carter512A_b_13	1891	29100	1.792	0.06	0.174	0.00	5.764	0.15	0.074	0.00	0.057	0.00	1030.52	26.47
Carter512A_b_15	2160	23510	2.184	0.07	0.194	0.01	5.144	0.15	0.081	0.00	0.062	0.00	1141.11	31.45
Carter512A_b_17	563	5650	1.956	0.10	0.167	0.01	5.977	0.20	0.084	0.00	0.052	0.00	982.41	32.65
Carter512A_b_18	7960	29600	1.703	0.04	0.168	0.00	5.942	0.15	0.073	0.00	0.055	0.00	1002.40	23.92
Carter512A_b_2	2760	49400	1.820	0.04	0.173	0.00	5.767	0.13	0.076	0.00	0.056	0.00	1028.20	23.09
Carter512A_b_5	4700	37200	1.943	0.08	0.181	0.01	5.540	0.19	0.078	0.00	0.054	0.00	1065.82	36.29
Carter512A_b_6	2420	14000	1.882	0.05	0.176	0.00	5.679	0.15	0.078	0.00	0.059	0.00	1040.52	25.86
Carter512A_b_7	1180	14800	1.230	0.21	0.122	0.02	8.197	1.02	0.070	0.00	0.033	0.00	736.10	89.15
Carter512A_b_9	2970	30900	2.242	0.10	0.181	0.01	5.528	0.18	0.090	0.00	0.047	0.00	1052.27	34.10
Carter512A_b_large_2	3830	30600	2.217	0.06	0.204	0.01	4.892	0.13	0.080	0.00	0.065	0.00	1198.70	31.08
Carter512A_b_large_3	10050	23870	1.789	0.05	0.175	0.00	5.718	0.15	0.076	0.00	0.055	0.00	1036.12	26.52
Carter512A_b_large_5	2080	33200	1.928	0.07	0.184	0.01	5.426	0.16	0.077	0.00	0.059	0.00	1088.79	31.64
FB1_1	2670	23230	0.589	0.02	0.074	0.00	13.459	0.38	0.057	0.00	0.025	0.00	461.59	12.87
FB1_10	8660	27700	0.566	0.02	0.074	0.00	13.605	0.40	0.056	0.00	0.025	0.00	457.32	13.26
FB1_11	4010	20400	0.586	0.02	0.075	0.00	13.423	0.34	0.057	0.00	0.025	0.00	462.74	11.66

Table S1. Detrital monazite U-Th-Pb data LASS-ICP-MS
Table S2. Detrital monazite Nd isotopic data LASS-ICP-MS
Table S3. Detrital monazite REE data LASS-ICP-MS

FB1_12	6600	28300	0.595	0.03	0.074	0.00	13.514	0.41	0.058	0.00	0.025	0.00	458.99	13.78
FB1_13	3070	24950	0.574	0.02	0.074	0.00	13.441	0.37	0.057	0.00	0.024	0.00	462.45	12.46
FB1_15	4750	31200	0.578	0.02	0.074	0.00	13.569	0.37	0.057	0.00	0.024	0.00	458.06	12.40
FB1_16	4722	18360	0.568	0.02	0.073	0.00	13.643	0.36	0.056	0.00	0.024	0.00	455.80	11.96
FB1_17	672	35300	0.570	0.03	0.073	0.00	13.661	0.40	0.056	0.00	0.023	0.00	455.34	13.28
FB1_18	720	33700	0.598	0.03	0.073	0.00	13.624	0.51	0.057	0.00	0.024	0.00	455.98	16.64
FB1_19	1280	28700	0.553	0.02	0.071	0.00	14.085	0.49	0.057	0.00	0.024	0.00	441.31	14.97
FB1_2	1650	42700	0.420	0.02	0.055	0.00	18.182	0.54	0.055	0.00	0.018	0.00	344.49	10.07
FB1_20	2433	25340	0.563	0.02	0.070	0.00	14.306	0.48	0.059	0.00	0.023	0.00	433.87	14.38
FB1_21	3460	23040	0.562	0.02	0.072	0.00	13.947	0.35	0.057	0.00	0.024	0.00	445.52	11.04
FB1_23	3010	56600	0.413	0.01	0.053	0.00	18.907	0.49	0.057	0.00	0.017	0.00	330.69	8.41
FB1_26	3670	63600	0.382	0.01	0.053	0.00	18.950	0.50	0.053	0.00	0.017	0.00	331.41	8.68
FB1_27	5040	68800	0.376	0.01	0.052	0.00	19.346	0.47	0.053	0.00	0.017	0.00	324.83	7.78
FB1_29	1320	35060	0.598	0.02	0.073	0.00	13.793	0.38	0.059	0.00	0.024	0.00	449.43	12.29
FB1_3	3580	25270	0.569	0.02	0.073	0.00	13.643	0.35	0.056	0.00	0.025	0.00	455.95	11.57
FB1_30	2740	29700	0.548	0.02	0.072	0.00	13.908	0.37	0.056	0.00	0.024	0.00	447.75	11.86
FB1_31	2770	16400	0.668	0.02	0.076	0.00	13.193	0.41	0.064	0.00	0.024	0.00	466.55	14.22
FB1_32	479	29500	0.520	0.03	0.064	0.00	15.576	0.68	0.059	0.00	0.021	0.00	399.06	17.19
FB1_33	2720	35700	0.568	0.02	0.072	0.00	13.850	0.35	0.057	0.00	0.024	0.00	448.73	11.09
FB1_4	1081	56400	0.633	0.02	0.081	0.00	12.376	0.41	0.057	0.00	0.026	0.00	500.99	16.10
FB1_6	1290	20500	0.645	0.02	0.077	0.00	13.021	0.34	0.061	0.00	0.026	0.00	474.49	12.23
FB1_7	3400	23920	0.500	0.04	0.064	0.00	15.601	1.19	0.056	0.00	0.021	0.00	399.93	29.84
FB1_8	3780	30600	0.572	0.02	0.073	0.00	13.624	0.35	0.056	0.00	0.025	0.00	456.78	11.59
FB1_9	3590	17300	0.574	0.02	0.074	0.00	13.569	0.47	0.057	0.00	0.025	0.00	458.06	15.63
FB10_1	3490	105500	1.751	0.05	0.172	0.00	5.817	0.15	0.074	0.00	0.053	0.00	1021.31	24.88
FB10_10	3650	36800	0.574	0.02	0.075	0.00	13.387	0.39	0.056	0.00	0.025	0.00	464.74	13.36
FB10_11	3010	25700	0.543	0.03	0.070	0.00	14.245	0.60	0.056	0.00	0.022	0.00	437.24	18.05
FB10_12	1955	26750	0.580	0.02	0.074	0.00	13.605	0.42	0.057	0.00	0.024	0.00	456.65	13.71
FB10_13	1517	31100	0.564	0.02	0.073	0.00	13.661	0.43	0.056	0.00	0.024	0.00	455.51	14.17
FB10_14	3610	16280	0.569	0.02	0.074	0.00	13.581	0.32	0.056	0.00	0.025	0.00	458.10	10.51
FB10_16	7660	28600	0.604	0.02	0.075	0.00	13.316	0.36	0.058	0.00	0.025	0.00	465.56	12.49

Table S1. Detrital monazite U-Th-Pb data LASS-ICP-MS
Table S2. Detrital monazite Nd isotopic data LASS-ICP-MS
Table S3. Detrital monazite REE data LASS-ICP-MS

FB10_17	7230	23200	0.569	0.01	0.074	0.00	13.514	0.36	0.056	0.00	0.025	0.00	460.42	12.02
FB10_18	6500	23800	0.572	0.02	0.074	0.00	13.514	0.36	0.056	0.00	0.024	0.00	460.27	12.02
FB10_19	1017	18430	2.783	0.09	0.228	0.01	4.382	0.12	0.088	0.00	0.070	0.00	1321.48	35.12
FB10_2	7910	23300	0.559	0.01	0.072	0.00	13.947	0.40	0.056	0.00	0.025	0.00	446.15	12.67
FB10_20	6630	55600	1.788	0.05	0.174	0.00	5.741	0.15	0.074	0.00	0.054	0.00	1035.32	26.91
FB10_21	5920	43500	0.571	0.02	0.073	0.00	13.680	0.39	0.056	0.00	0.024	0.00	454.64	12.78
FB10_22	1535	37600	0.576	0.02	0.073	0.00	13.643	0.38	0.057	0.00	0.024	0.00	455.72	12.37
FB10_23	2174	37100	1.534	0.05	0.157	0.01	6.373	0.20	0.071	0.00	0.045	0.00	938.80	29.08
FB10_24	1472	43700	0.604	0.02	0.076	0.00	13.175	0.38	0.057	0.00	0.023	0.00	471.12	13.44
FB10_25	506	30200	0.591	0.03	0.077	0.00	13.038	0.50	0.057	0.00	0.024	0.00	475.98	17.90
FB10_26	3600	21700	0.553	0.01	0.074	0.00	13.514	0.37	0.055	0.00	0.024	0.00	461.19	12.46
FB10_27	861	23380	0.617	0.02	0.076	0.00	13.193	0.44	0.059	0.00	0.024	0.00	469.63	15.27
FB10_28	5340	18390	0.569	0.02	0.074	0.00	13.459	0.36	0.055	0.00	0.025	0.00	462.57	12.06
FB10_29	1725	32300	0.642	0.02	0.076	0.00	13.245	0.35	0.061	0.00	0.024	0.00	466.81	12.11
FB10_3	5860	22740	0.600	0.02	0.075	0.00	13.423	0.41	0.058	0.00	0.025	0.00	462.26	13.76
FB10_30	658	29100	0.595	0.03	0.076	0.00	13.245	0.47	0.057	0.00	0.024	0.00	468.69	16.28
FB10_31	5700	18900	0.579	0.02	0.074	0.00	13.532	0.41	0.056	0.00	0.024	0.00	459.51	13.74
FB10_32	268	28000	0.651	0.04	0.078	0.00	12.837	0.49	0.060	0.00	0.024	0.00	481.87	17.97
FB10_33	7570	24330	0.560	0.02	0.073	0.00	13.717	0.41	0.056	0.00	0.024	0.00	453.89	13.22
FB10_34	7020	40770	0.571	0.02	0.075	0.00	13.369	0.42	0.055	0.00	0.024	0.00	465.70	14.28
FB10_35	4590	24900	0.570	0.02	0.074	0.00	13.477	0.36	0.055	0.00	0.024	0.00	461.91	12.05
FB10_36	990	57500	0.586	0.02	0.073	0.00	13.680	0.39	0.058	0.00	0.024	0.00	453.70	12.80
FB10_37	519	49100	0.616	0.03	0.075	0.00	13.333	0.50	0.060	0.00	0.024	0.00	464.31	17.21
FB10_4	2062	42500	0.573	0.02	0.074	0.00	13.550	0.36	0.056	0.00	0.024	0.00	458.93	12.01
FB10_5	2860	41100	1.756	0.05	0.176	0.00	5.692	0.16	0.074	0.00	0.056	0.00	1044.08	28.21
FB10_6	6140	20560	0.558	0.02	0.073	0.00	13.736	0.37	0.056	0.00	0.025	0.00	453.24	11.93
FB10_8	663	48300	1.937	0.08	0.188	0.01	5.333	0.20	0.075	0.00	0.057	0.00	1109.78	41.16
FB11_1	1115	57400	0.632	0.02	0.080	0.00	12.531	0.33	0.058	0.00	0.026	0.00	494.67	12.91
FB11_10	8190	43800	0.562	0.01	0.073	0.00	13.663	0.30	0.056	0.00	0.024	0.00	455.62	9.67
FB11_11	5530	26700	0.555	0.01	0.073	0.00	13.725	0.31	0.056	0.00	0.024	0.00	453.46	9.99
FB11_12	5440	17100	0.580	0.01	0.074	0.00	13.466	0.30	0.057	0.00	0.025	0.00	461.25	10.04

Table S1. Detrital monazite U-Th-Pb data LASS-ICP-MS
Table S2. Detrital monazite Nd isotopic data LASS-ICP-MS
Table S3. Detrital monazite REE data LASS-ICP-MS

FB11_13	5890	22900	0.579	0.01	0.075	0.00	13.405	0.30	0.056	0.00	0.025	0.00	463.75	10.17
FB11_14	2960	36300	0.570	0.01	0.074	0.00	13.548	0.29	0.056	0.00	0.024	0.00	459.19	9.68
FB11_15	3270	19530	0.571	0.02	0.074	0.00	13.546	0.32	0.057	0.00	0.024	0.00	458.94	10.60
FB11_16	3760	21200	0.572	0.01	0.075	0.00	13.423	0.33	0.056	0.00	0.024	0.00	463.42	11.31
FB11_17	4020	48000	0.564	0.02	0.074	0.00	13.576	0.30	0.055	0.00	0.024	0.00	458.58	10.03
FB11_18	3310	26600	0.566	0.02	0.074	0.00	13.495	0.34	0.056	0.00	0.024	0.00	460.86	11.27
FB11_19	2780	76400	1.680	0.04	0.169	0.00	5.935	0.14	0.073	0.00	0.052	0.00	1003.00	22.40
FB11_2	1135	58200	0.640	0.02	0.081	0.00	12.407	0.30	0.058	0.00	0.026	0.00	499.52	11.89
FB11_20	4150	23620	0.590	0.02	0.075	0.00	13.250	0.28	0.057	0.00	0.024	0.00	468.89	9.71
FB11_21	1402	42200	1.849	0.05	0.180	0.00	5.571	0.14	0.075	0.00	0.055	0.00	1064.53	25.57
FB11_22	643	30100	0.593	0.03	0.075	0.00	13.298	0.35	0.057	0.00	0.024	0.00	466.93	12.15
FB11_23	741	30800	0.571	0.02	0.073	0.00	13.717	0.38	0.057	0.00	0.024	0.00	453.17	12.38
FB11_24	5190	32800	0.571	0.01	0.074	0.00	13.439	0.31	0.056	0.00	0.024	0.00	462.98	10.53
FB11_25	7230	31800	0.575	0.01	0.074	0.00	13.441	0.32	0.056	0.00	0.024	0.00	462.70	10.81
FB11_26	5350	21410	0.570	0.01	0.074	0.00	13.535	0.30	0.056	0.00	0.024	0.00	459.71	9.89
FB11_27	7680	32100	0.568	0.01	0.074	0.00	13.545	0.31	0.056	0.00	0.024	0.00	459.07	10.17
FB11_28	7130	28130	0.583	0.02	0.075	0.00	13.389	0.32	0.057	0.00	0.024	0.00	464.17	10.86
FB11_3	1173	39100	0.565	0.02	0.073	0.00	13.717	0.33	0.057	0.00	0.024	0.00	453.28	10.83
FB11_4	6540	22390	0.571	0.01	0.074	0.00	13.517	0.30	0.056	0.00	0.025	0.00	460.08	10.13
FB11_5	8150	27700	0.585	0.01	0.075	0.00	13.396	0.30	0.057	0.00	0.024	0.00	463.60	10.11
FB11_6	6060	17260	0.588	0.01	0.074	0.00	13.508	0.31	0.058	0.00	0.025	0.00	459.62	10.23
FB11_7	4630	21200	0.582	0.02	0.075	0.00	13.414	0.30	0.057	0.00	0.025	0.00	463.30	10.03
FB11_8	3590	30900	0.576	0.01	0.074	0.00	13.452	0.30	0.057	0.00	0.024	0.00	461.95	10.19
FB11_9	4990	14220	0.591	0.01	0.074	0.00	13.550	0.31	0.058	0.00	0.025	0.00	457.96	10.32
FB13_1	3120	76600	1.717	0.05	0.168	0.00	5.952	0.17	0.073	0.00	0.052	0.00	1000.13	27.22
FB13_10	1627	48100	0.541	0.02	0.067	0.00	14.970	0.45	0.059	0.00	0.022	0.00	414.92	12.28
FB13_11	6190	31010	0.565	0.02	0.073	0.00	13.791	0.33	0.056	0.00	0.024	0.00	451.26	10.59
FB13_12	10490	5690	0.575	0.01	0.074	0.00	13.532	0.33	0.056	0.00	0.025	0.00	459.54	10.89
FB13_13	1687	27510	0.563	0.02	0.072	0.00	13.908	0.48	0.056	0.00	0.024	0.00	447.52	15.05
FB13_16	4140	24860	0.570	0.02	0.072	0.00	13.889	0.34	0.056	0.00	0.024	0.00	447.91	10.71
FB13_17	8810	37600	0.555	0.02	0.072	0.00	13.908	0.37	0.055	0.00	0.024	0.00	447.83	11.85

Table S1. Detrital monazite U-Th-Pb data LASS-ICP-MS
Table S2. Detrital monazite Nd isotopic data LASS-ICP-MS
Table S3. Detrital monazite REE data LASS-ICP-MS

FB13_2	6240	24070	0.583	0.02	0.074	0.00	13.514	0.45	0.057	0.00	0.025	0.00	459.94	15.16
FB13_3	4730	11800	0.572	0.02	0.074	0.00	13.459	0.38	0.055	0.00	0.026	0.00	462.51	12.89
FB13_4	11010	6890	0.566	0.02	0.073	0.00	13.661	0.39	0.056	0.00	0.024	0.00	455.39	12.79
FB13_5	1612	44800	0.575	0.02	0.073	0.00	13.624	0.42	0.057	0.00	0.024	0.00	456.09	13.71
FB13_7	3880	23900	0.560	0.02	0.073	0.00	13.680	0.54	0.056	0.00	0.024	0.00	454.95	17.67
FB13_8	5770	23450	0.574	0.02	0.074	0.00	13.587	0.38	0.056	0.00	0.024	0.00	457.69	12.40
FB14_1	1161	31800	0.553	0.02	0.071	0.00	14.045	0.42	0.056	0.00	0.024	0.00	443.03	13.09
FB14_10	360	28400	0.579	0.03	0.075	0.00	13.423	0.62	0.056	0.00	0.024	0.00	463.14	21.00
FB14_11	6170	20020	0.576	0.02	0.075	0.00	13.316	0.35	0.056	0.00	0.025	0.00	467.28	12.13
FB14_12	5480	23200	0.575	0.02	0.075	0.00	13.387	0.39	0.056	0.00	0.024	0.00	464.86	13.36
FB14_13	828	34800	0.569	0.03	0.074	0.00	13.495	0.45	0.056	0.00	0.024	0.00	460.88	15.20
FB14_14	499	23630	0.608	0.04	0.073	0.00	13.736	0.51	0.060	0.00	0.024	0.00	450.51	16.59
FB14_15	752	25600	0.551	0.02	0.071	0.00	14.025	0.42	0.055	0.00	0.024	0.00	444.20	13.12
FB14_17	6170	24710	0.566	0.02	0.074	0.00	13.550	0.41	0.056	0.00	0.024	0.00	459.37	13.74
FB14_18	2370	61100	1.916	0.06	0.182	0.01	5.485	0.16	0.075	0.00	0.057	0.00	1080.29	30.72
FB14_19	3920	37900	0.562	0.02	0.074	0.00	13.604	0.32	0.055	0.00	0.024	0.00	457.84	10.48
FB14_2	3030	26260	0.564	0.02	0.073	0.00	13.717	0.41	0.056	0.00	0.024	0.00	453.79	13.23
FB14_20	5430	25790	0.554	0.02	0.072	0.00	13.850	0.40	0.056	0.00	0.024	0.00	449.60	12.73
FB14_21	6040	22700	0.561	0.01	0.074	0.00	13.550	0.36	0.055	0.00	0.024	0.00	459.53	12.02
FB14_22	1479	75700	0.573	0.02	0.073	0.00	13.699	0.41	0.056	0.00	0.023	0.00	454.17	13.25
FB14_23	2670	20000	0.568	0.02	0.074	0.00	13.587	0.34	0.056	0.00	0.024	0.00	457.84	11.23
FB14_24	232	17070	0.420	0.05	0.058	0.00	17.391	1.00	0.055	0.01	0.018	0.00	359.97	20.51
FB14_25	4600	32100	0.561	0.01	0.073	0.00	13.643	0.34	0.055	0.00	0.024	0.00	456.48	11.20
FB14_26	7250	30300	1.797	0.05	0.175	0.00	5.714	0.15	0.075	0.00	0.055	0.00	1038.16	26.56
FB14_27	658	37900	0.544	0.03	0.073	0.00	13.699	0.51	0.055	0.00	0.023	0.00	455.09	16.68
FB14_28	2550	32800	0.577	0.02	0.074	0.00	13.569	0.34	0.056	0.00	0.024	0.00	458.35	11.23
FB14_29	1888	24890	1.792	0.05	0.176	0.00	5.685	0.15	0.074	0.00	0.055	0.00	1045.31	27.45
FB14_3	2154	38900	0.575	0.02	0.073	0.00	13.699	0.38	0.057	0.00	0.024	0.00	453.60	12.34
FB14_4	7840	26400	0.566	0.02	0.073	0.00	13.699	0.37	0.056	0.00	0.024	0.00	454.22	11.94
FB14_5	3440	40200	0.578	0.02	0.074	0.00	13.495	0.40	0.057	0.00	0.024	0.00	460.55	13.30
FB14_6	9190	39200	0.562	0.01	0.073	0.00	13.699	0.35	0.056	0.00	0.024	0.00	454.33	11.54

Table S1. Detrital monazite U-Th-Pb data LASS-ICP-MS
Table S2. Detrital monazite Nd isotopic data LASS-ICP-MS
Table S3. Detrital monazite REE data LASS-ICP-MS

FB14_7	1038	34200	0.599	0.03	0.074	0.00	13.605	0.44	0.059	0.00	0.023	0.00	455.67	14.69
FB14_8	6150	21260	0.565	0.02	0.073	0.00	13.699	0.42	0.056	0.00	0.024	0.00	454.32	13.68
FB14_9	3790	46700	0.564	0.02	0.073	0.00	13.643	0.35	0.055	0.00	0.024	0.00	456.57	11.58
FB15_1	4440	26140	0.575	0.02	0.074	0.00	13.441	0.32	0.056	0.00	0.025	0.00	462.70	10.94
FB15_10	6660	24600	0.583	0.01	0.075	0.00	13.287	0.31	0.057	0.00	0.025	0.00	467.64	10.60
FB15_11	5680	19700	0.594	0.02	0.075	0.00	13.387	0.31	0.058	0.00	0.025	0.00	463.33	10.68
FB15_12	6450	17040	0.579	0.01	0.075	0.00	13.337	0.29	0.056	0.00	0.025	0.00	466.26	9.95
FB15_13	8280	29440	0.583	0.01	0.075	0.00	13.396	0.29	0.057	0.00	0.024	0.00	463.89	9.98
FB15_14	1740	31600	0.575	0.02	0.074	0.00	13.569	0.34	0.057	0.00	0.024	0.00	457.81	11.23
FB15_15	8270	31900	0.583	0.01	0.073	0.00	13.624	0.32	0.058	0.00	0.024	0.00	455.67	10.60
FB15_16	3320	25390	0.572	0.02	0.074	0.00	13.519	0.32	0.057	0.00	0.024	0.00	459.85	10.61
FB15_17	2420	84500	0.403	0.01	0.054	0.00	18.399	0.44	0.054	0.00	0.017	0.00	340.68	7.99
FB15_18	5370	24300	0.570	0.01	0.074	0.00	13.556	0.31	0.056	0.00	0.024	0.00	458.83	10.46
FB15_19	3030	20600	0.626	0.02	0.076	0.00	13.106	0.33	0.059	0.00	0.026	0.00	472.25	11.79
FB15_20	10610	28500	0.575	0.01	0.074	0.00	13.428	0.29	0.057	0.00	0.024	0.00	462.83	9.84
FB15_21	5540	26900	0.574	0.01	0.075	0.00	13.407	0.29	0.056	0.00	0.024	0.00	463.78	9.89
FB15_22	7170	23300	0.595	0.02	0.076	0.00	13.228	0.30	0.058	0.00	0.024	0.00	469.11	10.48
FB15_23	1990	39900	0.591	0.02	0.076	0.00	13.245	0.35	0.057	0.00	0.024	0.00	468.81	12.15
FB15_24	10790	40900	0.573	0.02	0.074	0.00	13.569	0.37	0.057	0.00	0.024	0.00	457.93	12.39
FB15_25	2530	35300	0.547	0.01	0.074	0.00	13.552	0.33	0.054	0.00	0.023	0.00	459.98	10.88
FB15_26	3750	35700	0.558	0.01	0.073	0.00	13.644	0.31	0.056	0.00	0.024	0.00	456.19	10.33
FB15_29	6480	25400	0.597	0.01	0.076	0.00	13.175	0.32	0.058	0.00	0.024	0.00	471.00	11.07
FB15_3	2510	20000	0.554	0.03	0.073	0.00	13.680	0.59	0.056	0.00	0.023	0.00	454.79	19.27
FB15_30	4530	27160	0.581	0.02	0.075	0.00	13.405	0.32	0.057	0.00	0.024	0.00	463.55	10.96
FB15_31	1549	27400	0.595	0.02	0.075	0.00	13.280	0.32	0.058	0.00	0.024	0.00	467.06	11.02
FB15_32	855	8520	0.566	0.02	0.074	0.00	13.605	0.34	0.056	0.00	0.024	0.00	457.57	11.25
FB15_4	4060	38700	0.572	0.01	0.075	0.00	13.423	0.32	0.056	0.00	0.024	0.00	463.35	10.96
FB15_5	6940	26000	0.574	0.01	0.074	0.00	13.495	0.31	0.056	0.00	0.025	0.00	460.83	10.37
FB15_6	2780	39800	0.580	0.01	0.075	0.00	13.392	0.30	0.056	0.00	0.024	0.00	464.51	10.08
FB15_7	5560	21990	0.571	0.02	0.075	0.00	13.333	0.34	0.056	0.00	0.025	0.00	466.65	11.72
FB15_8	2480	28000	0.615	0.02	0.076	0.00	13.158	0.37	0.059	0.00	0.024	0.00	470.60	12.98

Table S1. Detrital monazite U-Th-Pb data LASS-ICP-MS
Table S2. Detrital monazite Nd isotopic data LASS-ICP-MS
Table S3. Detrital monazite REE data LASS-ICP-MS

FB15_9	4080	19040	0.577	0.02	0.076	0.00	13.175	0.33	0.056	0.00	0.023	0.00	472.15	11.45
FB1SR-AsheSchist_1	2750	18060	0.574	0.02	0.073	0.00	13.609	0.31	0.057	0.00	0.024	0.00	456.85	10.11
FB1SR-AsheSchist_10	2862	14190	0.590	0.02	0.076	0.00	13.141	0.31	0.056	0.00	0.025	0.00	473.05	11.12
FB1SR-AsheSchist_11	2400	12140	0.583	0.02	0.076	0.00	13.123	0.32	0.056	0.00	0.025	0.00	473.72	11.47
FB1SR-AsheSchist_12	2650	21200	0.553	0.02	0.073	0.00	13.755	0.34	0.055	0.00	0.024	0.00	452.91	11.16
FB1SR-AsheSchist_13	3110	15670	0.569	0.02	0.074	0.00	13.493	0.30	0.056	0.00	0.025	0.00	461.05	10.05
FB1SR-AsheSchist_2	1660	14810	0.576	0.02	0.074	0.00	13.569	0.35	0.057	0.00	0.024	0.00	457.98	11.61
FB1SR-AsheSchist_3	2990	14690	0.574	0.01	0.073	0.00	13.791	0.32	0.057	0.00	0.025	0.00	450.56	10.42
FB1SR-AsheSchist_4	2650	32500	0.605	0.02	0.075	0.00	13.333	0.33	0.058	0.00	0.026	0.00	465.06	11.32
FB1SR-AsheSchist_5	2420	29600	0.620	0.02	0.074	0.00	13.552	0.33	0.061	0.00	0.025	0.00	456.05	10.79
FB1SR-AsheSchist_6	2260	17820	0.560	0.02	0.073	0.00	13.680	0.35	0.056	0.00	0.024	0.00	455.13	11.56
FB1SR-AsheSchist_8	2480	17800	0.587	0.02	0.074	0.00	13.441	0.33	0.058	0.00	0.025	0.00	461.89	11.29
FB1SR-AsheSchist_9	2590	15000	0.593	0.02	0.076	0.00	13.226	0.32	0.057	0.00	0.025	0.00	469.66	11.03
FB2_1	9280	15620	0.572	0.02	0.073	0.00	13.755	0.36	0.057	0.00	0.024	0.00	451.75	11.50
FB2_10	7720	41800	0.573	0.01	0.074	0.00	13.604	0.32	0.057	0.00	0.024	0.00	456.89	10.40
FB2_11	2589	31800	0.616	0.02	0.075	0.00	13.369	0.32	0.060	0.00	0.024	0.00	462.86	10.95
FB2_12	3700	31500	0.584	0.02	0.073	0.00	13.641	0.32	0.058	0.00	0.024	0.00	455.19	10.40
FB2_13	9020	29000	0.583	0.01	0.073	0.00	13.648	0.32	0.057	0.00	0.024	0.00	455.06	10.39
FB2_15	5650	24300	0.579	0.02	0.074	0.00	13.605	0.35	0.057	0.00	0.024	0.00	456.57	11.57
FB2_16	5980	38700	0.577	0.02	0.074	0.00	13.605	0.35	0.057	0.00	0.024	0.00	456.83	11.57
FB2_17	4420	20640	0.591	0.02	0.075	0.00	13.387	0.32	0.057	0.00	0.025	0.00	464.21	10.97
FB2_18	2640	31000	0.595	0.02	0.076	0.00	13.089	0.34	0.056	0.00	0.024	0.00	474.74	12.23
FB2_19	4380	33130	0.582	0.02	0.074	0.00	13.556	0.32	0.056	0.00	0.024	0.00	458.67	10.65
FB2_2	4940	42900	0.584	0.02	0.074	0.00	13.441	0.35	0.057	0.00	0.024	0.00	462.06	11.65
FB2_20	5070	21700	0.580	0.02	0.074	0.00	13.441	0.33	0.056	0.00	0.024	0.00	462.52	11.29
FB2_21	5670	21800	0.579	0.01	0.074	0.00	13.495	0.34	0.056	0.00	0.024	0.00	460.66	11.26
FB2_24	3700	35800	0.576	0.02	0.075	0.00	13.333	0.34	0.055	0.00	0.024	0.00	466.76	11.73
FB2_25	2910	19270	0.567	0.02	0.076	0.00	13.210	0.35	0.055	0.00	0.024	0.00	471.33	12.19
FB2_26	5860	21600	0.560	0.02	0.073	0.00	13.624	0.34	0.055	0.00	0.024	0.00	457.21	11.21
FB2_27	755	31540	0.555	0.02	0.073	0.00	13.755	0.47	0.056	0.00	0.023	0.00	452.69	15.12
FB2_3	3620	14150	0.582	0.02	0.074	0.00	13.550	0.36	0.058	0.00	0.024	0.00	458.15	11.99

Table S1. Detrital monazite U-Th-Pb data LASS-ICP-MS
Table S2. Detrital monazite Nd isotopic data LASS-ICP-MS
Table S3. Detrital monazite REE data LASS-ICP-MS

FB2_4	7990	30880	0.574	0.02	0.074	0.00	13.605	0.35	0.057	0.00	0.024	0.00	456.99	11.58
FB2_5	2430	32500	0.591	0.02	0.075	0.00	13.423	0.36	0.058	0.00	0.024	0.00	462.38	12.06
FB2_6	5330	49200	0.390	0.01	0.052	0.00	19.113	0.47	0.054	0.00	0.017	0.00	328.36	7.97
FB2_7	2080	17480	0.570	0.02	0.074	0.00	13.587	0.39	0.057	0.00	0.024	0.00	457.43	12.83
FB2_8	5630	64700	0.577	0.02	0.074	0.00	13.585	0.31	0.057	0.00	0.024	0.00	457.61	10.12
FB2_9	1420	70000	0.564	0.02	0.073	0.00	13.791	0.32	0.057	0.00	0.023	0.00	450.62	10.36
FB2lowrow_1	4890	33200	0.437	0.01	0.053	0.00	18.818	0.41	0.059	0.00	0.018	0.00	331.22	7.19
FB2lowrow_10	5740	27000	0.512	0.03	0.066	0.00	15.083	0.77	0.056	0.00	0.022	0.00	413.51	20.64
FB2lowrow_11	7870	21000	0.576	0.02	0.074	0.00	13.441	0.39	0.056	0.00	0.024	0.00	463.05	13.34
FB2lowrow_12	2220	23130	0.609	0.02	0.075	0.00	13.405	0.37	0.059	0.00	0.025	0.00	462.52	12.45
FB2lowrow_13	3690	32900	0.430	0.01	0.057	0.00	17.668	0.54	0.055	0.00	0.019	0.00	354.49	10.63
FB2lowrow_14	5490	20470	0.580	0.01	0.075	0.00	13.423	0.34	0.056	0.00	0.025	0.00	463.17	11.67
FB2lowrow_15	6070	37100	0.482	0.01	0.062	0.00	16.077	0.43	0.056	0.00	0.021	0.00	388.38	10.20
FB2lowrow_16	3370	52700	0.419	0.01	0.054	0.00	18.416	0.52	0.056	0.00	0.018	0.00	339.75	9.54
FB2lowrow_17	3060	36700	0.585	0.02	0.075	0.00	13.405	0.32	0.057	0.00	0.025	0.00	463.54	10.96
FB2lowrow_18	6770	29650	0.585	0.02	0.074	0.00	13.441	0.32	0.056	0.00	0.025	0.00	462.49	10.94
FB2lowrow_19	6510	30200	0.552	0.02	0.072	0.00	13.810	0.32	0.055	0.00	0.024	0.00	451.07	10.40
FB2lowrow_2	5520	21080	0.577	0.02	0.074	0.00	13.514	0.34	0.056	0.00	0.025	0.00	460.23	11.26
FB2lowrow_20	3290	43500	0.590	0.02	0.075	0.00	13.333	0.33	0.057	0.00	0.024	0.00	465.95	11.35
FB2lowrow_21	2820	42400	0.567	0.02	0.074	0.00	13.514	0.35	0.056	0.00	0.024	0.00	460.56	11.65
FB2lowrow_22	2400	32400	0.570	0.02	0.072	0.00	13.812	0.40	0.057	0.00	0.024	0.00	449.91	12.72
FB2lowrow_24	2640	40500	0.590	0.02	0.075	0.00	13.405	0.34	0.057	0.00	0.024	0.00	463.28	11.68
FB2lowrow_25	2810	39200	0.585	0.02	0.074	0.00	13.459	0.38	0.057	0.00	0.024	0.00	461.63	12.88
FB2lowrow_28	8490	138800	0.996	0.03	0.107	0.00	9.320	0.23	0.067	0.00	0.033	0.00	652.83	15.90
FB2lowrow_29	5480	85700	0.580	0.02	0.074	0.00	13.495	0.33	0.057	0.00	0.024	0.00	460.31	10.90
FB2lowrow_3	3220	26000	0.454	0.01	0.060	0.00	16.694	0.45	0.055	0.00	0.020	0.00	374.75	10.02
FB2lowrow_30	1120	22840	0.458	0.02	0.059	0.00	16.892	0.64	0.056	0.00	0.019	0.00	369.68	13.77
FB2lowrow_31	2860	33800	0.580	0.02	0.075	0.00	13.333	0.38	0.056	0.00	0.024	0.00	466.30	12.95
FB2lowrow_4	3600	29900	0.586	0.02	0.075	0.00	13.280	0.37	0.056	0.00	0.025	0.00	468.29	12.97
FB2lowrow_5	3100	17510	0.408	0.01	0.055	0.00	18.265	0.44	0.053	0.00	0.019	0.00	343.60	8.18
FB2lowrow_6	6180	33900	0.412	0.01	0.054	0.00	18.376	0.39	0.055	0.00	0.018	0.00	340.96	7.22

Table S1. Detrital monazite U-Th-Pb data LASS-ICP-MS
Table S2. Detrital monazite Nd isotopic data LASS-ICP-MS
Table S3. Detrital monazite REE data LASS-ICP-MS

FB2lowrow_7	3400	17170	0.412	0.01	0.053	0.00	18.762	0.48	0.055	0.00	0.018	0.00	333.81	8.39
FB2lowrow_8	7260	29800	0.392	0.01	0.053	0.00	19.011	0.47	0.054	0.00	0.017	0.00	330.12	8.03
FB2lowrow_9	2230	36400	0.420	0.01	0.057	0.00	17.575	0.47	0.054	0.00	0.018	0.00	356.68	9.37
FB3_10	5360	34900	0.559	0.01	0.072	0.00	13.829	0.32	0.056	0.00	0.024	0.00	450.08	10.13
FB3_11	6600	26200	0.564	0.01	0.074	0.00	13.598	0.31	0.055	0.00	0.025	0.00	457.94	10.15
FB3_12	6510	34400	0.562	0.02	0.074	0.00	13.532	0.32	0.055	0.00	0.024	0.00	460.11	10.84
FB3_13	3670	17500	0.557	0.02	0.072	0.00	13.928	0.36	0.056	0.00	0.024	0.00	447.03	11.44
FB3_14	996	41200	0.583	0.02	0.075	0.00	13.423	0.37	0.058	0.00	0.024	0.00	462.46	12.46
FB3_16	2920	17590	0.578	0.02	0.075	0.00	13.405	0.33	0.056	0.00	0.024	0.00	463.86	11.31
FB3_18	5840	35600	0.393	0.01	0.053	0.00	18.936	0.48	0.054	0.00	0.018	0.00	331.49	8.20
FB3_19	3920	50000	0.575	0.01	0.074	0.00	13.578	0.29	0.056	0.00	0.024	0.00	458.08	9.72
FB3_20	6640	18800	0.421	0.01	0.054	0.00	18.484	0.50	0.056	0.00	0.020	0.00	338.29	9.08
FB3_21	6980	22530	0.568	0.01	0.074	0.00	13.481	0.31	0.055	0.00	0.024	0.00	461.88	10.27
FB3_22	6590	26820	0.453	0.01	0.061	0.00	16.393	0.36	0.054	0.00	0.020	0.00	381.76	8.35
FB3_23	3960	39000	0.565	0.02	0.073	0.00	13.659	0.32	0.056	0.00	0.024	0.00	455.34	10.47
FB3_24	6840	31000	0.564	0.01	0.073	0.00	13.648	0.32	0.055	0.00	0.024	0.00	456.20	10.54
FB3_25	7290	31300	0.565	0.02	0.074	0.00	13.569	0.35	0.056	0.00	0.024	0.00	458.68	11.60
FB3_26	3830	30310	0.464	0.01	0.060	0.00	16.714	0.40	0.056	0.00	0.020	0.00	373.74	8.90
FB3_27	5850	19720	0.458	0.01	0.061	0.00	16.474	0.39	0.055	0.00	0.020	0.00	379.64	8.76
FB3_28	5990	34300	0.576	0.01	0.074	0.00	13.488	0.30	0.056	0.00	0.024	0.00	461.03	10.06
FB3_29	5750	26000	0.571	0.01	0.074	0.00	13.530	0.30	0.056	0.00	0.024	0.00	459.78	10.04
FB3_3	5940	26430	0.581	0.02	0.075	0.00	13.335	0.32	0.057	0.00	0.025	0.00	465.78	10.82
FB3_30	10160	21200	0.387	0.01	0.053	0.00	18.776	0.44	0.053	0.00	0.018	0.00	334.69	7.70
FB3_33	779	24000	0.556	0.02	0.071	0.00	14.045	0.44	0.057	0.00	0.024	0.00	442.75	13.57
FB3_34	5200	34200	0.408	0.01	0.052	0.00	19.099	0.45	0.057	0.00	0.017	0.00	327.54	7.61
FB3_35	1980	60900	0.399	0.01	0.054	0.00	18.685	0.44	0.054	0.00	0.017	0.00	335.83	7.73
FB3_36	3650	46410	0.566	0.02	0.073	0.00	13.699	0.34	0.056	0.00	0.023	0.00	454.18	11.17
FB3_4	4960	28420	0.618	0.02	0.074	0.00	13.439	0.31	0.060	0.00	0.024	0.00	460.55	10.45
FB3_5	5660	28100	0.448	0.01	0.059	0.00	17.010	0.43	0.055	0.00	0.020	0.00	367.58	9.23
FB3_6	4750	22700	0.577	0.01	0.073	0.00	13.618	0.32	0.057	0.00	0.025	0.00	456.44	10.54
FB3_7	4530	22800	0.575	0.01	0.074	0.00	13.556	0.30	0.057	0.00	0.025	0.00	458.26	10.12

Table S1. Detrital monazite U-Th-Pb data LASS-ICP-MS
Table S2. Detrital monazite Nd isotopic data LASS-ICP-MS
Table S3. Detrital monazite REE data LASS-ICP-MS

FB3_9	4560	37800	0.562	0.01	0.073	0.00	13.643	0.34	0.056	0.00	0.024	0.00	456.29	11.20
FB4_1	1106	57000	0.627	0.02	0.078	0.00	12.771	0.33	0.058	0.00	0.025	0.00	485.45	12.41
FB4_10	2559	36800	0.554	0.02	0.069	0.00	14.493	0.40	0.058	0.00	0.022	0.00	428.64	11.58
FB4_11	4960	25890	0.552	0.02	0.072	0.00	13.947	0.33	0.056	0.00	0.023	0.00	446.43	10.36
FB4_12	5920	19950	0.583	0.01	0.074	0.00	13.600	0.31	0.057	0.00	0.025	0.00	457.01	10.08
FB4_13	2460	56300	0.574	0.01	0.074	0.00	13.574	0.31	0.056	0.00	0.024	0.00	458.03	10.30
FB4_14	6300	24000	0.578	0.02	0.074	0.00	13.561	0.31	0.057	0.00	0.025	0.00	458.33	10.36
FB4_15	6130	27260	0.564	0.01	0.072	0.00	13.816	0.30	0.056	0.00	0.024	0.00	450.54	9.70
FB4_16	2940	37900	0.577	0.02	0.074	0.00	13.492	0.32	0.056	0.00	0.024	0.00	461.00	10.76
FB4_17	3160	51100	0.591	0.01	0.075	0.00	13.417	0.31	0.057	0.00	0.024	0.00	462.82	10.44
FB4_18	5630	45900	0.390	0.01	0.052	0.00	19.113	0.45	0.054	0.00	0.017	0.00	328.31	7.69
FB4_2	1110	57500	0.635	0.02	0.079	0.00	12.626	0.34	0.058	0.00	0.025	0.00	490.85	12.87
FB4_20	1338	10090	0.393	0.01	0.053	0.00	18.893	0.47	0.053	0.00	0.017	0.00	332.35	8.12
FB4_21	3630	27400	0.415	0.01	0.054	0.00	18.474	0.40	0.056	0.00	0.018	0.00	338.66	7.32
FB4_22	1610	18490	0.599	0.03	0.074	0.00	13.495	0.73	0.058	0.00	0.022	0.00	459.74	24.23
FB4_23	2310	27600	0.391	0.01	0.052	0.00	19.246	0.42	0.055	0.00	0.017	0.00	325.74	7.08
FB4_24	7690	32600	0.562	0.01	0.073	0.00	13.721	0.33	0.056	0.00	0.024	0.00	453.36	10.73
FB4_25	1410	21870	0.576	0.02	0.070	0.00	14.337	0.35	0.060	0.00	0.022	0.00	432.33	10.28
FB4_26	4630	22490	0.572	0.02	0.073	0.00	13.680	0.39	0.057	0.00	0.024	0.00	454.47	12.78
FB4_27	224	5990	0.537	0.04	0.066	0.00	15.106	0.85	0.060	0.00	0.020	0.00	410.59	22.86
FB4_28	3980	34300	0.566	0.01	0.072	0.00	13.816	0.32	0.057	0.00	0.024	0.00	449.93	10.13
FB4_29	4380	27100	0.385	0.01	0.052	0.00	19.242	0.44	0.054	0.00	0.017	0.00	326.04	7.40
FB4_30	5050	25470	0.570	0.01	0.073	0.00	13.648	0.30	0.056	0.00	0.024	0.00	455.64	9.82
FB4_31	7830	31300	0.571	0.01	0.073	0.00	13.609	0.31	0.056	0.00	0.024	0.00	456.87	10.15
FB4_32	6350	25530	0.565	0.01	0.072	0.00	13.803	0.32	0.057	0.00	0.024	0.00	450.43	10.29
FB4_4	823	28300	0.589	0.02	0.075	0.00	13.333	0.38	0.057	0.00	0.024	0.00	466.12	12.96
FB4_6	403	32900	0.636	0.03	0.077	0.00	13.004	0.53	0.060	0.00	0.024	0.00	475.46	18.89
FB4_7	4440	32100	0.384	0.01	0.052	0.00	19.264	0.46	0.053	0.00	0.017	0.00	326.09	7.66
FB4_8	2830	35800	0.567	0.02	0.074	0.00	13.602	0.33	0.056	0.00	0.024	0.00	457.68	10.84
FB4_9	3010	27200	0.571	0.02	0.073	0.00	13.738	0.33	0.056	0.00	0.024	0.00	452.67	10.72
FB5_1	4520	32600	0.563	0.02	0.072	0.00	13.986	0.37	0.057	0.00	0.024	0.00	444.67	11.40

Table S1. Detrital monazite U-Th-Pb data LASS-ICP-MS
Table S2. Detrital monazite Nd isotopic data LASS-ICP-MS
Table S3. Detrital monazite REE data LASS-ICP-MS

FB5_10	2230	26910	0.566	0.02	0.071	0.00	14.104	0.37	0.058	0.00	0.021	0.00	440.48	11.34
FB5_11	4450	28730	0.564	0.02	0.073	0.00	13.793	0.41	0.056	0.00	0.024	0.00	450.97	13.18
FB5_12	3940	29680	0.564	0.02	0.073	0.00	13.630	0.31	0.056	0.00	0.024	0.00	456.38	10.15
FB5_13	1560	37700	0.556	0.02	0.072	0.00	13.889	0.35	0.057	0.00	0.024	0.00	447.63	11.08
FB5_14	3640	66500	0.563	0.02	0.073	0.00	13.755	0.34	0.056	0.00	0.023	0.00	452.36	11.14
FB5_15	3230	34850	0.560	0.01	0.072	0.00	13.850	0.35	0.057	0.00	0.024	0.00	449.04	11.09
FB5_16	6340	27200	0.576	0.01	0.074	0.00	13.569	0.32	0.056	0.00	0.025	0.00	458.40	10.45
FB5_17	2190	24830	0.568	0.02	0.072	0.00	13.889	0.39	0.057	0.00	0.024	0.00	447.31	12.25
FB5_18	6090	28500	0.570	0.02	0.072	0.00	13.908	0.42	0.057	0.00	0.024	0.00	446.87	13.12
FB5_19	5950	23460	0.582	0.02	0.074	0.00	13.514	0.35	0.057	0.00	0.024	0.00	459.93	11.62
FB5_2	4150	30000	0.570	0.02	0.073	0.00	13.755	0.37	0.057	0.00	0.024	0.00	452.06	11.90
FB5_20	10000	29500	0.569	0.02	0.073	0.00	13.736	0.37	0.057	0.00	0.024	0.00	452.59	11.91
FB5_21	7290	33600	0.577	0.02	0.073	0.00	13.624	0.36	0.057	0.00	0.024	0.00	456.36	11.96
FB5_22	779	29700	0.566	0.03	0.072	0.00	13.850	0.50	0.057	0.00	0.024	0.00	448.73	16.07
FB5_23	4980	25000	0.588	0.01	0.073	0.00	13.624	0.35	0.058	0.00	0.024	0.00	455.68	11.56
FB5_25	1668	23690	0.574	0.02	0.074	0.00	13.605	0.38	0.057	0.00	0.024	0.00	456.53	12.40
FB5_26	989	38100	0.573	0.03	0.073	0.00	13.793	0.40	0.058	0.00	0.024	0.00	450.05	12.76
FB5_27	3670	32780	0.568	0.02	0.072	0.00	13.891	0.31	0.057	0.00	0.024	0.00	447.57	9.74
FB5_28	1589	30000	0.570	0.02	0.073	0.00	13.643	0.36	0.056	0.00	0.023	0.00	456.04	11.97
FB5_29	5190	30200	0.559	0.02	0.073	0.00	13.699	0.38	0.056	0.00	0.024	0.00	454.13	12.35
FB5_3	3430	20160	0.569	0.02	0.073	0.00	13.680	0.31	0.057	0.00	0.024	0.00	454.53	10.21
FB5_30	6650	24520	0.566	0.02	0.071	0.00	14.019	0.33	0.058	0.00	0.024	0.00	443.08	10.10
FB5_31	4300	25600	0.594	0.02	0.076	0.00	13.242	0.31	0.057	0.00	0.024	0.00	468.94	10.94
FB5_32	4940	7930	0.598	0.01	0.075	0.00	13.277	0.30	0.057	0.00	0.025	0.00	467.56	10.21
FB5_33	6950	42540	0.563	0.01	0.072	0.00	13.908	0.34	0.057	0.00	0.024	0.00	446.89	10.69
FB5_34	2100	36490	0.595	0.02	0.077	0.00	12.970	0.45	0.057	0.00	0.020	0.00	478.77	16.36
FB5_35	6370	20310	0.580	0.01	0.075	0.00	13.387	0.33	0.056	0.00	0.024	0.00	464.41	11.32
FB5_36	6470	115100	0.580	0.01	0.074	0.00	13.477	0.31	0.057	0.00	0.023	0.00	460.84	10.43
FB5_37	4910	45300	0.567	0.01	0.073	0.00	13.624	0.32	0.056	0.00	0.024	0.00	456.83	10.62
FB5_38	4000	25500	0.585	0.01	0.075	0.00	13.392	0.32	0.057	0.00	0.024	0.00	463.73	10.72
FB5_39	3400	33800	0.577	0.02	0.076	0.00	13.245	0.35	0.056	0.00	0.024	0.00	469.59	12.16

Table S1. Detrital monazite U-Th-Pb data LASS-ICP-MS
Table S2. Detrital monazite Nd isotopic data LASS-ICP-MS
Table S3. Detrital monazite REE data LASS-ICP-MS

FB5_4	1196	36100	0.545	0.02	0.072	0.00	13.928	0.45	0.056	0.00	0.024	0.00	447.03	14.08
FB5_5	891	34800	0.547	0.02	0.070	0.00	14.225	0.48	0.056	0.00	0.023	0.00	437.54	14.46
FB5_6	4120	27710	0.571	0.02	0.073	0.00	13.755	0.37	0.057	0.00	0.024	0.00	451.87	11.90
FB5_7	2170	27390	0.598	0.02	0.076	0.00	13.210	0.34	0.058	0.00	0.024	0.00	469.79	11.77
FB5_8	1014	33110	0.589	0.02	0.072	0.00	13.928	0.42	0.060	0.00	0.024	0.00	444.72	13.11
FB5_9	10350	31750	0.565	0.01	0.072	0.00	13.839	0.32	0.057	0.00	0.024	0.00	449.28	10.24
FB6_1	3800	21630	0.574	0.02	0.074	0.00	13.532	0.36	0.056	0.00	0.025	0.00	459.51	12.01
FB6_10	3680	37200	0.566	0.02	0.073	0.00	13.755	0.38	0.056	0.00	0.024	0.00	452.32	12.32
FB6_11	9100	181000	0.657	0.03	0.078	0.00	12.771	0.39	0.061	0.00	0.023	0.00	483.25	14.46
FB6_12	1596	31000	0.563	0.02	0.072	0.00	13.966	0.43	0.057	0.00	0.023	0.00	445.02	13.57
FB6_13	3880	25000	0.574	0.01	0.075	0.00	13.351	0.34	0.056	0.00	0.024	0.00	465.87	11.71
FB6_14	2920	19300	0.631	0.04	0.075	0.00	13.387	0.41	0.062	0.00	0.024	0.00	461.09	13.82
FB6_15	5710	23400	0.568	0.02	0.073	0.00	13.643	0.46	0.056	0.00	0.024	0.00	456.29	15.14
FB6_16	3090	31400	0.566	0.02	0.074	0.00	13.587	0.40	0.057	0.00	0.024	0.00	457.54	13.26
FB6_17	2580	41200	0.567	0.02	0.074	0.00	13.605	0.38	0.056	0.00	0.024	0.00	457.41	12.40
FB6_18	7850	36990	0.565	0.02	0.073	0.00	13.744	0.33	0.056	0.00	0.024	0.00	452.82	10.69
FB6_19	3800	19910	0.565	0.02	0.074	0.00	13.569	0.40	0.056	0.00	0.025	0.00	458.39	13.27
FB6_2	5310	31500	0.558	0.01	0.073	0.00	13.755	0.38	0.056	0.00	0.024	0.00	452.59	12.33
FB6_20	2300	28410	0.548	0.02	0.072	0.00	13.870	0.47	0.055	0.00	0.024	0.00	449.42	15.09
FB6_21	1600	24200	0.566	0.02	0.073	0.00	13.774	0.38	0.057	0.00	0.024	0.00	451.28	12.33
FB6_22	6980	25390	0.565	0.02	0.073	0.00	13.717	0.39	0.056	0.00	0.024	0.00	453.59	12.77
FB6_23	5230	30600	0.572	0.02	0.074	0.00	13.459	0.42	0.056	0.00	0.024	0.00	462.17	14.24
FB6_24	1866	73400	0.569	0.02	0.073	0.00	13.661	0.39	0.055	0.00	0.024	0.00	455.79	12.82
FB6_25	2262	97700	0.559	0.02	0.071	0.00	14.025	0.44	0.057	0.00	0.023	0.00	443.53	13.56
FB6_26	3250	31500	0.581	0.02	0.074	0.00	13.514	0.41	0.057	0.00	0.024	0.00	459.73	13.73
FB6_27	2068	24960	0.570	0.02	0.073	0.00	13.717	0.45	0.057	0.00	0.024	0.00	453.11	14.61
FB6_28	4570	32300	0.571	0.02	0.074	0.00	13.605	0.38	0.055	0.00	0.024	0.00	457.62	12.41
FB6_29	317	35400	0.587	0.03	0.074	0.00	13.569	0.60	0.059	0.00	0.024	0.00	456.60	19.86
FB6_3	1092	3900	0.571	0.02	0.073	0.00	13.661	0.37	0.057	0.00	0.025	0.00	455.11	11.98
FB6_30	2540	58800	0.583	0.02	0.075	0.00	13.387	0.42	0.057	0.00	0.024	0.00	464.12	14.26
FB6_31	3620	28400	0.576	0.02	0.074	0.00	13.514	0.40	0.057	0.00	0.024	0.00	459.98	13.29

Table S1. Detrital monazite U-Th-Pb data LASS-ICP-MS
Table S2. Detrital monazite Nd isotopic data LASS-ICP-MS
Table S3. Detrital monazite REE data LASS-ICP-MS

FB6_32	1232	54600	0.580	0.02	0.072	0.00	13.889	0.40	0.058	0.00	0.024	0.00	447.01	12.69
FB6_33	2852	21350	0.589	0.02	0.073	0.00	13.680	0.37	0.058	0.00	0.024	0.00	453.97	11.93
FB6_34	2550	40600	0.590	0.02	0.072	0.00	13.947	0.35	0.059	0.00	0.023	0.00	444.68	11.01
FB6_35	3730	33900	0.559	0.02	0.071	0.00	14.006	0.37	0.056	0.00	0.023	0.00	444.31	11.40
FB6_36	4030	32800	0.557	0.02	0.072	0.00	13.889	0.39	0.055	0.00	0.024	0.00	448.47	12.28
FB6_37	3490	27000	0.570	0.02	0.073	0.00	13.717	0.41	0.056	0.00	0.024	0.00	453.50	13.22
FB6_38	7180	26870	0.573	0.02	0.073	0.00	13.772	0.33	0.057	0.00	0.024	0.00	451.26	10.52
FB6_39	5990	23410	0.588	0.02	0.074	0.00	13.587	0.38	0.057	0.00	0.024	0.00	457.23	12.38
FB6_4	4330	29040	0.564	0.02	0.073	0.00	13.755	0.37	0.055	0.00	0.024	0.00	452.75	11.92
FB6_40	1680	31000	0.574	0.02	0.072	0.00	13.812	0.43	0.057	0.00	0.024	0.00	449.84	13.62
FB6_5	902	32300	0.562	0.03	0.074	0.00	13.605	0.47	0.055	0.00	0.024	0.00	457.74	15.67
FB6_6	1898	32500	0.551	0.02	0.073	0.00	13.774	0.42	0.056	0.00	0.024	0.00	452.02	13.67
FB6_7	3890	24100	0.575	0.02	0.074	0.00	13.550	0.39	0.056	0.00	0.025	0.00	458.94	12.84
FB6_8	3780	18700	0.575	0.02	0.073	0.00	13.624	0.39	0.057	0.00	0.025	0.00	456.28	12.80
FB6_9	5590	20130	0.570	0.02	0.073	0.00	13.661	0.37	0.057	0.00	0.024	0.00	455.11	11.95
FB8_11	6260	30200	0.580	0.01	0.074	0.00	13.477	0.33	0.057	0.00	0.024	0.00	461.03	10.91
FB8_12	2161	39300	0.564	0.02	0.073	0.00	13.774	0.36	0.056	0.00	0.023	0.00	451.57	11.51
FB8_13	4392	23500	0.574	0.02	0.073	0.00	13.691	0.32	0.057	0.00	0.024	0.00	454.07	10.38
FB8_14	4260	61700	0.604	0.02	0.075	0.00	13.330	0.32	0.059	0.00	0.025	0.00	464.99	10.84
FB8_15	4840	26200	0.575	0.02	0.074	0.00	13.514	0.38	0.057	0.00	0.024	0.00	459.73	12.84
FB8_16	6100	17950	0.578	0.01	0.074	0.00	13.435	0.30	0.056	0.00	0.024	0.00	462.83	10.07
FB8_2	3220	17370	0.586	0.02	0.076	0.00	13.245	0.32	0.057	0.00	0.024	0.00	468.86	11.04
FB8_3	4450	36580	0.586	0.02	0.075	0.00	13.314	0.30	0.057	0.00	0.024	0.00	466.51	10.19
FB8_4	2870	15280	0.570	0.02	0.074	0.00	13.569	0.33	0.057	0.00	0.024	0.00	458.01	10.87
FB8_5	8980	37200	0.583	0.02	0.074	0.00	13.441	0.33	0.057	0.00	0.024	0.00	462.25	11.28
FB8_6	6260	22900	0.601	0.02	0.076	0.00	13.245	0.37	0.057	0.00	0.025	0.00	468.60	12.96
FB8_7	3570	22300	0.579	0.02	0.073	0.00	13.680	0.37	0.058	0.00	0.024	0.00	453.63	11.92
FB8_8	6300	16670	0.578	0.02	0.074	0.00	13.524	0.32	0.057	0.00	0.024	0.00	459.40	10.72
FB8_9	485	30030	0.560	0.02	0.074	0.00	13.587	0.42	0.055	0.00	0.024	0.00	458.58	13.78
FB9_1	4330	11880	0.583	0.02	0.075	0.00	13.351	0.33	0.057	0.00	0.025	0.00	465.20	11.33
FB9_11	4930	31100	0.568	0.02	0.073	0.00	13.755	0.33	0.056	0.00	0.024	0.00	452.29	10.79

Table S1. Detrital monazite U-Th-Pb data LASS-ICP-MS
Table S2. Detrital monazite Nd isotopic data LASS-ICP-MS
Table S3. Detrital monazite REE data LASS-ICP-MS

FB9_12	1569	29000	0.555	0.02	0.071	0.00	14.065	0.36	0.056	0.00	0.023	0.00	442.92	11.01
FB9_13	5870	22170	0.563	0.02	0.072	0.00	13.805	0.31	0.056	0.00	0.024	0.00	450.63	9.84
FB9_14	6070	23710	0.576	0.01	0.074	0.00	13.563	0.32	0.056	0.00	0.024	0.00	458.56	10.49
FB9_15	5590	24400	0.564	0.01	0.073	0.00	13.751	0.30	0.056	0.00	0.024	0.00	452.42	9.82
FB9_16	6630	28570	0.561	0.01	0.072	0.00	13.852	0.31	0.056	0.00	0.023	0.00	449.17	9.76
FB9_17	4650	21090	0.564	0.02	0.073	0.00	13.774	0.30	0.056	0.00	0.024	0.00	451.55	9.72
FB9_18	5870	22530	0.548	0.01	0.072	0.00	13.972	0.32	0.055	0.00	0.024	0.00	445.99	10.10
FB9_19	4530	27760	0.548	0.01	0.072	0.00	13.849	0.31	0.055	0.00	0.024	0.00	449.92	9.91
FB9_2	622	58100	2.052	0.09	0.178	0.01	5.627	0.17	0.083	0.00	0.053	0.00	1042.69	30.62
FB9_20	1211	78600	1.747	0.05	0.171	0.00	5.858	0.14	0.074	0.00	0.052	0.00	1015.29	23.50
FB9_21	6280	25210	0.566	0.02	0.073	0.00	13.691	0.32	0.056	0.00	0.024	0.00	454.50	10.42
FB9_22	4550	31600	0.554	0.01	0.073	0.00	13.630	0.32	0.055	0.00	0.024	0.00	457.02	10.69
FB9_23	6630	26300	0.566	0.01	0.073	0.00	13.657	0.31	0.056	0.00	0.024	0.00	455.77	10.32
FB9_25	7780	36000	0.560	0.01	0.073	0.00	13.723	0.30	0.056	0.00	0.024	0.00	453.54	9.83
FB9_26	1537	41200	0.563	0.02	0.072	0.00	13.974	0.32	0.056	0.00	0.023	0.00	445.28	10.13
FB9_27	4850	23370	0.545	0.01	0.073	0.00	13.776	0.30	0.055	0.00	0.024	0.00	452.53	9.59
FB9_28	3330	25830	0.551	0.02	0.073	0.00	13.774	0.31	0.055	0.00	0.024	0.00	452.26	10.12
FB9_29	973	37300	0.559	0.02	0.072	0.00	13.889	0.35	0.056	0.00	0.023	0.00	447.91	11.11
FB9_3	3560	51100	0.589	0.02	0.074	0.00	13.479	0.31	0.057	0.00	0.024	0.00	460.69	10.31
FB9_30	5370	24060	0.554	0.02	0.073	0.00	13.643	0.33	0.055	0.00	0.024	0.00	456.63	10.82
FB9_31	6280	24480	0.552	0.01	0.072	0.00	13.889	0.31	0.056	0.00	0.024	0.00	448.34	9.69
FB9_32	3770	31580	0.566	0.01	0.074	0.00	13.459	0.33	0.055	0.00	0.024	0.00	462.56	11.29
FB9_33	3780	23210	0.544	0.02	0.070	0.00	14.312	0.34	0.057	0.00	0.023	0.00	434.70	10.21
FB9_34	3770	20700	0.563	0.01	0.073	0.00	13.674	0.32	0.056	0.00	0.024	0.00	455.30	10.41
FB9_35	7000	24000	0.548	0.01	0.072	0.00	13.849	0.31	0.055	0.00	0.023	0.00	449.99	9.91
FB9_36	5690	32800	0.568	0.01	0.073	0.00	13.618	0.32	0.056	0.00	0.024	0.00	456.86	10.43
FB9_37	2610	30100	0.558	0.02	0.073	0.00	13.736	0.34	0.056	0.00	0.024	0.00	453.18	11.17
FB9_38	5960	43600	0.561	0.01	0.073	0.00	13.789	0.31	0.056	0.00	0.024	0.00	451.20	10.09
FB9_39	1460	33400	0.571	0.02	0.073	0.00	13.793	0.34	0.057	0.00	0.023	0.00	450.39	10.76
FB9_4	3780	23550	0.583	0.01	0.074	0.00	13.556	0.31	0.057	0.00	0.024	0.00	458.35	10.27
FB9_40	3420	17090	0.552	0.01	0.072	0.00	13.893	0.32	0.056	0.00	0.024	0.00	448.27	10.02

Table S1. Detrital monazite U-Th-Pb data LASS-ICP-MS
Table S2. Detrital monazite Nd isotopic data LASS-ICP-MS
Table S3. Detrital monazite REE data LASS-ICP-MS

FB9_41	2263	63700	0.573	0.02	0.072	0.00	13.961	0.33	0.057	0.00	0.023	0.00	445.09	10.22
FB9_42	5090	27800	0.580	0.01	0.073	0.00	13.701	0.31	0.057	0.00	0.024	0.00	453.57	10.22
FB9_43	5100	32900	0.552	0.01	0.072	0.00	13.845	0.33	0.055	0.00	0.024	0.00	450.00	10.48
FB9_44	7070	29200	0.564	0.01	0.072	0.00	13.845	0.33	0.057	0.00	0.024	0.00	449.22	10.49
FB9_46	2815	30800	0.543	0.01	0.071	0.00	14.168	0.31	0.056	0.00	0.023	0.00	439.65	9.52
FB9_5	4360	22000	0.569	0.02	0.073	0.00	13.656	0.32	0.057	0.00	0.024	0.00	455.29	10.59
FB9_6	2339	20120	0.581	0.02	0.075	0.00	13.369	0.30	0.056	0.00	0.025	0.00	465.14	10.23
FB9_7	4410	20180	0.602	0.02	0.074	0.00	13.466	0.30	0.059	0.00	0.024	0.00	460.16	10.08
FB9_8	4550	35200	0.603	0.02	0.074	0.00	13.508	0.29	0.059	0.00	0.024	0.00	459.00	9.67
FB9_9	10740	32900	0.574	0.01	0.073	0.00	13.753	0.32	0.057	0.00	0.024	0.00	452.06	10.25
FinesCreek-Schist_1	5930	26700	0.572	0.02	0.073	0.00	13.793	0.38	0.056	0.00	0.024	0.00	450.96	12.30
FinesCreek-Schist_10	6070	17760	0.559	0.02	0.072	0.00	13.908	0.42	0.056	0.00	0.024	0.00	447.44	13.14
FinesCreek-Schist_11	6090	19190	0.561	0.02	0.071	0.00	14.006	0.44	0.056	0.00	0.024	0.00	444.30	13.56
FinesCreek-Schist_12	6280	20700	0.567	0.02	0.072	0.00	13.872	0.32	0.057	0.00	0.024	0.00	448.28	10.07
FinesCreek-Schist_13	4700	18600	0.602	0.02	0.072	0.00	13.966	0.42	0.061	0.00	0.024	0.00	443.01	13.07
FinesCreek-Schist_14	6460	28500	0.559	0.02	0.072	0.00	13.966	0.42	0.057	0.00	0.024	0.00	445.40	13.11
FinesCreek-Schist_15	6490	27800	0.553	0.02	0.071	0.00	14.045	0.47	0.056	0.00	0.024	0.00	443.15	14.50
FinesCreek-Schist_16	5850	19120	0.559	0.02	0.071	0.00	14.025	0.45	0.057	0.00	0.024	0.00	443.52	14.02
FinesCreek-Schist_17	6750	24630	0.556	0.01	0.072	0.00	13.931	0.34	0.056	0.00	0.024	0.00	446.85	10.63
FinesCreek-Schist_18	6300	28400	0.559	0.02	0.071	0.00	14.045	0.45	0.056	0.00	0.024	0.00	443.26	14.02
FinesCreek-Schist_2	6410	20240	0.597	0.02	0.072	0.00	13.850	0.40	0.060	0.00	0.024	0.00	447.18	12.66
FinesCreek-Schist_3	6650	21170	0.558	0.01	0.071	0.00	14.006	0.37	0.057	0.00	0.024	0.00	444.05	11.39
FinesCreek-Schist_4	6610	29100	0.565	0.02	0.072	0.00	13.879	0.32	0.056	0.00	0.024	0.00	448.19	10.04
FinesCreek-Schist_5	6650	33700	0.559	0.02	0.071	0.00	14.085	0.38	0.057	0.00	0.023	0.00	441.76	11.76
FinesCreek-Schist_6	6110	27600	0.584	0.02	0.073	0.00	13.624	0.38	0.057	0.00	0.024	0.00	455.92	12.37
FinesCreek-Schist_7	5920	20300	0.583	0.02	0.073	0.00	13.680	0.46	0.058	0.00	0.024	0.00	453.98	15.09
FinesCreek-Schist_8	5900	26900	0.577	0.02	0.073	0.00	13.755	0.38	0.057	0.00	0.024	0.00	451.83	12.31
FinesCreek-Schist_9	5520	17100	0.581	0.02	0.071	0.00	14.006	0.42	0.058	0.00	0.024	0.00	443.34	13.08
FL7_large_1	1900	57000	1.790	0.05	0.177	0.00	5.663	0.13	0.074	0.00	0.053	0.00	1048.37	23.17
FL7_large_10	8850	41200	1.771	0.04	0.173	0.00	5.774	0.13	0.075	0.00	0.055	0.00	1027.36	21.78
FL7_large_11	2840	54700	1.862	0.05	0.179	0.00	5.583	0.13	0.076	0.00	0.056	0.00	1060.45	24.51

Table S1. Detrital monazite U-Th-Pb data LASS-ICP-MS
Table S2. Detrital monazite Nd isotopic data LASS-ICP-MS
Table S3. Detrital monazite REE data LASS-ICP-MS

FL7_large_13	4460	40700	2.129	0.05	0.197	0.00	5.066	0.11	0.080	0.00	0.061	0.00	1159.94	25.33
FL7_large_14	4410	46800	2.142	0.05	0.198	0.00	5.040	0.12	0.079	0.00	0.061	0.00	1166.25	25.97
FL7_large_15	5020	34500	1.912	0.04	0.183	0.00	5.464	0.12	0.077	0.00	0.058	0.00	1082.01	23.46
FL7_large_16	1174	33500	1.807	0.07	0.175	0.00	5.724	0.16	0.076	0.00	0.053	0.00	1035.81	28.51
FL7_large_17	2360	28700	1.772	0.05	0.177	0.00	5.640	0.14	0.073	0.00	0.056	0.00	1054.03	25.41
FL7_large_18	2840	30800	1.763	0.05	0.176	0.00	5.679	0.14	0.073	0.00	0.056	0.00	1047.01	24.97
FL7_large_19	4530	21640	2.114	0.06	0.197	0.01	5.071	0.13	0.078	0.00	0.063	0.00	1161.52	28.73
FL7_large_2	1267	59300	1.740	0.05	0.176	0.00	5.692	0.14	0.073	0.00	0.054	0.00	1045.34	24.95
FL7_large_20	2240	70600	1.697	0.04	0.169	0.00	5.928	0.16	0.074	0.00	0.052	0.00	1003.65	26.09
FL7_large_21	1134	63300	1.849	0.05	0.175	0.00	5.705	0.15	0.076	0.00	0.054	0.00	1038.19	26.23
FL7_large_22	1237	48800	1.808	0.05	0.177	0.00	5.637	0.14	0.074	0.00	0.054	0.00	1052.91	25.07
FL7_large_24	1545	55900	2.072	0.08	0.186	0.00	5.376	0.14	0.081	0.00	0.052	0.00	1093.32	28.49
FL7_large_25	2080	62800	2.130	0.12	0.200	0.01	5.013	0.27	0.078	0.00	0.049	0.00	1174.17	60.42
FL7_large_26	1880	35100	1.782	0.05	0.176	0.00	5.698	0.14	0.074	0.00	0.056	0.00	1042.52	25.58
FL7_large_29	5130	20900	1.891	0.05	0.185	0.00	5.417	0.13	0.075	0.00	0.059	0.00	1092.65	25.34
FL7_large_30	9260	32200	2.186	0.05	0.199	0.00	5.030	0.12	0.080	0.00	0.062	0.00	1167.34	27.46
FL7_large_34	5180	26900	1.648	0.04	0.168	0.00	5.942	0.14	0.072	0.00	0.054	0.00	1003.27	22.98
FL7_large_35	4830	23590	1.658	0.04	0.169	0.00	5.917	0.16	0.072	0.00	0.055	0.00	1007.42	26.16
FL7_large_37	7040	34800	2.020	0.05	0.189	0.00	5.291	0.13	0.079	0.00	0.060	0.00	1112.96	26.93
FL7_large_5	1307	65100	2.243	0.06	0.194	0.00	5.144	0.12	0.085	0.00	0.059	0.00	1135.20	25.17
FL7_large_6	5950	81400	1.709	0.04	0.165	0.00	6.050	0.14	0.076	0.00	0.050	0.00	981.45	22.61
FL7_large_8	5700	25400	2.193	0.05	0.198	0.00	5.051	0.12	0.081	0.00	0.062	0.00	1160.97	25.87
FL7_large_9	8710	38000	1.786	0.04	0.172	0.00	5.800	0.14	0.076	0.00	0.055	0.00	1022.42	23.89
FL7_small_1	5010	14570	2.108	0.05	0.193	0.00	5.181	0.11	0.079	0.00	0.063	0.00	1136.08	23.35
FL7_small_10	5130	20750	2.129	0.05	0.194	0.00	5.163	0.12	0.080	0.00	0.062	0.00	1138.56	26.07
FL7_small_11	9780	41000	1.852	0.04	0.175	0.00	5.721	0.13	0.077	0.00	0.056	0.00	1035.01	23.48
FL7_small_13	4457	29610	2.123	0.05	0.195	0.00	5.126	0.12	0.079	0.00	0.063	0.00	1147.73	25.11
FL7_small_14	2100	22300	1.774	0.04	0.173	0.00	5.787	0.14	0.074	0.00	0.056	0.00	1026.66	23.37
FL7_small_16	2250	21100	2.002	0.05	0.187	0.00	5.350	0.12	0.078	0.00	0.060	0.00	1102.41	24.90
FL7_small_17	121	3500	1.510	0.13	0.153	0.01	6.536	0.49	0.073	0.00	0.051	0.00	913.97	66.25
FL7_small_18	1959	39200	2.293	0.05	0.199	0.00	5.018	0.12	0.083	0.00	0.060	0.00	1165.48	26.23

Table S1. Detrital monazite U-Th-Pb data LASS-ICP-MS
Table S2. Detrital monazite Nd isotopic data LASS-ICP-MS
Table S3. Detrital monazite REE data LASS-ICP-MS

FL7_small_21	358	10690	0.668	0.03	0.083	0.00	12.005	0.49	0.060	0.00	0.027	0.00	514.51	20.79
FL7_small_22	5780	29100	2.074	0.05	0.191	0.00	5.238	0.12	0.078	0.00	0.061	0.00	1124.69	25.26
FL7_small_24	970	70400	1.893	0.06	0.178	0.01	5.634	0.16	0.078	0.00	0.053	0.00	1048.93	29.05
FL7_small_26	6550	27600	2.274	0.05	0.205	0.00	4.890	0.11	0.080	0.00	0.065	0.00	1199.50	26.53
FL7_small_27	2530	24000	2.194	0.06	0.197	0.00	5.066	0.13	0.080	0.00	0.064	0.00	1159.93	28.34
FL7_small_28	12470	27600	2.018	0.04	0.185	0.00	5.397	0.12	0.078	0.00	0.061	0.00	1092.75	22.94
FL7_small_29	190	18460	2.080	0.14	0.188	0.01	5.319	0.33	0.080	0.00	0.061	0.00	1105.70	66.37
FL7_small_3	6420	36900	2.106	0.05	0.190	0.00	5.258	0.11	0.080	0.00	0.061	0.00	1118.80	23.42
FL7_small_30	7600	56600	1.849	0.05	0.177	0.00	5.653	0.14	0.076	0.00	0.055	0.00	1048.19	25.97
FL7_small_31	1450	17850	2.060	0.05	0.190	0.00	5.258	0.12	0.079	0.00	0.062	0.00	1120.29	24.14
FL7_small_32	4470	48960	2.010	0.05	0.188	0.00	5.325	0.13	0.077	0.00	0.058	0.00	1108.68	26.23
FL7_small_34	5640	16250	2.001	0.05	0.188	0.00	5.328	0.12	0.077	0.00	0.062	0.00	1108.42	25.28
FL7_small_35	1071	23200	1.831	0.06	0.178	0.00	5.618	0.14	0.075	0.00	0.058	0.00	1055.75	26.12
FL7_small_5	47	32600	1.840	0.59	0.174	0.05	5.747	1.62	0.075	0.01	0.049	0.00	1032.84	########
FL7_small_7	1235	32100	1.753	0.05	0.173	0.00	5.794	0.14	0.074	0.00	0.056	0.00	1025.97	23.68
FL7_small_8	1880	25740	1.822	0.05	0.177	0.00	5.666	0.14	0.075	0.00	0.056	0.00	1047.07	24.31
FL7_small_9	7850	33800	1.823	0.04	0.175	0.00	5.714	0.12	0.075	0.00	0.056	0.00	1037.94	21.96
KS12-2C_large_1	1210	67500	1.840	0.05	0.179	0.00	5.593	0.13	0.074	0.00	0.054	0.00	1061.22	23.98
KS12-2C_large_10	3240	59300	1.793	0.05	0.177	0.00	5.666	0.14	0.074	0.00	0.053	0.00	1047.51	25.98
KS12-2C_large_13	1278	69700	1.827	0.05	0.174	0.00	5.750	0.15	0.076	0.00	0.054	0.00	1030.03	25.38
KS12-2C_large_14	1197	67400	1.742	0.05	0.173	0.00	5.770	0.14	0.073	0.00	0.053	0.00	1030.52	25.07
KS12-2C_large_15	18560	24800	1.739	0.04	0.168	0.00	5.945	0.13	0.076	0.00	0.055	0.00	998.22	21.50
KS12-2C_large_16	20900	19900	1.750	0.04	0.167	0.00	5.984	0.13	0.077	0.00	0.053	0.00	990.63	21.37
KS12-2C_large_2	1213	68600	1.812	0.05	0.176	0.00	5.688	0.14	0.075	0.00	0.054	0.00	1043.13	24.89
KS12-2C_large_5	9390	41600	1.787	0.04	0.174	0.00	5.764	0.14	0.074	0.00	0.054	0.00	1030.67	24.35
KS12-2C_large_7	1950	69700	1.690	0.21	0.171	0.02	5.848	0.69	0.073	0.00	0.030	0.00	1018.05	########
KS12-2C_large_8	1670	63200	1.775	0.05	0.176	0.01	5.692	0.16	0.074	0.00	0.053	0.00	1043.63	29.02
KS12-2C_large_9	1880	67100	1.806	0.05	0.176	0.00	5.685	0.15	0.074	0.00	0.053	0.00	1044.30	26.67
KS12-2C_small_10	14400	49000	2.050	0.38	0.173	0.04	5.780	1.24	0.088	0.00	0.054	0.00	1010.23	########
KS12-2C_small_11	1480	47800	0.498	0.01	0.062	0.00	16.103	0.41	0.057	0.00	0.021	0.00	387.12	9.80
KS12-2C_small_12	1370	34000	0.456	0.01	0.059	0.00	16.906	0.38	0.056	0.00	0.020	0.00	369.66	8.30

Table S1. Detrital monazite U-Th-Pb data LASS-ICP-MS
Table S2. Detrital monazite Nd isotopic data LASS-ICP-MS
Table S3. Detrital monazite REE data LASS-ICP-MS

KS12-2C_small_14	78	50000	2.600	1.10	0.245	0.10	4.082	1.58	0.071	0.01	0.024	0.00	1446.81	##### #
KS12-2C_small_2	4570	15510	1.893	0.04	0.180	0.00	5.543	0.12	0.076	0.00	0.059	0.00	1068.09	22.10
KS12-2C_small_3	19500	16780	1.770	0.04	0.167	0.00	5.981	0.13	0.076	0.00	0.057	0.00	991.61	20.92
KS12-2C_small_4	3911	50700	1.729	0.04	0.167	0.00	5.974	0.13	0.074	0.00	0.052	0.00	995.77	21.47
KS12-2C_small_5	3540	59900	1.903	0.08	0.174	0.00	5.747	0.14	0.079	0.00	0.055	0.00	1027.06	24.36
KS12-2C_small_6	3910	23600	1.787	0.04	0.172	0.00	5.807	0.13	0.075	0.00	0.056	0.00	1021.61	22.17
KS12-2C_small_7	1641	38500	0.434	0.01	0.056	0.00	17.828	0.40	0.056	0.00	0.019	0.00	350.92	7.74
KS12-2C_small_8	2590	7240	2.129	0.05	0.192	0.00	5.198	0.11	0.079	0.00	0.064	0.00	1131.81	23.88
LookingGlass-Granite_1	2560	60200	0.395	0.02	0.053	0.00	18.868	0.50	0.054	0.00	0.017	0.00	332.49	8.65
LookingGlass-Granite_11	2920	52100	0.415	0.01	0.054	0.00	18.674	0.49	0.057	0.00	0.017	0.00	334.79	8.68
LookingGlass-Granite_12	1540	52300	0.418	0.02	0.054	0.00	18.587	0.61	0.056	0.00	0.017	0.00	336.75	10.91
LookingGlass-Granite_13	2280	58600	0.405	0.03	0.054	0.00	18.546	0.45	0.054	0.00	0.018	0.00	338.09	8.22
LookingGlass-Granite_2	4010	75900	0.439	0.02	0.054	0.00	18.605	0.47	0.058	0.00	0.017	0.00	335.34	8.39
LookingGlass-Granite_20	3010	55500	0.392	0.01	0.053	0.00	18.804	0.48	0.053	0.00	0.017	0.00	334.07	8.37
LookingGlass-Granite_23	2590	59100	0.427	0.02	0.054	0.00	18.519	0.53	0.057	0.00	0.017	0.00	337.64	9.53
LookingGlass-Granite_25	5690	48600	0.406	0.01	0.054	0.00	18.519	0.50	0.054	0.00	0.018	0.00	338.58	9.10
LookingGlass-Granite_3	2460	25810	0.377	0.02	0.051	0.00	19.455	0.60	0.052	0.00	0.017	0.00	323.38	9.81
LookingGlass-Granite_6	2320	54400	0.432	0.02	0.054	0.00	18.674	0.49	0.057	0.00	0.017	0.00	334.49	8.76
LookingGlass-Granite_8	2450	36600	0.382	0.01	0.051	0.00	19.573	0.47	0.054	0.00	0.017	0.00	320.78	7.55
PF12-1-Shields_1	2470	17000	1.568	0.04	0.163	0.00	6.143	0.14	0.070	0.00	0.052	0.00	974.13	20.87
PF12-1-Shields_10	808	48500	1.803	0.05	0.176	0.00	5.688	0.14	0.074	0.00	0.055	0.00	1043.82	25.59
PF12-1-Shields_11	889	53500	1.889	0.06	0.183	0.00	5.479	0.14	0.075	0.00	0.055	0.00	1081.66	26.89
PF12-1-Shields_12	1910	19500	1.728	0.05	0.174	0.00	5.757	0.14	0.073	0.00	0.054	0.00	1033.96	24.44
PF12-1-Shields_13	7440	32400	1.832	0.04	0.177	0.00	5.666	0.12	0.076	0.00	0.056	0.00	1046.14	21.89
PF12-1-Shields_14	7360	32800	1.822	0.04	0.176	0.00	5.692	0.13	0.076	0.00	0.056	0.00	1041.08	22.25
PF12-1-Shields_16	1105	57300	1.768	0.05	0.177	0.00	5.650	0.14	0.073	0.00	0.054	0.00	1052.92	26.10
PF12-1-Shields_17	2940	26400	2.124	0.06	0.193	0.00	5.181	0.13	0.080	0.00	0.052	0.00	1134.29	28.31
PF12-1-Shields_23	3360	30000	1.846	0.05	0.178	0.00	5.634	0.13	0.076	0.00	0.055	0.00	1051.53	24.07
PF12-1-Shields_6	518	16700	1.935	0.06	0.183	0.01	5.467	0.17	0.076	0.00	0.058	0.00	1082.57	32.06
PF12-1-Shields_7	510	6300	1.980	0.33	0.178	0.01	5.618	0.40	0.079	0.01	0.048	0.00	1050.04	71.89
PF12-1-Shields_8	1520	32400	2.232	0.06	0.205	0.00	4.888	0.12	0.080	0.00	0.062	0.00	1200.63	28.05

Table S1. Detrital monazite U-Th-Pb data LASS-ICP-MS
Table S2. Detrital monazite Nd isotopic data LASS-ICP-MS
Table S3. Detrital monazite REE data LASS-ICP-MS

PF12-1-Shields_9	1890	30200	2.229	0.06	0.203	0.00	4.931	0.12	0.080	0.00	0.063	0.00	1189.60	28.49
SixmileSchist_1	4900	17730	0.429	0.01	0.058	0.00	17.230	0.40	0.053	0.00	0.020	0.00	364.04	8.31
SixmileSchist_10	4350	17100	0.430	0.01	0.058	0.00	17.388	0.42	0.054	0.00	0.019	0.00	360.28	8.61
SixmileSchist_11	4410	23700	0.435	0.01	0.057	0.00	17.452	0.46	0.055	0.00	0.019	0.00	358.83	9.38
SixmileSchist_12	4080	20200	0.441	0.02	0.058	0.00	17.097	0.42	0.054	0.00	0.019	0.00	366.20	8.82
SixmileSchist_13	1550	25200	0.446	0.01	0.057	0.00	17.575	0.43	0.056	0.00	0.019	0.00	355.74	8.55
SixmileSchist_14	1477	28700	0.442	0.02	0.058	0.00	17.153	0.49	0.054	0.00	0.019	0.00	365.35	10.34
SixmileSchist_15	5080	21500	0.501	0.01	0.065	0.00	15.330	0.36	0.056	0.00	0.022	0.00	407.02	9.42
SixmileSchist_16	4690	24200	0.445	0.01	0.059	0.00	16.981	0.39	0.054	0.00	0.019	0.00	368.76	8.33
SixmileSchist_17	3980	34100	0.504	0.01	0.065	0.00	15.340	0.35	0.056	0.00	0.021	0.00	406.40	9.23
SixmileSchist_18	7280	23900	0.463	0.01	0.059	0.00	16.892	0.44	0.056	0.00	0.020	0.00	369.73	9.53
SixmileSchist_19	3270	26200	0.458	0.01	0.060	0.00	16.647	0.39	0.055	0.00	0.020	0.00	375.64	8.70
SixmileSchist_2	1540	26390	0.469	0.02	0.061	0.00	16.367	0.44	0.057	0.00	0.020	0.00	381.24	10.11
SixmileSchist_20	4830	27900	0.457	0.01	0.059	0.00	16.941	0.41	0.057	0.00	0.020	0.00	368.53	8.77
SixmileSchist_3	5400	16500	0.469	0.02	0.061	0.00	16.502	0.48	0.055	0.00	0.020	0.00	378.81	10.93
SixmileSchist_4	5550	20100	0.488	0.01	0.063	0.00	15.883	0.37	0.055	0.00	0.021	0.00	393.18	9.00
SixmileSchist_5	4970	25800	0.428	0.01	0.057	0.00	17.618	0.39	0.054	0.00	0.019	0.00	355.61	7.79
SixmileSchist_6	2450	17940	0.474	0.01	0.062	0.00	16.234	0.40	0.055	0.00	0.020	0.00	384.89	9.25
SixmileSchist_7	5520	23130	0.442	0.01	0.059	0.00	16.895	0.40	0.054	0.00	0.020	0.00	370.54	8.71
SixmileSchist_8	2040	25600	0.469	0.02	0.061	0.00	16.313	0.56	0.056	0.00	0.019	0.00	382.90	12.89
SixmileSchist_9	6390	17890	0.443	0.01	0.059	0.00	17.021	0.41	0.054	0.00	0.020	0.00	367.93	8.70
WCK12-1-Sandsuck_1	3330	30600	1.926	0.05	0.178	0.00	5.609	0.13	0.078	0.00	0.055	0.00	1053.22	22.96
WCK12-1-Sandsuck_2	862	35400	1.878	0.06	0.181	0.00	5.531	0.15	0.075	0.00	0.057	0.00	1071.49	27.48
WCK12-1-Sandsuck_3	2210	47300	1.958	0.06	0.185	0.00	5.405	0.13	0.076	0.00	0.057	0.00	1094.05	26.38
WCK12-1-Sandsuck_4	2860	45100	1.812	0.05	0.176	0.00	5.688	0.14	0.075	0.00	0.055	0.00	1043.28	25.57
WCK12-1-Sandsuck_5	935	36200	1.874	0.05	0.176	0.00	5.695	0.14	0.077	0.00	0.055	0.00	1038.59	24.82
WCK12-1-Sandsuck_6	2003	62900	1.857	0.05	0.177	0.00	5.656	0.14	0.075	0.00	0.054	0.00	1047.97	25.98
WCK12-1-Sandsuck_8	681	62400	1.948	0.06	0.181	0.01	5.537	0.17	0.077	0.00	0.054	0.00	1068.30	32.74

Table S1. Detrital monazite U-Th-Pb data LASS-ICP-MS
Table S2. Detrital monazite Nd isotopic data LASS-ICP-MS
Table S3. Detrital monazite REE data LASS-ICP-MS

Table S2:

Sample	Best Age Estimate	2s	Sm conc. (ppm)	2σ	Nd conc. (ppm)	2σ	Finalized present day 143Nd/144Nd	Initial 143Nd/144Nd	ENdi	2σ
01-TN-02A_1	1080.37	35	22390	220	110600	1200	0.5120	0.5112	-1.3	1.2
01-TN-02A_17	373.92	8	12690	140	84020	920	0.5122	0.5120	-2.8	1.3
01-TN-02A_2	1036.81	34	15210	180	91000	1200	0.5121	0.5114	1.9	1.3
01-TN-02A_21	438.90	10	17250	170	95750	910	0.5118	0.5114	-12.4	1.2
01-TN-02A_25	463.11	10	17650	220	98100	1100	0.5118	0.5115	-10.4	1.2
01-TN-02A_29	380.48	8	18670	200	93200	1100	0.5119	0.5116	-10.8	1.2
01-TN-02A_3	445.53	14	14630	180	93200	1100	0.5123	0.5120	-0.4	1.3
01-TN-02A_30	380.30	8	18230	170	95850	880	0.5119	0.5116	-10.2	1.2
01-TN-02A_31	1047.55	23	19720	190	95380	920	0.5121	0.5112	-1.7	1.2
01-TN-02A_36	1045.35	46	7484	79	66400	680	0.5118	0.5114	1.4	1.2
01-TN-02A_44	1070.20	29	21070	210	121900	1200	0.5120	0.5112	-0.2	1.0
01-TN-02A_49	1162.99	26	23320	190	111840	920	0.5121	0.5111	-0.5	1.1
01-TN-02A_51	467.80	18	25430	300	119200	1300	0.5119	0.5115	-10.7	1.0
01-TN04_1	370.29	9	19610	190	93520	860	0.5121	0.5118	-6.6	1.3
01-TN04_18	1025.50	28	17790	160	89150	810	0.5118	0.5110	-5.9	1.2
01-TN04_2	411.49	14	17510	140	101600	810	0.5121	0.5118	-6.0	1.3
01-TN05_12	407.01	9	28480	270	144900	1200	0.5120	0.5117	-8.2	1.1
01-TN05_19	484.45	12	16490	130	82830	670	0.5118	0.5114	-12.0	1.3
01-TN05_2	401.02	12	19060	170	94230	760	0.5123	0.5120	-2.1	1.2
01-TN05_28	414.82	11	21640	180	93910	790	0.5125	0.5121	0.9	1.2
01-TN05_29	468.10	12	14060	130	96650	840	0.5119	0.5116	-7.8	1.3
01-TN05_3	406.24	9	17040	160	87810	790	0.5122	0.5119	-4.0	1.4
01-TN05_31	423.61	12	16740	140	98560	830	0.5125	0.5122	2.1	1.2
01-TN05_32	420.35	12	13950	120	90300	740	0.5125	0.5122	2.4	1.3
01-TN05_36	380.43	9	21630	170	105060	800	0.5121	0.5118	-6.3	1.1

Table S1. Detrital monazite U-Th-Pb data LASS-ICP-MS
Table S2. Detrital monazite Nd isotopic data LASS-ICP-MS
Table S3. Detrital monazite REE data LASS-ICP-MS

01-TN05_37	1004.53	25	25300	210	111380	930	0.5120	0.5111	-4.7	1.1
01-TN05_38	1037.32	24	18770	160	96260	800	0.5121	0.5113	-0.9	1.2
01-TN05_42	1042.33	25	20150	160	107170	850	0.5121	0.5113	0.7	1.2
01-TN05_44	438.53	11	21350	180	104430	840	0.5122	0.5119	-3.9	1.2
01-TN05_45	470.79	19	13345	96	93770	710	0.5122	0.5119	-2.7	1.2
01-TN05_5	421.62	10	18440	160	81650	730	0.5124	0.5121	-0.6	1.4
01-TN05_9	461.06	12	14770	140	90010	850	0.5120	0.5117	-6.8	1.2
5-1-2_small_34	498.85	18	24890	310	136200	1400	0.5121	0.5117	-5.0	1.1
AsheGneiss_1	445.26	10	14860	140	80530	770	0.5120	0.5117	-7.5	1.4
AsheGneiss_10	464.83	11	14620	170	83990	960	0.5120	0.5116	-7.8	1.5
AsheGneiss_11	457.92	12	14200	170	85800	1000	0.5120	0.5117	-7.6	1.3
AsheGneiss_12	462.89	12	15580	190	88000	1100	0.5121	0.5117	-5.7	1.4
AsheGneiss_2	443.41	10	14700	150	78910	800	0.5120	0.5117	-6.9	1.3
AsheGneiss_3	442.56	11	13540	130	77320	730	0.5120	0.5117	-7.8	1.4
AsheGneiss_4	450.70	12	14800	130	81980	750	0.5120	0.5117	-7.3	1.4
AsheGneiss_5	446.28	11	14300	140	79910	800	0.5120	0.5117	-7.0	1.6
AsheGneiss_6	441.44	12	15590	130	84460	700	0.5120	0.5117	-6.6	1.4
AsheGneiss_7	455.61	11	15150	160	84860	910	0.5121	0.5117	-6.3	1.3
AsheGneiss_8	460.85	12	14370	140	83540	910	0.5120	0.5117	-7.6	1.5
AsheGneiss_9	454.15	13	16140	190	84330	980	0.5120	0.5117	-7.6	1.3
AsheSchist-newrow_1	451.34	11	15380	160	80890	800	0.5121	0.5118	-5.0	1.4
AsheSchist-newrow_10	440.68	11	17350	170	89130	790	0.5121	0.5118	-5.7	1.3
AsheSchist-newrow_11	455.76	12	16800	150	89460	800	0.5121	0.5117	-6.4	1.3
AsheSchist-newrow_2	441.30	11	15420	180	81940	840	0.5121	0.5118	-5.9	1.4
AsheSchist-newrow_3	450.79	11	15870	150	83210	710	0.5121	0.5117	-6.6	1.4
AsheSchist-newrow_4	444.81	11	13550	130	76100	710	0.5121	0.5117	-6.2	1.5
AsheSchist-newrow_5	442.85	12	14900	160	81570	840	0.5121	0.5118	-5.8	1.5
AsheSchist-newrow_6	443.85	12	15240	150	84730	800	0.5121	0.5118	-5.8	1.3
AsheSchist-newrow_7	439.54	12	15660	140	83980	740	0.5120	0.5117	-6.9	1.2

Table S1. Detrital monazite U-Th-Pb data LASS-ICP-MS
Table S2. Detrital monazite Nd isotopic data LASS-ICP-MS
Table S3. Detrital monazite REE data LASS-ICP-MS

AsheSchist-newrow_8	443.78	11	14820	150	83080	830	0.5121	0.5118	-6.1	1.4
AsheSchist-newrow_9	442.76	10	17490	170	90080	850	0.5121	0.5117	-6.5	1.3
Carter512A_a_1	1044.95	23	14820	130	92600	910	0.5119	0.5113	-0.6	1.2
Carter512A_a_11	1081.72	25	16400	160	87030	910	0.5120	0.5112	-0.6	1.3
Carter512A_a_12	1144.01	27	20250	240	102000	1500	0.5120	0.5111	-0.6	1.2
Carter512A_a_14	1064.15	28	11730	130	82710	880	0.5119	0.5113	0.8	1.2
Carter512A_a_15	1073.96	26	11570	120	82260	860	0.5119	0.5113	1.3	1.2
Carter512A_a_2	1032.18	39	12130	120	90780	900	0.5119	0.5114	1.0	1.2
Carter512A_a_5	1054.39	51	23280	650	114600	3400	0.5121	0.5112	-1.5	1.1
Carter512A_a_6	1044.88	25	22580	250	100700	1100	0.5123	0.5113	0.7	1.1
Carter512A_a_7	1043.58	24	22040	240	99690	1100	0.5122	0.5113	0.2	1.1
Carter512A_a_8	1035.34	27	18430	210	98000	1100	0.5121	0.5113	0.5	1.0
Carter512A_a_9	1057.66	23	17450	180	95650	960	0.5117	0.5109	-6.8	1.1
Carter512A_a_large_1	973.93	52	10790	120	77560	800	0.5120	0.5114	1.0	1.3
Carter512A_a_large_3	515.18	21	11810	110	84860	770	0.5121	0.5118	-3.2	1.2
Carter512A_a_large_4	1195.27	30	19110	190	96810	960	0.5121	0.5111	1.1	1.2
Carter512A_a_large_5	1130.48	41	19610	230	97100	1300	0.5122	0.5112	1.4	1.3
Carter512A_a_large_6	1157.41	26	20220	190	97780	940	0.5120	0.5110	-2.9	1.0
Carter512A_b_1	1099.01	26	20910	210	97850	980	0.5121	0.5111	-1.5	1.1
Carter512A_b_10	1060.75	27	13380	150	91820	990	0.5119	0.5113	0.6	1.2
Carter512A_b_11	1064.62	32	18350	120	105300	910	0.5121	0.5113	1.5	1.3
Carter512A_b_13	1030.52	26	15280	130	96220	910	0.5120	0.5113	0.5	1.3
Carter512A_b_15	1141.11	31	23890	240	108500	1100	0.5123	0.5113	1.7	1.1
Carter512A_b_17	982.41	33	8754	79	73260	680	0.5119	0.5114	0.3	1.3
Carter512A_b_18	1002.40	24	17510	180	90480	900	0.5118	0.5110	-5.8	1.3
Carter512A_b_2	1028.20	23	15440	160	91730	950	0.5120	0.5113	-0.8	1.3
Carter512A_b_5	1065.82	36	18080	280	95400	1500	0.5119	0.5111	-2.7	1.2
Carter512A_b_6	1040.52	26	25330	390	106100	1600	0.5123	0.5113	0.2	1.1
Carter512A_b_7	736.10	89	29450	970	135200	3100	0.5122	0.5115	-2.8	1.2

Table S1. Detrital monazite U-Th-Pb data LASS-ICP-MS
Table S2. Detrital monazite Nd isotopic data LASS-ICP-MS
Table S3. Detrital monazite REE data LASS-ICP-MS

Carter512A_b_9	1052.27	34	22100	350	116600	2100	0.5121	0.5113	0.1	1.1
Carter512A_b_large_2	1198.70	31	19310	170	100400	1000	0.5119	0.5109	-3.0	1.1
Carter512A_b_large_3	1036.12	27	18770	180	94860	860	0.5118	0.5110	-5.6	1.2
Carter512A_b_large_5	1088.79	32	19130	160	97880	870	0.5121	0.5112	-0.4	1.2
FB1_1	461.59	13	17170	160	91110	850	0.5121	0.5117	-6.0	1.5
FB1_10	457.32	13	17980	180	93400	930	0.5121	0.5117	-6.1	1.2
FB1_11	462.74	12	18070	180	93540	930	0.5121	0.5118	-5.5	1.3
FB1_12	458.99	14	17920	270	90000	1200	0.5119	0.5116	-9.3	1.2
FB1_13	462.45	12	18650	160	98990	830	0.5121	0.5118	-5.2	1.3
FB1_15	458.06	12	16110	160	92320	940	0.5118	0.5115	-10.2	1.3
FB1_16	455.80	12	16410	140	94890	830	0.5121	0.5118	-5.5	1.2
FB1_17	455.34	13	15050	150	92090	810	0.5119	0.5116	-8.3	1.2
FB1_18	455.98	17	18640	150	100320	850	0.5121	0.5117	-6.0	1.2
FB1_19	441.31	15	15770	130	96530	820	0.5121	0.5118	-5.8	1.3
FB1_2	344.49	10	9783	85	76140	690	0.5123	0.5121	-1.1	1.3
FB1_20	433.87	14	16680	140	92420	800	0.5121	0.5117	-6.5	1.3
FB1_21	445.52	11	18310	150	93750	760	0.5121	0.5117	-7.0	1.1
FB1_23	330.69	8	16250	140	82050	700	0.5122	0.5120	-4.6	1.3
FB1_26	331.41	9	15630	150	78580	770	0.5123	0.5121	-2.6	1.3
FB1_27	324.83	8	15890	170	77220	830	0.5124	0.5121	-2.0	1.2
FB1_29	449.43	12	17210	160	89060	890	0.5121	0.5117	-6.1	1.2
FB1_3	455.95	12	17940	160	89770	800	0.5122	0.5118	-4.4	1.2
FB1_30	447.75	12	9449	89	78610	740	0.5118	0.5116	-9.9	1.3
FB1_31	466.55	14	18150	220	94900	1100	0.5122	0.5118	-4.0	1.4
FB1_32	399.06	17	17690	160	102700	1000	0.5121	0.5118	-6.3	1.1
FB1_33	448.73	11	20540	190	101520	970	0.5120	0.5117	-7.3	1.1
FB1_4	500.99	16	27510	250	97110	890	0.5119	0.5114	-12.2	1.3
FB1_6	474.49	12	15300	140	90440	810	0.5121	0.5118	-5.2	1.4
FB1_7	399.93	30	17530	150	92540	760	0.5121	0.5118	-7.0	1.3

Table S1. Detrital monazite U-Th-Pb data LASS-ICP-MS
Table S2. Detrital monazite Nd isotopic data LASS-ICP-MS
Table S3. Detrital monazite REE data LASS-ICP-MS

FB1_8	456.78	12	18280	190	98680	970	0.5121	0.5117	-6.1	1.2
FB1_9	458.06	16	16760	160	89430	830	0.5121	0.5117	-5.8	1.3
FB10_1	1021.31	25	16830	160	88090	710	0.5120	0.5112	-2.7	1.3
FB10_10	464.74	13	19420	180	101470	940	0.5121	0.5118	-5.5	1.2
FB10_11	437.24	18	22450	220	100900	1100	0.5121	0.5117	-7.4	1.1
FB10_12	456.65	14	18210	150	96330	890	0.5121	0.5117	-6.5	1.2
FB10_13	455.51	14	16780	140	95530	770	0.5120	0.5117	-6.9	1.4
FB10_14	458.10	11	18240	150	99220	810	0.5120	0.5117	-6.5	1.2
FB10_16	465.56	12	18640	160	98630	800	0.5120	0.5116	-7.8	1.3
FB10_17	460.42	12	19630	220	100600	1100	0.5121	0.5117	-6.2	1.3
FB10_18	460.27	12	19580	170	103280	900	0.5120	0.5117	-6.8	1.2
FB10_19	1321.48	35	27360	390	142700	1400	0.5120	0.5110	2.2	1.2
FB10_2	446.15	13	17890	140	96370	710	0.5120	0.5117	-7.0	1.3
FB10_20	1035.32	27	19420	200	94620	910	0.5120	0.5111	-3.4	1.2
FB10_21	454.64	13	19200	160	94170	770	0.5120	0.5117	-7.3	1.1
FB10_22	455.72	12	17390	160	103500	930	0.5120	0.5117	-6.5	1.1
FB10_23	938.80	29	19460	180	99720	900	0.5119	0.5112	-4.1	1.1
FB10_24	471.12	13	16610	150	98770	890	0.5119	0.5116	-8.4	1.2
FB10_25	475.98	18	13220	140	91030	950	0.5120	0.5118	-5.1	1.4
FB10_26	461.19	12	16960	160	99660	950	0.5120	0.5117	-6.6	1.2
FB10_27	469.63	15	16400	120	100200	800	0.5120	0.5117	-5.8	1.1
FB10_28	462.57	12	18850	180	105200	1000	0.5120	0.5117	-6.3	1.2
FB10_29	466.81	12	12690	120	89540	870	0.5118	0.5116	-9.0	1.3
FB10_3	462.26	14	18560	170	100800	900	0.5121	0.5117	-6.4	1.3
FB10_30	468.69	16	15950	170	103720	980	0.5120	0.5117	-6.2	1.2
FB10_31	459.51	14	19640	190	103090	880	0.5120	0.5117	-7.0	1.2
FB10_32	481.87	18	12780	120	97310	940	0.5120	0.5117	-5.7	1.1
FB10_33	453.89	13	24500	220	107400	1000	0.5121	0.5117	-6.7	1.2
FB10_34	465.70	14	18810	170	98710	940	0.5121	0.5117	-6.3	1.2

Table S1. Detrital monazite U-Th-Pb data LASS-ICP-MS
Table S2. Detrital monazite Nd isotopic data LASS-ICP-MS
Table S3. Detrital monazite REE data LASS-ICP-MS

FB10_35	461.91	12	18460	170	102230	940	0.5121	0.5117	-6.3	1.1
FB10_36	453.70	13	14700	140	89900	750	0.5117	0.5114	-12.0	1.3
FB10_37	464.31	17	15140	140	89810	760	0.5116	0.5113	-14.3	1.1
FB10_4	458.93	12	16000	150	97660	900	0.5120	0.5117	-6.8	1.3
FB10_5	1044.08	28	14800	120	91740	750	0.5119	0.5113	-0.7	1.3
FB10_6	453.24	12	18920	170	102900	900	0.5121	0.5117	-6.3	1.3
FB10_8	1109.78	41	14110	120	96790	830	0.5120	0.5113	2.4	1.4
FB11_1	494.67	13	28530	310	101800	1100	0.5119	0.5113	-13.4	1.4
FB11_10	455.62	10	17540	150	96900	870	0.5121	0.5117	-6.4	1.2
FB11_11	453.46	10	17430	180	98200	1000	0.5120	0.5117	-7.6	1.4
FB11_12	461.25	10	18100	300	94500	1500	0.5120	0.5117	-6.8	1.2
FB11_13	463.75	10	18750	180	102610	970	0.5121	0.5117	-6.3	1.2
FB11_14	459.19	10	18380	190	98500	1000	0.5121	0.5118	-5.4	1.2
FB11_15	458.94	11	18380	210	102300	1100	0.5120	0.5117	-6.8	1.3
FB11_16	463.42	11	18320	210	99960	1300	0.5120	0.5117	-7.1	1.2
FB11_17	458.58	10	19530	220	99000	1100	0.5122	0.5118	-4.7	1.3
FB11_18	460.86	11	17580	170	101360	980	0.5120	0.5117	-7.2	1.2
FB11_19	1003.00	22	15780	120	98340	790	0.5118	0.5112	-2.7	1.2
FB11_2	499.52	12	28770	270	102640	960	0.5118	0.5113	-14.5	1.1
FB11_20	468.89	10	17540	210	99510	1100	0.5119	0.5116	-8.1	1.1
FB11_21	1064.53	26	14580	160	102800	1100	0.5117	0.5111	-3.5	1.2
FB11_22	466.93	12	14640	140	96860	950	0.5120	0.5117	-6.2	1.2
FB11_23	453.17	12	15420	170	99000	1100	0.5120	0.5118	-5.6	1.3
FB11_24	462.98	11	18790	210	100100	1200	0.5121	0.5117	-5.8	1.2
FB11_25	462.70	11	18430	180	98600	1000	0.5120	0.5116	-7.9	1.1
FB11_26	459.71	10	18960	200	98100	1000	0.5121	0.5117	-6.8	1.2
FB11_27	459.07	10	19200	200	100700	1000	0.5121	0.5117	-6.6	1.2
FB11_28	464.17	11	19500	210	106100	1200	0.5121	0.5117	-6.2	1.1
FB11_3	453.28	11	15360	150	100440	990	0.5121	0.5118	-5.4	1.3

Table S1. Detrital monazite U-Th-Pb data LASS-ICP-MS
Table S2. Detrital monazite Nd isotopic data LASS-ICP-MS
Table S3. Detrital monazite REE data LASS-ICP-MS

FB11_4	460.08	10	19110	180	101830	940	0.5121	0.5117	-6.0	1.2
FB11_5	463.60	10	18950	150	101510	780	0.5120	0.5116	-8.0	1.4
FB11_6	459.62	10	19090	190	101870	960	0.5121	0.5117	-6.4	1.2
FB11_7	463.30	10	18470	190	98310	950	0.5121	0.5117	-5.7	1.3
FB11_8	461.95	10	18120	190	98800	970	0.5121	0.5117	-6.0	1.3
FB11_9	457.96	10	19160	190	101600	1000	0.5121	0.5117	-6.5	1.2
FB13_1	1000.13	27	23310	210	110270	980	0.5119	0.5111	-4.6	1.2
FB13_10	414.92	12	17720	150	91060	760	0.5118	0.5115	-12.1	1.3
FB13_11	451.26	11	19520	180	97810	840	0.5121	0.5118	-5.3	1.2
FB13_12	459.54	11	17930	180	96680	930	0.5120	0.5117	-6.7	1.2
FB13_13	447.52	15	16690	140	95110	730	0.5120	0.5117	-6.4	1.2
FB13_16	447.91	11	17570	150	97710	840	0.5120	0.5117	-7.9	1.3
FB13_17	447.83	12	20600	170	101530	830	0.5121	0.5118	-5.5	1.2
FB13_2	459.94	15	18890	160	100650	830	0.5121	0.5117	-6.5	1.4
FB13_3	462.51	13	17950	160	96720	910	0.5120	0.5117	-7.6	1.2
FB13_4	455.39	13	15130	130	86230	700	0.5120	0.5117	-6.5	1.3
FB13_5	456.09	14	14510	140	92260	850	0.5119	0.5116	-8.0	1.4
FB13_7	454.95	18	18280	170	103980	930	0.5121	0.5118	-5.9	1.3
FB13_8	457.69	12	19820	160	102170	810	0.5121	0.5118	-5.5	1.2
FB14_1	443.03	13	17730	140	96440	760	0.5120	0.5117	-7.0	1.4
FB14_10	463.14	21	15100	130	100620	890	0.5120	0.5117	-6.5	1.2
FB14_11	467.28	12	17370	190	94100	1000	0.5121	0.5117	-6.2	1.2
FB14_12	464.86	13	18410	190	99850	1000	0.5120	0.5117	-6.6	1.1
FB14_13	460.88	15	16050	160	98210	960	0.5121	0.5118	-5.1	1.3
FB14_14	450.51	17	16150	170	91080	950	0.5117	0.5114	-13.3	1.3
FB14_15	444.20	13	17770	190	102600	1100	0.5121	0.5118	-5.8	1.3
FB14_17	459.37	14	18090	160	100910	890	0.5121	0.5117	-6.1	1.2
FB14_18	1080.29	31	15500	160	91880	820	0.5121	0.5114	3.5	1.2
FB14_19	457.84	10	18270	160	98140	870	0.5121	0.5118	-5.5	1.2

Table S1. Detrital monazite U-Th-Pb data LASS-ICP-MS
Table S2. Detrital monazite Nd isotopic data LASS-ICP-MS
Table S3. Detrital monazite REE data LASS-ICP-MS

FB14_2	453.79	13	17780	130	93280	710	0.5121	0.5117	-6.4	1.2
FB14_20	449.60	13	19180	170	102430	930	0.5121	0.5117	-6.4	1.3
FB14_21	459.53	12	19190	200	102100	990	0.5120	0.5117	-7.7	1.2
FB14_22	454.17	13	10100	100	71790	740	0.5117	0.5115	-11.0	1.3
FB14_23	457.84	11	19380	190	92220	810	0.5119	0.5115	-11.2	1.2
FB14_24	359.97	21	20320	170	115110	960	0.5121	0.5118	-7.1	1.1
FB14_25	456.48	11	17800	170	94610	870	0.5120	0.5117	-6.8	1.2
FB14_26	1038.16	27	18130	200	92700	860	0.5118	0.5110	-5.9	1.4
FB14_27	455.09	17	15820	130	103080	920	0.5120	0.5117	-7.0	1.1
FB14_28	458.35	11	17470	140	95050	770	0.5118	0.5114	-12.2	1.2
FB14_29	1045.31	27	15790	130	102660	880	0.5118	0.5111	-3.4	1.1
FB14_3	453.60	12	21710	190	103590	860	0.5121	0.5117	-6.7	1.2
FB14_4	454.22	12	19290	170	102320	840	0.5121	0.5117	-6.5	1.3
FB14_5	460.55	13	15860	150	94080	910	0.5118	0.5115	-9.9	1.2
FB14_6	454.33	12	18280	180	97450	940	0.5121	0.5117	-6.3	1.2
FB14_7	455.67	15	17180	150	100540	910	0.5120	0.5117	-6.3	1.2
FB14_8	454.32	14	16480	150	94430	830	0.5120	0.5117	-7.0	1.3
FB14_9	456.57	12	19230	170	89640	790	0.5121	0.5118	-5.7	1.3
FB15_1	462.70	11	17920	170	94410	840	0.5121	0.5117	-6.4	1.3
FB15_10	467.64	11	17980	180	92460	870	0.5120	0.5117	-6.8	1.3
FB15_11	463.33	11	16830	160	94990	890	0.5120	0.5117	-6.7	1.2
FB15_12	466.26	10	19210	190	100100	1000	0.5121	0.5117	-5.7	1.2
FB15_13	463.89	10	20850	210	106700	1100	0.5121	0.5117	-5.9	1.2
FB15_14	457.81	11	18620	180	96060	860	0.5121	0.5118	-5.8	1.2
FB15_15	455.67	11	18590	170	95830	890	0.5120	0.5116	-7.9	1.2
FB15_16	459.85	11	18510	190	102200	1000	0.5121	0.5117	-6.0	1.3
FB15_17	340.68	8	13700	140	86160	930	0.5121	0.5119	-5.2	1.2
FB15_18	458.83	10	18700	190	99660	1000	0.5120	0.5117	-6.9	1.3
FB15_19	472.25	12	12430	230	70400	1300	0.5120	0.5117	-6.3	1.5

Table S1. Detrital monazite U-Th-Pb data LASS-ICP-MS
Table S2. Detrital monazite Nd isotopic data LASS-ICP-MS
Table S3. Detrital monazite REE data LASS-ICP-MS

FB15_20	462.83	10	18800	200	98800	1100	0.5120	0.5117	-6.7	1.1
FB15_21	463.78	10	18880	190	97600	1000	0.5121	0.5117	-6.5	1.1
FB15_22	469.11	10	18290	200	98600	1100	0.5120	0.5116	-7.6	1.2
FB15_23	468.81	12	17740	170	95230	990	0.5120	0.5116	-7.5	1.2
FB15_24	457.93	12	21860	220	93310	990	0.5122	0.5117	-6.1	1.2
FB15_25	459.98	11	17680	180	98930	980	0.5121	0.5117	-6.2	1.2
FB15_26	456.19	10	17340	160	95660	880	0.5120	0.5117	-6.9	1.1
FB15_29	471.00	11	19850	220	103800	1200	0.5120	0.5117	-6.8	1.2
FB15_3	454.79	19	17410	170	97140	940	0.5120	0.5117	-6.9	1.3
FB15_30	463.55	11	18820	210	102500	1000	0.5120	0.5117	-7.1	1.1
FB15_31	467.06	11	19530	190	97830	950	0.5121	0.5117	-6.2	1.1
FB15_32	457.57	11	18460	180	108900	1100	0.5121	0.5117	-5.9	1.0
FB15_4	463.35	11	18140	160	96730	890	0.5120	0.5117	-6.7	1.3
FB15_5	460.83	10	19930	190	99140	890	0.5121	0.5117	-6.5	1.3
FB15_6	464.51	10	17070	150	95880	840	0.5120	0.5117	-6.5	1.2
FB15_7	466.65	12	17520	160	97310	940	0.5120	0.5117	-6.5	1.3
FB15_8	470.60	13	14800	160	95810	930	0.5120	0.5117	-6.7	1.2
FB15_9	472.15	11	18480	210	97700	1100	0.5121	0.5117	-6.3	1.2
FB1SR-AsheSchist_1	456.85	10	14380	200	77510	940	0.5121	0.5118	-4.5	1.3
FB1SR-AsheSchist_10	473.05	11	14690	170	79530	980	0.5121	0.5117	-6.1	1.3
FB1SR-AsheSchist_11	473.72	11	13410	140	73070	760	0.5121	0.5117	-5.7	1.5
FB1SR-AsheSchist_12	452.91	11	15140	190	81770	990	0.5121	0.5118	-5.5	1.5
FB1SR-AsheSchist_13	461.05	10	15490	160	84310	940	0.5121	0.5118	-4.9	1.4
FB1SR-AsheSchist_2	457.98	12	13660	160	77330	900	0.5121	0.5118	-4.9	1.5
FB1SR-AsheSchist_3	450.56	10	14490	160	78160	870	0.5121	0.5118	-5.2	1.2
FB1SR-AsheSchist_4	465.06	11	14020	180	74740	950	0.5121	0.5117	-6.2	1.4
FB1SR-AsheSchist_5	456.05	11	14790	190	78070	950	0.5121	0.5118	-5.8	1.3
FB1SR-AsheSchist_6	455.13	12	14330	160	78750	860	0.5121	0.5118	-5.1	1.4
FB1SR-AsheSchist_8	461.89	11	14720	140	80500	1000	0.5121	0.5118	-5.5	1.4

Table S1. Detrital monazite U-Th-Pb data LASS-ICP-MS
Table S2. Detrital monazite Nd isotopic data LASS-ICP-MS
Table S3. Detrital monazite REE data LASS-ICP-MS

FB1SR-AsheSchist_9	469.66	11	14480	230	78100	1200	0.5121	0.5118	-4.9	1.5
FB2_1	451.75	11	18730	240	94990	910	0.5120	0.5117	-7.6	1.3
FB2_10	456.89	10	16880	160	95790	900	0.5118	0.5115	-10.5	1.1
FB2_11	462.86	11	15650	150	92180	930	0.5119	0.5116	-9.1	1.2
FB2_12	455.19	10	19900	230	100800	1000	0.5120	0.5117	-7.1	1.2
FB2_13	455.06	10	18840	170	99490	900	0.5120	0.5117	-6.8	1.2
FB2_15	456.57	12	17830	170	95560	890	0.5120	0.5117	-7.2	1.3
FB2_16	456.83	12	18780	180	100630	950	0.5121	0.5117	-6.6	1.1
FB2_17	464.21	11	18310	200	103100	1100	0.5120	0.5116	-7.6	1.2
FB2_18	474.74	12	19180	190	105100	1100	0.5121	0.5117	-6.0	1.1
FB2_19	458.67	11	18550	170	99860	940	0.5120	0.5117	-7.2	1.1
FB2_2	462.06	12	18080	210	95500	1000	0.5120	0.5117	-6.7	1.4
FB2_20	462.52	11	18720	190	98260	980	0.5121	0.5117	-6.4	1.2
FB2_21	460.66	11	18580	190	98510	990	0.5120	0.5117	-6.7	1.1
FB2_24	466.76	12	18030	190	96530	950	0.5121	0.5117	-6.2	1.2
FB2_25	471.33	12	18930	220	102300	1100	0.5121	0.5117	-5.7	1.1
FB2_26	457.21	11	19740	170	101130	970	0.5120	0.5117	-7.3	1.1
FB2_27	452.69	15	18340	130	106820	870	0.5121	0.5118	-5.8	1.2
FB2_3	458.15	12	16760	160	96150	850	0.5121	0.5118	-5.7	1.2
FB2_4	456.99	12	19870	190	101270	960	0.5121	0.5118	-5.7	1.3
FB2_5	462.38	12	14490	140	88320	800	0.5119	0.5116	-7.7	1.3
FB2_6	328.36	8	19030	180	85260	820	0.5122	0.5119	-6.5	1.4
FB2_7	457.43	13	17880	150	89550	740	0.5117	0.5114	-12.9	1.3
FB2_8	457.61	10	18080	160	91520	830	0.5121	0.5118	-5.5	1.3
FB2_9	450.62	10	17390	230	99890	1000	0.5120	0.5117	-7.5	1.2
FB2lowrow_1	331.22	7	16200	160	85370	820	0.5120	0.5118	-8.5	1.3
FB2lowrow_10	413.51	21	18400	160	93920	740	0.5121	0.5118	-6.2	1.3
FB2lowrow_11	463.05	13	16690	150	86060	780	0.5119	0.5116	-9.5	1.3
FB2lowrow_12	462.52	12	16380	160	95610	880	0.5120	0.5117	-6.4	1.2

Table S1. Detrital monazite U-Th-Pb data LASS-ICP-MS
Table S2. Detrital monazite Nd isotopic data LASS-ICP-MS
Table S3. Detrital monazite REE data LASS-ICP-MS

FB2lowrow_13	354.49	11	16040	180	88760	910	0.5120	0.5118	-8.1	1.4
FB2lowrow_14	463.17	12	17910	160	96380	870	0.5120	0.5117	-7.4	1.2
FB2lowrow_15	388.38	10	15340	140	83950	740	0.5119	0.5116	-9.7	1.2
FB2lowrow_16	339.75	10	17140	150	89110	760	0.5120	0.5117	-9.6	1.2
FB2lowrow_17	463.54	11	15190	150	90730	820	0.5120	0.5117	-7.2	1.2
FB2lowrow_18	462.49	11	14700	120	85930	710	0.5118	0.5115	-10.5	1.3
FB2lowrow_19	451.07	10	17700	190	91830	890	0.5120	0.5117	-7.0	1.3
FB2lowrow_2	460.23	11	17130	160	93570	870	0.5120	0.5117	-7.1	1.4
FB2lowrow_20	465.95	11	14200	140	93790	890	0.5119	0.5116	-8.2	1.2
FB2lowrow_21	460.56	12	13590	120	91820	810	0.5118	0.5115	-9.7	1.3
FB2lowrow_22	449.91	13	15160	140	88380	830	0.5122	0.5119	-4.0	1.4
FB2lowrow_24	463.28	12	14010	150	92030	960	0.5121	0.5118	-4.8	1.3
FB2lowrow_25	461.63	13	14900	150	92950	900	0.5120	0.5117	-5.9	1.3
FB2lowrow_28	652.83	16	14800	160	82800	900	0.5120	0.5115	-5.0	1.2
FB2lowrow_29	460.31	11	15920	130	85090	700	0.5120	0.5117	-6.9	1.3
FB2lowrow_3	374.75	10	19070	190	94880	910	0.5121	0.5118	-6.1	1.3
FB2lowrow_30	369.68	14	18430	210	104530	990	0.5121	0.5118	-6.3	1.3
FB2lowrow_31	466.30	13	17390	190	100500	1100	0.5121	0.5117	-5.8	1.2
FB2lowrow_4	468.29	13	14950	150	88230	870	0.5118	0.5115	-10.1	1.4
FB2lowrow_5	343.60	8	17240	150	102970	900	0.5121	0.5118	-7.0	1.3
FB2lowrow_6	340.96	7	14960	150	84440	820	0.5119	0.5117	-10.4	1.2
FB2lowrow_7	333.81	8	15490	150	84780	790	0.5120	0.5117	-9.3	1.4
FB2lowrow_8	330.12	8	17690	210	93800	1000	0.5120	0.5118	-8.6	1.3
FB2lowrow_9	356.68	9	20630	160	98370	810	0.5122	0.5119	-5.4	1.4
FB3_10	450.08	10	18260	180	92400	910	0.5119	0.5115	-10.3	1.3
FB3_11	457.94	10	20510	200	94960	900	0.5122	0.5118	-5.1	1.2
FB3_12	460.11	11	19590	190	98020	960	0.5119	0.5115	-9.9	1.2
FB3_13	447.03	11	16390	160	90440	880	0.5120	0.5117	-6.7	1.3
FB3_14	462.46	12	14680	140	92590	870	0.5122	0.5119	-3.4	1.4

Table S1. Detrital monazite U-Th-Pb data LASS-ICP-MS
Table S2. Detrital monazite Nd isotopic data LASS-ICP-MS
Table S3. Detrital monazite REE data LASS-ICP-MS

FB3_16	463.86	11	16110	170	92320	910	0.5121	0.5117	-5.9	1.3
FB3_18	331.49	8	19000	200	99660	1000	0.5121	0.5119	-7.0	1.3
FB3_19	458.08	10	10280	100	71420	710	0.5117	0.5114	-12.1	1.5
FB3_20	338.29	9	10640	250	55700	1300	0.5120	0.5117	-9.1	1.5
FB3_21	461.88	10	20090	200	104800	1100	0.5121	0.5117	-6.2	1.2
FB3_22	381.76	8	18860	190	95070	960	0.5120	0.5117	-8.9	1.3
FB3_23	455.34	10	14380	140	88310	860	0.5118	0.5115	-11.0	1.4
FB3_24	456.20	11	21250	200	102570	960	0.5121	0.5117	-6.4	1.2
FB3_25	458.68	12	21460	190	102980	920	0.5121	0.5117	-7.0	1.2
FB3_26	373.74	9	17450	190	95200	1000	0.5119	0.5117	-9.9	1.3
FB3_27	379.64	9	17840	200	94400	1000	0.5120	0.5117	-9.2	1.3
FB3_28	461.03	10	18230	180	99000	1000	0.5119	0.5116	-9.0	1.2
FB3_29	459.78	10	21010	230	103000	1100	0.5121	0.5118	-5.5	1.2
FB3_3	465.78	11	17220	160	95180	880	0.5119	0.5116	-8.2	1.3
FB3_30	334.69	8	32290	310	99200	990	0.5126	0.5121	-1.6	1.2
FB3_33	442.75	14	10634	88	87700	770	0.5116	0.5114	-13.4	1.3
FB3_34	327.54	8	16420	220	91300	1100	0.5119	0.5117	-10.0	1.3
FB3_35	335.83	8	31300	310	107500	1000	0.5125	0.5121	-1.6	1.2
FB3_36	454.18	11	18010	170	98540	980	0.5119	0.5116	-9.7	1.2
FB3_4	460.55	10	15180	140	88750	810	0.5119	0.5116	-8.6	1.3
FB3_5	367.58	9	16980	150	90880	760	0.5120	0.5117	-9.1	1.3
FB3_6	456.44	11	18240	170	93030	870	0.5121	0.5117	-6.1	1.4
FB3_7	458.26	10	18370	150	93080	760	0.5121	0.5117	-6.6	1.2
FB3_9	456.29	11	15640	150	87650	810	0.5118	0.5114	-11.8	1.3
FB4_1	485.45	12	27910	270	99170	960	0.5119	0.5113	-13.6	1.3
FB4_10	428.64	12	16070	240	93800	1300	0.5120	0.5117	-7.8	1.3
FB4_11	446.43	10	16770	130	94550	820	0.5121	0.5118	-5.4	1.1
FB4_12	457.01	10	18960	180	99360	920	0.5121	0.5117	-5.9	1.2
FB4_13	458.03	10	15570	150	91600	910	0.5120	0.5116	-7.8	1.2

Table S1. Detrital monazite U-Th-Pb data LASS-ICP-MS
Table S2. Detrital monazite Nd isotopic data LASS-ICP-MS
Table S3. Detrital monazite REE data LASS-ICP-MS

FB4_14	458.33	10	19040	290	95700	1100	0.5121	0.5117	-6.4	1.5
FB4_15	450.54	10	18450	180	98130	910	0.5120	0.5117	-7.3	1.2
FB4_16	461.00	11	15520	180	92850	870	0.5119	0.5116	-8.4	1.2
FB4_17	462.82	10	16510	170	89420	900	0.5120	0.5116	-7.7	1.3
FB4_18	328.31	8	16970	170	87920	910	0.5120	0.5117	-9.4	1.3
FB4_2	490.85	13	28740	300	102000	1100	0.5118	0.5113	-14.3	1.2
FB4_20	332.35	8	9029	94	73800	750	0.5121	0.5120	-5.0	1.3
FB4_21	338.66	7	16650	160	93260	880	0.5120	0.5118	-8.1	1.2
FB4_22	459.74	24	13810	130	89870	830	0.5122	0.5119	-2.4	1.2
FB4_23	325.74	7	18790	200	97900	1000	0.5121	0.5118	-8.0	1.2
FB4_24	453.36	11	19440	210	93130	910	0.5119	0.5116	-9.4	1.3
FB4_25	432.33	10	17960	220	96000	1100	0.5120	0.5117	-7.2	1.2
FB4_26	454.47	13	18910	230	98100	1200	0.5121	0.5118	-5.3	1.3
FB4_27	410.59	23	9500	140	55020	810	0.5123	0.5121	-0.9	1.2
FB4_28	449.93	10	18930	170	100220	930	0.5119	0.5115	-10.0	1.3
FB4_29	326.04	7	18150	160	92600	800	0.5121	0.5118	-7.6	1.2
FB4_30	455.64	10	15910	150	91450	840	0.5118	0.5115	-10.5	1.1
FB4_31	456.87	10	14560	140	88210	820	0.5118	0.5115	-11.1	1.3
FB4_32	450.43	10	25020	250	106900	1100	0.5123	0.5119	-3.1	1.1
FB4_4	466.12	13	10181	93	81850	740	0.5116	0.5114	-12.1	1.3
FB4_6	475.46	19	16800	160	94490	900	0.5120	0.5117	-7.0	1.2
FB4_7	326.09	8	16460	160	90430	850	0.5120	0.5118	-9.1	1.2
FB4_8	457.68	11	17190	240	96510	970	0.5120	0.5116	-8.2	1.3
FB4_9	452.67	11	18190	150	98760	810	0.5120	0.5117	-6.9	1.3
FB5_1	444.67	11	20850	160	99330	720	0.5121	0.5118	-6.0	1.1
FB5_10	440.48	11	17650	130	92440	660	0.5121	0.5117	-6.9	1.2
FB5_11	450.97	13	17290	140	93780	730	0.5121	0.5117	-6.5	1.2
FB5_12	456.38	10	15980	120	93330	690	0.5119	0.5116	-9.3	1.2
FB5_13	447.63	11	15430	120	86140	630	0.5119	0.5116	-9.7	1.3

Table S1. Detrital monazite U-Th-Pb data LASS-ICP-MS
Table S2. Detrital monazite Nd isotopic data LASS-ICP-MS
Table S3. Detrital monazite REE data LASS-ICP-MS

FB5_14	452.36	11	12465	95	80120	610	0.5118	0.5115	-10.0	1.3
FB5_15	449.04	11	16750	140	98890	790	0.5121	0.5117	-6.1	1.3
FB5_16	458.40	10	17040	170	93990	830	0.5120	0.5117	-7.6	1.2
FB5_17	447.31	12	18400	130	100160	690	0.5121	0.5118	-5.5	1.3
FB5_18	446.87	13	20080	150	91460	660	0.5121	0.5117	-7.8	1.3
FB5_19	459.93	12	19600	180	105110	890	0.5121	0.5117	-6.0	1.2
FB5_2	452.06	12	18800	170	101060	960	0.5120	0.5117	-6.7	1.2
FB5_20	452.59	12	19740	170	103290	850	0.5120	0.5117	-6.8	1.0
FB5_21	456.36	12	17850	150	98450	830	0.5119	0.5116	-8.4	1.3
FB5_22	448.73	16	15340	120	104380	780	0.5120	0.5117	-6.1	1.1
FB5_23	455.68	12	18100	130	99620	760	0.5121	0.5117	-6.3	1.1
FB5_25	456.53	12	17730	140	90040	710	0.5121	0.5117	-6.0	1.1
FB5_26	450.05	13	16490	130	100630	770	0.5120	0.5118	-6.0	1.2
FB5_27	447.57	10	18990	140	101170	710	0.5120	0.5116	-8.1	1.3
FB5_28	456.04	12	20070	180	101260	980	0.5121	0.5117	-6.2	1.2
FB5_29	454.13	12	18500	150	101240	800	0.5120	0.5117	-7.6	1.2
FB5_3	454.53	10	18520	150	99550	760	0.5121	0.5118	-5.6	1.2
FB5_30	443.08	10	19830	150	105550	790	0.5121	0.5117	-6.6	1.1
FB5_31	468.94	11	18590	180	98720	970	0.5121	0.5117	-6.1	1.2
FB5_32	467.56	10	17300	180	93600	1000	0.5121	0.5117	-5.7	1.2
FB5_33	446.89	11	19160	130	98310	660	0.5121	0.5117	-6.2	1.2
FB5_34	478.77	16	15190	110	91580	650	0.5120	0.5116	-7.5	1.2
FB5_35	464.41	11	19220	190	102400	1000	0.5120	0.5117	-6.8	1.2
FB5_36	460.84	10	15290	150	82100	830	0.5121	0.5118	-5.3	1.3
FB5_37	456.83	11	17850	180	95070	980	0.5121	0.5118	-4.8	1.2
FB5_38	463.73	11	19290	260	102100	1300	0.5121	0.5117	-6.0	1.1
FB5_39	469.59	12	16040	170	92600	1000	0.5119	0.5115	-9.5	1.2
FB5_4	447.03	14	16790	130	103270	750	0.5120	0.5117	-6.7	1.3
FB5_5	437.54	14	17070	150	101800	870	0.5121	0.5118	-5.4	1.2

Table S1. Detrital monazite U-Th-Pb data LASS-ICP-MS
Table S2. Detrital monazite Nd isotopic data LASS-ICP-MS
Table S3. Detrital monazite REE data LASS-ICP-MS

FB5_6	451.87	12	18480	150	98990	750	0.5121	0.5118	-5.8	1.2
FB5_7	469.79	12	17570	150	99060	800	0.5120	0.5117	-6.4	1.2
FB5_8	444.72	13	19460	150	105780	840	0.5121	0.5117	-6.5	1.2
FB5_9	449.28	10	18970	160	98720	810	0.5121	0.5117	-6.1	1.2
FB6_1	459.51	12	18060	150	95870	810	0.5120	0.5117	-6.7	1.3
FB6_10	452.32	12	19240	170	101270	890	0.5121	0.5117	-6.6	1.2
FB6_11	483.25	14	14810	180	66820	730	0.5121	0.5117	-6.3	1.4
FB6_12	445.02	14	17770	190	94910	940	0.5121	0.5118	-5.3	1.3
FB6_13	465.87	12	18730	180	98520	950	0.5121	0.5118	-4.9	1.2
FB6_14	461.09	14	16440	310	89600	1500	0.5120	0.5117	-6.7	1.2
FB6_15	456.29	15	18520	170	98910	870	0.5120	0.5117	-6.7	1.2
FB6_16	457.54	13	15510	140	87490	770	0.5119	0.5115	-10.1	1.3
FB6_17	457.41	12	16820	130	95560	780	0.5120	0.5117	-7.0	1.2
FB6_18	452.82	11	18940	180	98070	920	0.5121	0.5118	-5.7	1.3
FB6_19	458.39	13	18840	180	98390	920	0.5121	0.5118	-5.3	1.3
FB6_2	452.59	12	15650	130	88340	740	0.5120	0.5117	-6.4	1.4
FB6_20	449.42	15	20640	170	103760	900	0.5121	0.5118	-5.7	1.3
FB6_21	451.28	12	18290	150	100910	810	0.5121	0.5117	-6.4	1.2
FB6_22	453.59	13	17880	160	99990	940	0.5120	0.5117	-7.5	1.3
FB6_23	462.17	14	19720	180	99810	880	0.5121	0.5117	-6.1	1.3
FB6_24	455.79	13	10630	110	81480	810	0.5117	0.5114	-12.1	1.3
FB6_25	443.53	14	10249	99	78270	780	0.5117	0.5115	-11.7	1.3
FB6_26	459.73	14	18980	150	98610	830	0.5120	0.5117	-7.6	1.2
FB6_27	453.11	15	17150	140	97970	890	0.5121	0.5118	-5.8	1.3
FB6_28	457.62	12	19560	170	101690	870	0.5121	0.5118	-5.5	1.2
FB6_29	456.60	20	10830	78	92320	800	0.5119	0.5117	-7.6	1.3
FB6_3	455.11	12	18560	140	100410	720	0.5120	0.5117	-7.8	1.3
FB6_30	464.12	14	15780	150	86170	870	0.5117	0.5114	-12.8	1.1
FB6_31	459.98	13	18640	180	101910	990	0.5120	0.5117	-7.0	1.2

Table S1. Detrital monazite U-Th-Pb data LASS-ICP-MS
Table S2. Detrital monazite Nd isotopic data LASS-ICP-MS
Table S3. Detrital monazite REE data LASS-ICP-MS

FB6_32	447.01	13	13760	120	86300	850	0.5116	0.5114	-13.9	1.2
FB6_33	453.97	12	18400	160	98060	860	0.5120	0.5117	-7.1	1.2
FB6_34	444.68	11	12730	130	77360	790	0.5117	0.5114	-13.0	1.3
FB6_35	444.31	11	18170	140	96380	730	0.5121	0.5118	-6.1	1.2
FB6_36	448.47	12	18790	140	97590	760	0.5121	0.5118	-5.9	1.2
FB6_37	453.50	13	18890	150	99450	870	0.5120	0.5117	-6.9	1.2
FB6_38	451.26	11	18740	140	101850	750	0.5120	0.5117	-7.1	1.3
FB6_39	457.23	12	18580	160	99670	900	0.5121	0.5117	-6.0	1.1
FB6_4	452.75	12	18410	160	96840	880	0.5121	0.5118	-5.3	1.3
FB6_40	449.84	14	17790	180	101700	1000	0.5120	0.5117	-6.6	1.1
FB6_5	457.74	16	15450	140	97400	860	0.5120	0.5118	-5.7	1.3
FB6_6	452.02	14	15500	140	94570	820	0.5121	0.5118	-5.8	1.3
FB6_7	458.94	13	16360	120	97200	750	0.5119	0.5116	-9.2	1.2
FB6_8	456.28	13	17720	160	100630	890	0.5121	0.5117	-6.0	1.3
FB6_9	455.11	12	16970	140	96860	800	0.5120	0.5117	-6.7	1.2
FB8_11	461.03	11	19740	190	104320	980	0.5120	0.5117	-7.7	1.1
FB8_12	451.57	12	15440	150	89090	890	0.5117	0.5114	-12.3	1.2
FB8_13	454.07	10	18800	180	103400	1000	0.5121	0.5117	-6.3	1.3
FB8_14	464.99	11	14500	200	88100	1100	0.5118	0.5115	-10.3	1.2
FB8_15	459.73	13	17480	140	96500	1000	0.5121	0.5118	-5.6	1.2
FB8_16	462.83	10	21650	210	104800	1000	0.5122	0.5118	-5.2	1.2
FB8_2	468.86	11	16030	150	93910	800	0.5119	0.5116	-8.0	1.1
FB8_3	466.51	10	22450	170	109710	860	0.5121	0.5118	-5.4	1.2
FB8_4	458.01	11	22360	220	105200	1000	0.5121	0.5117	-7.1	1.2
FB8_5	462.25	11	18930	170	99730	920	0.5121	0.5118	-5.0	1.2
FB8_6	468.60	13	18670	180	102050	950	0.5121	0.5117	-6.2	1.2
FB8_7	453.63	12	18140	190	95460	980	0.5120	0.5116	-8.1	1.1
FB8_8	459.40	11	19360	170	103400	910	0.5120	0.5117	-6.7	1.0
FB8_9	458.58	14	15630	150	100020	950	0.5120	0.5117	-7.1	1.2

Table S1. Detrital monazite U-Th-Pb data LASS-ICP-MS
Table S2. Detrital monazite Nd isotopic data LASS-ICP-MS
Table S3. Detrital monazite REE data LASS-ICP-MS

FB9_1	465.20	11	17240	190	94240	900	0.5121	0.5118	-4.9	1.3
FB9_11	452.29	11	17900	190	93080	950	0.5121	0.5118	-5.7	1.3
FB9_12	442.92	11	17900	170	101590	940	0.5121	0.5117	-6.4	1.1
FB9_13	450.63	10	19630	180	104020	970	0.5121	0.5118	-5.9	1.1
FB9_14	458.56	10	19130	180	102660	930	0.5120	0.5117	-7.7	1.3
FB9_15	452.42	10	20010	210	101540	930	0.5121	0.5117	-6.4	1.2
FB9_16	449.17	10	18620	190	100300	1000	0.5120	0.5116	-8.2	1.3
FB9_17	451.55	10	18960	180	102330	950	0.5121	0.5117	-6.3	1.2
FB9_18	445.99	10	18310	180	97630	940	0.5121	0.5117	-6.5	1.2
FB9_19	449.92	10	15750	140	91040	790	0.5120	0.5117	-7.9	1.3
FB9_2	1042.69	31	10170	100	82770	800	0.5118	0.5113	-0.6	1.4
FB9_20	1015.29	24	10390	100	74970	740	0.5116	0.5111	-4.9	1.4
FB9_21	454.50	10	18760	170	99380	950	0.5121	0.5118	-5.8	1.2
FB9_22	457.02	11	18750	170	101330	900	0.5121	0.5117	-6.2	1.1
FB9_23	455.77	10	18280	200	95800	1000	0.5121	0.5117	-6.1	1.2
FB9_25	453.54	10	20280	190	100550	940	0.5120	0.5117	-7.5	1.1
FB9_26	445.28	10	16260	140	99680	940	0.5120	0.5117	-6.4	1.1
FB9_27	452.53	10	19510	170	102000	880	0.5121	0.5117	-6.2	1.2
FB9_28	452.26	10	19320	180	108300	1000	0.5121	0.5118	-5.4	1.3
FB9_29	447.91	11	14160	120	100400	860	0.5121	0.5118	-5.1	1.1
FB9_3	460.69	10	24100	220	100800	1200	0.5122	0.5118	-5.5	1.3
FB9_30	456.63	11	19900	200	107200	1000	0.5121	0.5118	-5.2	1.2
FB9_31	448.34	10	18920	160	101510	900	0.5121	0.5118	-5.8	1.4
FB9_32	462.56	11	17800	180	104720	950	0.5121	0.5117	-5.7	1.0
FB9_33	434.70	10	17930	150	95340	810	0.5121	0.5117	-6.6	1.2
FB9_34	455.30	10	18810	170	99900	900	0.5121	0.5118	-5.8	1.2
FB9_35	449.99	10	17190	150	98480	870	0.5121	0.5118	-5.7	1.3
FB9_36	456.86	10	18540	190	95540	950	0.5121	0.5117	-6.6	1.2
FB9_37	453.18	11	19720	160	106490	880	0.5121	0.5117	-5.9	1.2

Table S1. Detrital monazite U-Th-Pb data LASS-ICP-MS
Table S2. Detrital monazite Nd isotopic data LASS-ICP-MS
Table S3. Detrital monazite REE data LASS-ICP-MS

FB9_38	451.20	10	19260	210	100500	1000	0.5121	0.5118	-5.9	1.2
FB9_39	450.39	11	18240	130	104600	870	0.5120	0.5117	-6.8	1.2
FB9_4	458.35	10	17690	160	95380	860	0.5121	0.5117	-5.9	1.2
FB9_40	448.27	10	18330	150	99920	830	0.5121	0.5118	-5.9	1.1
FB9_41	445.09	10	14910	120	92890	770	0.5117	0.5114	-13.3	1.2
FB9_42	453.57	10	19940	160	106560	840	0.5121	0.5118	-5.1	1.1
FB9_43	450.00	10	19710	170	105110	880	0.5120	0.5117	-7.2	1.2
FB9_44	449.22	10	17960	160	98010	870	0.5119	0.5116	-9.1	1.2
FB9_46	439.65	10	16680	130	103980	790	0.5120	0.5117	-6.7	1.1
FB9_5	455.29	11	20990	220	98640	980	0.5121	0.5117	-7.0	1.3
FB9_6	465.14	10	18520	170	104600	1100	0.5121	0.5118	-5.6	1.2
FB9_7	460.16	10	18170	150	97410	820	0.5120	0.5116	-8.3	1.2
FB9_8	459.00	10	18860	180	99100	1000	0.5121	0.5118	-5.4	1.3
FB9_9	452.06	10	18390	170	97980	950	0.5121	0.5117	-6.2	1.4
FinesCreek-Schist_1	450.96	12	16040	240	80700	1300	0.5121	0.5117	-6.2	1.5
FinesCreek-Schist_10	447.44	13	16020	140	84820	770	0.5121	0.5118	-6.0	1.5
FinesCreek-Schist_11	444.30	14	15680	150	85820	820	0.5120	0.5117	-7.1	1.3
FinesCreek-Schist_12	448.28	10	16740	180	84970	740	0.5121	0.5117	-6.9	1.3
FinesCreek-Schist_13	443.01	13	14500	400	73700	2000	0.5121	0.5118	-6.2	1.6
FinesCreek-Schist_14	445.40	13	17310	160	84380	790	0.5121	0.5117	-7.2	1.5
FinesCreek-Schist_15	443.15	14	16680	150	82890	710	0.5121	0.5117	-6.6	1.4
FinesCreek-Schist_16	443.52	14	16000	150	86560	820	0.5120	0.5117	-7.0	1.4
FinesCreek-Schist_17	446.85	11	16950	140	84940	750	0.5121	0.5118	-5.5	1.4
FinesCreek-Schist_18	443.26	14	17450	160	85860	850	0.5121	0.5118	-6.1	1.4
FinesCreek-Schist_2	447.18	13	16590	160	87370	870	0.5121	0.5117	-6.7	1.4
FinesCreek-Schist_3	444.05	11	16010	140	87010	760	0.5120	0.5117	-6.6	1.3
FinesCreek-Schist_4	448.19	10	16620	170	83350	850	0.5121	0.5117	-7.1	1.4
FinesCreek-Schist_5	441.76	12	17090	170	83620	840	0.5121	0.5117	-6.6	1.4
FinesCreek-Schist_6	455.92	12	17010	160	85280	850	0.5121	0.5117	-6.0	1.4

Table S1. Detrital monazite U-Th-Pb data LASS-ICP-MS
Table S2. Detrital monazite Nd isotopic data LASS-ICP-MS
Table S3. Detrital monazite REE data LASS-ICP-MS

FinesCreek-Schist_7	453.98	15	17300	170	86970	780	0.5121	0.5117	-6.0	1.4
FinesCreek-Schist_8	451.83	12	17210	160	84320	780	0.5121	0.5118	-5.9	1.3
FinesCreek-Schist_9	443.34	13	14660	250	77200	1300	0.5121	0.5118	-6.1	1.5
FL7_large_1	1048.37	23	25240	250	121000	1100	0.5121	0.5113	-0.4	1.0
FL7_large_10	1027.36	22	25470	280	103300	1100	0.5122	0.5112	-1.7	1.1
FL7_large_11	1060.45	25	17240	190	100800	1200	0.5119	0.5112	-1.1	1.1
FL7_large_13	1159.94	25	18850	210	95400	1100	0.5121	0.5111	-0.1	1.1
FL7_large_14	1166.25	26	19570	220	94800	1100	0.5121	0.5111	0.2	1.1
FL7_large_15	1082.01	23	14700	180	87200	1100	0.5120	0.5113	1.1	1.2
FL7_large_16	1035.81	29	15260	160	88430	930	0.5121	0.5114	1.3	1.2
FL7_large_17	1054.03	25	16300	190	89500	1000	0.5119	0.5111	-3.8	1.2
FL7_large_18	1047.01	25	16640	190	89160	990	0.5118	0.5110	-4.6	1.2
FL7_large_19	1161.52	29	18370	200	89440	940	0.5116	0.5107	-8.8	1.2
FL7_large_2	1045.34	25	22370	170	113750	940	0.5121	0.5112	-1.2	1.0
FL7_large_20	1003.65	26	19650	220	102500	1100	0.5120	0.5112	-2.5	1.1
FL7_large_21	1038.19	26	27290	300	116900	1300	0.5122	0.5112	-1.1	1.0
FL7_large_22	1052.91	25	25930	230	118100	1100	0.5122	0.5113	-0.1	1.1
FL7_large_24	1093.32	28	16880	210	92800	1100	0.5121	0.5113	1.8	1.2
FL7_large_25	1174.17	60	17330	200	92400	1000	0.5121	0.5112	2.0	1.2
FL7_large_26	1042.52	26	14370	140	100260	970	0.5119	0.5112	-0.8	1.1
FL7_large_29	1092.65	25	22510	230	107300	1100	0.5120	0.5111	-3.2	1.0
FL7_large_30	1167.34	27	20070	230	96200	1000	0.5122	0.5112	1.4	1.1
FL7_large_34	1003.27	23	21750	230	97300	1000	0.5122	0.5113	-1.2	1.1
FL7_large_35	1007.42	26	21390	210	97120	970	0.5121	0.5112	-2.3	1.1
FL7_large_37	1112.96	27	20550	210	103350	980	0.5121	0.5112	-0.7	1.2
FL7_large_5	1135.20	25	18540	180	100980	960	0.5120	0.5112	0.1	1.0
FL7_large_6	981.45	23	20410	220	95050	970	0.5121	0.5112	-2.8	1.1
FL7_large_8	1160.97	26	20710	220	103300	1100	0.5120	0.5110	-2.3	1.1
FL7_large_9	1022.42	24	25300	280	103100	1100	0.5123	0.5113	-1.2	1.1

Table S1. Detrital monazite U-Th-Pb data LASS-ICP-MS
Table S2. Detrital monazite Nd isotopic data LASS-ICP-MS
Table S3. Detrital monazite REE data LASS-ICP-MS

FL7_small_1	1136.08	23	24560	280	108400	1200	0.5122	0.5112	0.2	1.1
FL7_small_10	1138.56	26	16390	170	95900	1100	0.5118	0.5110	-2.8	1.1
FL7_small_11	1035.01	23	26150	290	100400	980	0.5123	0.5112	-1.1	1.2
FL7_small_13	1147.73	25	19850	200	98300	1000	0.5120	0.5111	-1.5	1.1
FL7_small_14	1026.66	23	20340	220	102800	1100	0.5121	0.5113	-0.9	1.2
FL7_small_16	1102.41	25	23600	230	110400	1100	0.5122	0.5113	0.9	1.1
FL7_small_17	913.97	66	20160	560	109100	1300	0.5122	0.5115	1.7	1.5
FL7_small_18	1165.48	26	14630	210	82690	980	0.5119	0.5111	-1.3	1.4
FL7_small_21	514.51	21	35520	320	177100	1500	0.5123	0.5119	-2.1	1.0
FL7_small_22	1124.69	25	16620	210	92500	1100	0.5117	0.5109	-5.1	1.2
FL7_small_24	1048.93	29	15370	300	100300	1900	0.5119	0.5113	-0.1	1.2
FL7_small_26	1199.50	27	18750	200	95400	1000	0.5120	0.5111	0.2	1.2
FL7_small_27	1159.93	28	22190	250	100500	1200	0.5122	0.5111	0.2	1.1
FL7_small_28	1092.75	23	20740	210	89620	910	0.5120	0.5110	-4.7	1.1
FL7_small_29	1105.70	66	16310	180	120900	1400	0.5119	0.5113	1.7	1.1
FL7_small_3	1118.80	23	24290	250	103500	1100	0.5121	0.5111	-2.2	1.1
FL7_small_30	1048.19	26	20150	240	97100	1100	0.5120	0.5111	-3.4	1.1
FL7_small_31	1120.29	24	14770	140	82720	830	0.5119	0.5111	-1.2	1.4
FL7_small_32	1108.68	26	26800	260	123000	1200	0.5121	0.5111	-1.2	1.2
FL7_small_34	1108.42	25	21320	220	109600	1100	0.5122	0.5113	2.7	1.2
FL7_small_35	1055.75	26	16230	180	98000	1100	0.5120	0.5113	-0.2	1.1
FL7_small_5	1032.84	283	16120	160	87880	820	0.5122	0.5114	2.2	1.2
FL7_small_7	1025.97	24	13980	130	96400	1000	0.5119	0.5113	-0.9	1.2
FL7_small_8	1047.07	24	19370	160	99460	860	0.5121	0.5113	-0.6	1.1
FL7_small_9	1037.94	22	18730	180	100040	930	0.5118	0.5110	-5.8	1.2
KS12-2C_large_1	1061.22	24	18670	250	104100	1300	0.5119	0.5112	-2.0	1.1
KS12-2C_large_10	1047.51	26	19450	170	102430	830	0.5119	0.5111	-4.2	1.2
KS12-2C_large_13	1030.03	25	19670	210	108700	1100	0.5119	0.5112	-3.1	1.1
KS12-2C_large_14	1030.52	25	19440	180	108500	1000	0.5119	0.5111	-3.3	1.1

Table S1. Detrital monazite U-Th-Pb data LASS-ICP-MS
Table S2. Detrital monazite Nd isotopic data LASS-ICP-MS
Table S3. Detrital monazite REE data LASS-ICP-MS

KS12-2C_large_15	998.22	22	29580	290	100340	990	0.5124	0.5112	-2.7	1.1
KS12-2C_large_16	990.63	21	29500	270	99290	970	0.5124	0.5112	-2.5	1.1
KS12-2C_large_2	1043.13	25	18730	220	104100	1200	0.5119	0.5111	-3.0	1.1
KS12-2C_large_5	1030.67	24	25570	320	102100	1300	0.5122	0.5112	-2.5	1.1
KS12-2C_large_7	1018.05	117	9160	110	73500	1000	0.5119	0.5114	1.0	1.2
KS12-2C_large_8	1043.63	29	19600	200	106200	1100	0.5119	0.5111	-3.3	1.2
KS12-2C_large_9	1044.30	27	19590	210	106700	1100	0.5119	0.5111	-3.1	1.2
KS12-2C_small_10	1010.23	210	24360	540	94300	2300	0.5122	0.5112	-3.2	1.2
KS12-2C_small_11	387.12	10	17300	200	97100	1000	0.5123	0.5120	-2.8	1.2
KS12-2C_small_12	369.66	8	17880	180	92640	940	0.5123	0.5120	-3.0	1.1
KS12-2C_small_14	1446.81	549	21050	300	109100	1500	0.5119	0.5108	1.2	1.1
KS12-2C_small_2	1068.09	22	24540	240	104400	1100	0.5124	0.5114	2.0	1.2
KS12-2C_small_3	991.61	21	30320	300	97480	940	0.5124	0.5112	-2.8	1.1
KS12-2C_small_4	995.77	21	22050	310	109400	1800	0.5120	0.5112	-3.3	1.2
KS12-2C_small_5	1027.06	24	22630	220	101600	1000	0.5120	0.5111	-3.7	1.0
KS12-2C_small_6	1021.61	22	18090	200	95200	1100	0.5118	0.5110	-5.4	1.3
KS12-2C_small_7	350.92	8	17390	200	92400	1100	0.5123	0.5120	-3.3	1.1
KS12-2C_small_8	1131.81	24	18140	180	94320	970	0.5118	0.5109	-5.0	1.2
LookingGlass-Granite_1	332.49	9	23010	340	83460	940	0.5125	0.5122	-0.6	1.3
LookingGlass-Granite_11	334.79	9	21780	200	79900	720	0.5124	0.5121	-2.9	1.4
LookingGlass-Granite_12	336.75	11	24360	210	86370	750	0.5125	0.5122	-0.8	1.3
LookingGlass-Granite_13	338.09	8	21850	220	81250	770	0.5125	0.5121	-1.6	1.4
LookingGlass-Granite_2	335.34	8	19630	200	72050	710	0.5125	0.5122	-0.4	1.3
LookingGlass-Granite_20	334.07	8	22440	240	82430	840	0.5126	0.5122	0.5	1.3
LookingGlass-Granite_23	337.64	10	22860	270	84420	930	0.5125	0.5122	-0.8	1.4
LookingGlass-Granite_25	338.58	9	25570	210	76200	640	0.5126	0.5122	0.0	1.2
LookingGlass-Granite_3	323.38	10	24310	210	87810	750	0.5125	0.5121	-2.2	1.3
LookingGlass-Granite_6	334.49	9	20680	200	77750	680	0.5125	0.5122	-0.8	1.5
LookingGlass-Granite_8	320.78	8	22310	190	80330	660	0.5126	0.5122	0.2	1.2

Table S1. Detrital monazite U-Th-Pb data LASS-ICP-MS
Table S2. Detrital monazite Nd isotopic data LASS-ICP-MS
Table S3. Detrital monazite REE data LASS-ICP-MS

PF12-1-Shields_1	974.13	21	27120	300	112500	1200	0.5125	0.5115	3.0	1.2
PF12-1-Shields_10	1043.82	26	14800	160	97200	1100	0.5119	0.5112	-1.1	1.2
PF12-1-Shields_11	1081.66	27	15150	170	97800	1000	0.5120	0.5113	1.4	1.2
PF12-1-Shields_12	1033.96	24	14790	150	87610	900	0.5121	0.5114	2.2	1.2
PF12-1-Shields_13	1046.14	22	24570	250	106200	1100	0.5122	0.5113	-0.3	1.1
PF12-1-Shields_14	1041.08	22	24830	280	107300	1200	0.5121	0.5112	-2.0	1.1
PF12-1-Shields_16	1052.92	26	11940	110	83350	850	0.5120	0.5114	1.6	1.3
PF12-1-Shields_17	1134.29	28	19740	180	99380	960	0.5120	0.5111	-1.0	1.2
PF12-1-Shields_23	1051.53	24	15860	240	85590	940	0.5120	0.5113	-0.4	1.3
PF12-1-Shields_6	1082.57	32	21040	210	107400	1100	0.5122	0.5113	1.8	1.3
PF12-1-Shields_7	1050.04	72	13800	1100	61900	5700	0.5123	0.5115	3.7	1.8
PF12-1-Shields_8	1200.63	28	10060	100	79510	790	0.5119	0.5113	3.9	1.4
PF12-1-Shields_9	1189.60	28	9340	100	76960	810	0.5118	0.5112	2.3	1.6
SixmileSchist_1	364.04	8	16100	170	82530	870	0.5120	0.5117	-9.1	1.2
SixmileSchist_10	360.28	9	16670	180	85380	950	0.5120	0.5117	-8.7	1.3
SixmileSchist_11	358.83	9	14950	230	80000	1100	0.5120	0.5118	-8.0	1.4
SixmileSchist_12	366.20	9	16840	200	86500	980	0.5120	0.5118	-7.9	1.3
SixmileSchist_13	355.74	9	12780	150	74620	890	0.5119	0.5117	-9.4	1.4
SixmileSchist_14	365.35	10	13730	160	86100	1000	0.5120	0.5118	-7.5	1.3
SixmileSchist_15	407.02	9	16190	210	83340	970	0.5120	0.5117	-7.9	1.5
SixmileSchist_16	368.76	8	15920	180	86190	990	0.5120	0.5117	-8.3	1.3
SixmileSchist_17	406.40	9	13740	200	81700	1200	0.5120	0.5118	-7.1	1.4
SixmileSchist_18	369.73	10	16660	200	85900	1000	0.5120	0.5117	-8.6	1.3
SixmileSchist_19	375.64	9	17410	200	88200	1100	0.5121	0.5118	-6.8	1.4
SixmileSchist_2	381.24	10	14110	290	80960	850	0.5120	0.5117	-8.6	1.5
SixmileSchist_20	368.53	9	17060	200	86900	1100	0.5121	0.5118	-7.5	1.3
SixmileSchist_3	378.81	11	14590	240	77900	1200	0.5120	0.5117	-8.2	1.4
SixmileSchist_4	393.18	9	18620	180	85410	820	0.5121	0.5118	-7.1	1.4
SixmileSchist_5	355.61	8	15730	180	80540	920	0.5121	0.5118	-7.7	1.3

Table S1. Detrital monazite U-Th-Pb data LASS-ICP-MS
Table S2. Detrital monazite Nd isotopic data LASS-ICP-MS
Table S3. Detrital monazite REE data LASS-ICP-MS

SixmileSchist_6	384.89	9	16120	210	81860	960	0.5120	0.5117	-7.8	1.4
SixmileSchist_7	370.54	9	14210	150	75240	840	0.5120	0.5118	-7.6	1.3
SixmileSchist_8	382.90	13	13960	270	81310	850	0.5120	0.5118	-7.5	1.4
SixmileSchist_9	367.93	9	16060	190	78790	980	0.5120	0.5117	-8.2	1.3
WCK12-1-Sandsuck_1	1053.22	23	12550	140	89680	920	0.5118	0.5113	-0.2	1.3
WCK12-1-Sandsuck_2	1071.49	27	13420	140	90960	970	0.5120	0.5113	1.5	1.3
WCK12-1-Sandsuck_3	1094.05	26	14570	130	85730	750	0.5120	0.5113	1.0	1.3
WCK12-1-Sandsuck_4	1043.28	26	19560	210	94700	1000	0.5123	0.5115	3.8	1.2
WCK12-1-Sandsuck_5	1038.59	25	19930	170	104100	1000	0.5122	0.5114	2.1	1.2
WCK12-1-Sandsuck_6	1047.97	26	14240	220	90100	1100	0.5119	0.5113	-0.3	1.3
WCK12-1-Sandsuck_8	1068.30	33	14990	170	97800	1100	0.5120	0.5114	1.9	1.2

Table S1. Detrital monazite U-Th-Pb data LASS-ICP-MS
Table S2. Detrital monazite Nd isotopic data LASS-ICP-MS
Table S3. Detrital monazite REE data LASS-ICP-MS

Table S3: Measured ppm were divided by the Mg-normalized abundances in the Silicate Earth (u)

Sample	Best Age	Ce	Pr	Nd	Sm	Eu	Gd	Eu*	Th/U
01-TN-02A_1	1080	350408	297953	242013	151284	6265	85025	0.1	16
01-TN-02A_17	374	410114	280280	183851	85743	7442	64372	0.1	3
01-TN-02A_2	1037	371289	274677	199125	102770	11018	66332	0.1	3
01-TN-02A_21	439	367374	279095	209519	116554	45471	79598	0.5	11
01-TN-02A_25	463	365742	284159	214661	119257	12167	81307	0.1	9
01-TN-02A_29	380	337194	265194	203939	126149	53925	88693	0.5	7
01-TN-02A_3	446	392333	293319	203939	98851	2829	55879	0.0	17
01-TN-02A_30	380	355302	277694	209737	123176	55151	84422	0.5	8
01-TN-02A_31	1048	354976	277047	208709	133243	4327	85176	0.0	11
01-TN-02A_36	1045	394943	239655	145295	50568	4039	54271	0.1	139
01-TN-02A_44	1070	384176	332328	266740	142365	732	60653	0.0	46
01-TN-02A_49	1163	369168	309483	244726	157568	22309	87739	0.2	12
01-TN-02A_51	468	296411	296121	260832	171824	126732	63367	1.2	6
01-TN04_1	370	352855	267457	204639	132500	51403	89447	0.5	7
01-TN04_18	1025	335889	259914	195077	120203	43446	83467	0.4	6
01-TN04_2	411	366884	303125	222319	118311	74547	64955	0.9	15
01-TN05_12	407	385644	372306	317068	192432	138224	78090	1.1	1
01-TN05_19	484	339641	246444	181247	111419	38615	72663	0.4	11
01-TN05_2	401	355628	274784	206193	128784	2025	79246	0.0	21
01-TN05_28	415	342088	264978	205492	146216	82877	101960	0.7	15
01-TN05_29	468	397879	296228	211488	95000	7860	56337	0.1	12
01-TN05_3	406	380914	256142	192144	115135	39929	73769	0.4	3
01-TN05_31	424	378956	287500	215667	113108	22824	60729	0.3	40
01-TN05_32	420	407667	286638	197593	94257	20263	56226	0.3	30
01-TN05_36	380	353670	288039	229891	146149	99751	92965	0.9	4
01-TN05_37	1005	345840	305172	243720	170946	3085	96683	0.0	3
01-TN05_38	1037	345840	279526	210635	126824	7238	80603	0.1	6

Table S1. Detrital monazite U-Th-Pb data LASS-ICP-MS
Table S2. Detrital monazite Nd isotopic data LASS-ICP-MS
Table S3. Detrital monazite REE data LASS-ICP-MS

01-TN05_42	1042	336868	296552	234508	136149	17655	83417	0.2	5
01-TN05_44	439	358401	288254	228512	144257	7664	84925	0.1	15
01-TN05_45	471	399347	289763	205186	90169	26234	55759	0.4	63
01-TN05_5	422	304894	233728	178665	124595	9281	85427	0.1	21
01-TN05_9	461	359706	282435	196958	99797	68579	64221	0.9	1
5-1-2_small_34	499	367374	350862	298031	168176	110089	42668	1.3	5
AsheGneiss_1	445	300816	232328	176214	100405	29183	61558	0.4	4
AsheGneiss_10	465	328222	249784	183786	98784	31829	57688	0.4	5
AsheGneiss_11	458	334421	255388	187746	95946	12707	53668	0.2	14
AsheGneiss_12	463	334421	257974	192560	105270	32398	61859	0.4	4
AsheGneiss_2	443	295432	227478	172670	99324	30515	60151	0.4	5
AsheGneiss_3	443	311746	232974	169190	91486	28259	54111	0.4	4
AsheGneiss_4	451	306199	238254	179387	100000	21599	58397	0.3	6
AsheGneiss_5	446	316966	236315	174858	96622	28384	59497	0.4	3
AsheGneiss_6	441	317129	243534	184814	105338	30764	61980	0.4	4
AsheGneiss_7	456	321697	249353	185689	102365	31705	58844	0.4	5
AsheGneiss_8	461	322512	247629	182801	97095	14458	54754	0.2	10
AsheGneiss_9	454	308646	241487	184530	109054	34192	67286	0.4	4
AsheSchist-newrow_1	451	295269	230172	177002	103919	30639	64472	0.4	4
AsheSchist-newrow_10	441	328059	258297	195033	117230	32469	70503	0.4	4
AsheSchist-newrow_11	456	333605	260668	195755	113514	29005	65879	0.3	5
AsheSchist-newrow_2	441	301468	235991	179300	104189	29840	63417	0.4	4
AsheSchist-newrow_3	451	301305	238362	182079	107230	32362	64472	0.4	3
AsheSchist-newrow_4	445	313866	230496	166521	91554	31652	55879	0.4	4
AsheSchist-newrow_5	443	307341	238362	178490	100676	29467	60603	0.4	4
AsheSchist-newrow_6	444	316313	245474	185405	102973	29325	61709	0.4	5
AsheSchist-newrow_7	440	318597	246983	183764	105811	32274	63563	0.4	4
AsheSchist-newrow_8	444	325122	246767	181794	100135	29716	60302	0.4	4
AsheSchist-newrow_9	443	329364	260129	197112	118176	29236	70251	0.3	4

Table S1. Detrital monazite U-Th-Pb data LASS-ICP-MS
Table S2. Detrital monazite Nd isotopic data LASS-ICP-MS
Table S3. Detrital monazite REE data LASS-ICP-MS

Carter512A_a_1	1045	388581	288578	202626	100135	15790	62734	0.2	4
Carter512A_a_11	1082	369168	257974	190438	110811	30906	66784	0.4	4
Carter512A_a_12	1144	340457	277909	223195	136824	47531	80201	0.5	5
Carter512A_a_14	1064	371289	266056	180985	79257	16927	48528	0.3	12
Carter512A_a_15	1074	370147	264547	180000	78176	15247	47688	0.2	12
Carter512A_a_2	1032	378303	275108	198643	81959	7799	47754	0.1	119
Carter512A_a_5	1054	351060	303772	250766	157297	70515	78744	0.6	3
Carter512A_a_6	1045	327243	273707	220350	152568	66412	84724	0.6	2
Carter512A_a_7	1044	333931	275216	218140	148919	64405	82563	0.6	2
Carter512A_a_8	1035	357259	283405	214442	124527	5513	72513	0.1	27
Carter512A_a_9	1058	372594	280280	209300	117905	66643	71206	0.7	2
Carter512A_a_large_1	974	367537	255927	169716	72905	13179	57286	0.2	13
Carter512A_a_large_3	515	398042	269397	185689	79797	59556	52955	0.9	2
Carter512A_a_large_4	1195	335073	269720	211838	129122	19840	82714	0.2	32
Carter512A_a_large_5	1130	344046	279095	212473	132500	23162	79347	0.2	17
Carter512A_a_large_6	1157	312724	268858	213961	136622	9964	89749	0.1	14
Carter512A_b_1	1099	318597	268103	214114	141284	19538	88945	0.2	4
Carter512A_b_10	1061	372268	274138	200919	90405	14849	50402	0.2	61
Carter512A_b_11	1065	347471	286099	230416	123986	26874	71442	0.3	28
Carter512A_b_13	1031	369168	285560	210547	103243	4425	61608	0.1	15
Carter512A_b_15	1141	330179	282112	237418	161419	18828	99397	0.1	11
Carter512A_b_17	982	395759	251940	160306	59149	19165	41578	0.4	10
Carter512A_b_18	1002	325938	259591	197987	118311	7741	74121	0.1	4
Carter512A_b_2	1028	348613	274030	200722	104324	13517	60251	0.2	18
Carter512A_b_5	1066	351876	279957	208753	122162	20959	70151	0.2	8
Carter512A_b_6	1041	306688	271121	232166	171149	25968	97638	0.2	6
Carter512A_b_7	736	372757	331789	295842	198986	121314	75126	1.0	13
Carter512A_b_9	1052	366069	311422	255142	149324	52931	74075	0.5	10
Carter512A_b_large_2	1199	349103	284159	219694	130473	17268	85477	0.2	8

Table S1. Detrital monazite U-Th-Pb data LASS-ICP-MS
Table S2. Detrital monazite Nd isotopic data LASS-ICP-MS
Table S3. Detrital monazite REE data LASS-ICP-MS

Carter512A_b_large_3	1036	335726	268642	207571	126824	23419	81106	0.2	2
Carter512A_b_large_5	1089	325122	265625	214179	129257	14103	84221	0.1	16
FB1_1	462	334910	261961	199365	116014	55240	68291	0.6	9
FB1_10	457	324470	266810	204376	121486	41901	78241	0.4	3
FB1_11	463	350408	267888	204683	122095	68472	77085	0.7	5
FB1_12	459	341762	260345	196937	121081	18792	79698	0.2	4
FB1_13	462	350408	278664	216608	126014	13229	73015	0.1	8
FB1_15	458	377162	273707	202013	108851	30053	64824	0.4	7
FB1_16	456	355139	275216	207637	110878	26607	68307	0.3	4
FB1_17	455	371289	269073	201510	101689	38330	59045	0.5	53
FB1_18	456	373083	289009	219519	125946	24210	62518	0.3	47
FB1_19	441	354976	275216	211225	106554	30622	63166	0.4	22
FB1_2	344	375041	251832	166608	66101	23517	36538	0.5	26
FB1_20	434	352692	269181	202232	112703	50728	67538	0.6	10
FB1_21	446	356607	268642	205142	123716	70018	78291	0.7	7
FB1_23	331	352855	258836	179540	109797	21066	65980	0.2	19
FB1_26	331	337357	240517	171947	105608	27638	67035	0.3	17
FB1_27	325	331485	238793	168972	107365	28988	67739	0.3	14
FB1_29	449	347798	261746	194880	116284	67798	73166	0.7	27
FB1_3	456	323491	251509	196433	121216	56039	76181	0.6	7
FB1_30	448	406852	270151	172013	63845	5901	37874	0.1	11
FB1_31	467	360685	272522	207659	122635	83481	80854	0.8	6
FB1_32	399	379935	297414	224726	119527	53446	67085	0.6	62
FB1_33	449	364274	285991	222144	138784	15922	88894	0.1	13
FB1_4	501	342414	291918	212495	185878	1558	80854	0.0	52
FB1_6	474	343393	260560	197899	103378	53286	62563	0.7	16
FB1_7	400	331158	259591	202495	118446	58970	69749	0.6	7
FB1_8	457	363948	282543	215930	123514	11750	66533	0.1	8
FB1_9	458	347635	261853	195689	113243	61439	71156	0.7	5

Table S1. Detrital monazite U-Th-Pb data LASS-ICP-MS
Table S2. Detrital monazite Nd isotopic data LASS-ICP-MS
Table S3. Detrital monazite REE data LASS-ICP-MS

FB10_1	1021	315498	252371	192757	113716	1993	70553	0.0	30
FB10_10	465	351223	284483	222035	131216	18313	81357	0.2	10
FB10_11	437	337194	271767	220788	151689	17407	96834	0.1	9
FB10_12	457	364274	278125	210788	123041	15126	74121	0.2	14
FB10_13	456	369984	279095	209037	113378	16014	68442	0.2	21
FB10_14	458	376346	288147	217112	123243	41652	72714	0.4	5
FB10_16	466	375856	287500	215821	125946	25346	78894	0.3	4
FB10_17	460	356281	289978	220131	132635	50178	84975	0.5	3
FB10_18	460	371289	297414	225996	132297	44778	87085	0.4	4
FB10_19	1321	390212	358944	312254	184865	5769	73116	0.0	18
FB10_2	446	339315	278772	210875	120878	51989	76030	0.5	3
FB10_20	1035	348450	272414	207046	131216	6462	81658	0.1	8
FB10_21	455	362480	275647	206061	129730	13300	82563	0.1	7
FB10_22	456	383361	299138	226477	117500	7876	59286	0.1	24
FB10_23	939	387113	301078	218206	131486	29165	66734	0.3	17
FB10_24	471	380098	289547	216127	112230	6872	62663	0.1	30
FB10_25	476	390538	280603	199190	89324	14206	49754	0.2	60
FB10_26	461	373736	294289	218074	114595	22202	69095	0.2	6
FB10_27	470	392985	296552	219256	110811	16941	62156	0.2	27
FB10_28	463	392496	310237	230197	127365	47282	66181	0.5	3
FB10_29	467	403426	280065	195930	85743	6558	51256	0.1	19
FB10_3	462	377977	291595	220569	125405	39272	78090	0.4	4
FB10_30	469	389070	295582	226958	107770	24121	58945	0.3	44
FB10_31	460	361011	298276	225580	132703	57194	82663	0.5	3
FB10_32	482	391843	287500	212932	86351	14671	47447	0.2	104
FB10_33	454	336215	283297	235011	165541	17211	111960	0.1	3
FB10_34	466	366721	281573	215996	127095	25346	79196	0.3	6
FB10_35	462	380914	296552	223698	124730	17975	75126	0.2	5
FB10_36	454	374062	271983	196718	99324	22131	58442	0.3	58

Table S1. Detrital monazite U-Th-Pb data LASS-ICP-MS
Table S2. Detrital monazite Nd isotopic data LASS-ICP-MS
Table S3. Detrital monazite REE data LASS-ICP-MS

FB10_37	464	378303	272953	196521	102297	25524	60302	0.3	95
FB10_4	459	378303	285668	213698	108108	6391	58342	0.1	21
FB10_5	1044	369821	273168	200744	100000	2471	65025	0.0	14
FB10_6	453	362316	300862	225164	127838	46696	78543	0.5	3
FB10_8	1110	378956	288254	211794	95338	2364	50930	0.0	73
FB11_1	495	360685	307004	222757	192770	1622	84472	0.0	51
FB11_10	456	379772	282328	212035	118514	11297	73367	0.1	5
FB11_11	453	377488	290409	214880	117770	31492	69347	0.3	5
FB11_12	461	340457	274353	206783	122297	62789	77839	0.6	3
FB11_13	464	379935	298384	224530	126689	41155	75779	0.4	4
FB11_14	459	369821	287716	215536	124189	26998	78543	0.3	12
FB11_15	459	380914	302263	223851	124189	41794	79598	0.4	6
FB11_16	463	349592	291164	218731	123784	29378	77889	0.3	6
FB11_17	459	327080	262823	216630	131959	61492	81156	0.6	12
FB11_18	461	383361	296444	221794	118784	15826	69799	0.2	8
FB11_19	1003	382055	292457	215186	106622	3385	44623	0.0	27
FB11_2	500	361664	309375	224595	194392	1604	85025	0.0	51
FB11_20	469	378630	296336	217746	118514	39574	71709	0.4	6
FB11_21	1065	388744	294828	224945	98514	5615	46302	0.1	30
FB11_22	467	389233	288362	211947	98919	15464	51508	0.2	47
FB11_23	453	385481	289547	216630	104189	13609	53869	0.2	42
FB11_24	463	372431	286207	219037	126959	20710	76281	0.2	6
FB11_25	463	354323	282112	215755	124527	38934	80503	0.4	4
FB11_26	460	362153	281142	214661	128108	28686	83317	0.3	4
FB11_27	459	358238	291056	220350	129730	40568	81608	0.4	4
FB11_28	464	389396	299892	232166	131757	39449	73417	0.4	4
FB11_3	453	375367	288470	219781	103784	17389	53613	0.2	33
FB11_4	460	373083	294935	222823	129122	42256	76533	0.4	3
FB11_5	464	376346	294181	222123	128041	41510	77990	0.4	3

Table S1. Detrital monazite U-Th-Pb data LASS-ICP-MS
Table S2. Detrital monazite Nd isotopic data LASS-ICP-MS
Table S3. Detrital monazite REE data LASS-ICP-MS

FB11_6	460	354160	294720	222910	128986	50995	81658	0.5	3
FB11_7	463	362480	284375	215120	124797	85293	79246	0.9	5
FB11_8	462	369984	282543	216193	122432	17211	73668	0.2	9
FB11_9	458	366069	296552	222319	129459	69130	76683	0.7	3
FB13_1	1000	327080	285884	241291	157500	3710	68442	0.0	25
FB13_10	415	354160	265841	199256	119730	22877	75578	0.2	30
FB13_11	451	348287	270690	214026	131892	17229	82864	0.2	5
FB13_12	460	353018	281681	211554	121149	58615	75980	0.6	1
FB13_13	448	376835	282328	208118	112770	17083	68241	0.2	16
FB13_16	448	376509	289978	213807	118716	33943	74774	0.4	6
FB13_17	448	358728	284483	222166	139189	16815	87085	0.2	4
FB13_2	460	362153	286422	220241	127635	38650	80352	0.4	4
FB13_3	463	388254	285884	211641	121284	58632	71668	0.6	2
FB13_4	455	396411	280280	188687	102230	29876	67824	0.4	1
FB13_5	456	382219	278556	201882	98041	8993	55528	0.1	28
FB13_7	455	371126	288578	227527	123514	9501	70804	0.1	6
FB13_8	458	352855	285991	223567	133919	16991	80201	0.2	4
FB14_1	443	353507	275108	211028	119797	23037	72814	0.2	27
FB14_10	463	393801	295366	220175	102027	11202	51990	0.2	79
FB14_11	467	365905	276616	205908	117365	40124	74774	0.4	3
FB14_12	465	370310	289655	218490	124392	50888	76432	0.5	4
FB14_13	461	378956	285776	214902	108446	16270	60955	0.2	42
FB14_14	451	384013	274138	199300	109122	30053	76683	0.3	47
FB14_15	444	381077	292888	224508	120068	22256	68090	0.2	34
FB14_17	459	371941	298168	220810	122230	42860	73518	0.5	4
FB14_18	1080	366884	282112	201050	104730	4774	54774	0.1	26
FB14_19	458	362643	282328	214748	123446	17650	73769	0.2	10
FB14_2	454	351060	268534	204114	120135	19057	74372	0.2	9
FB14_20	450	374225	296659	224136	129595	34529	78191	0.3	5

Table S1. Detrital monazite U-Th-Pb data LASS-ICP-MS
Table S2. Detrital monazite Nd isotopic data LASS-ICP-MS
Table S3. Detrital monazite REE data LASS-ICP-MS

FB14_21	460	365742	297845	223414	129662	55187	81809	0.5	4
FB14_22	454	370310	242457	157090	68243	4680	44663	0.1	51
FB14_23	458	403426	283190	201794	130946	33961	77236	0.3	7
FB14_24	360	390538	314224	251882	137297	4369	79799	0.0	74
FB14_25	456	363622	282974	207024	120270	27211	77136	0.3	7
FB14_26	1038	369005	275970	202845	122500	10959	75126	0.1	4
FB14_27	455	385644	296228	225558	106892	17703	56759	0.2	58
FB14_28	458	384992	284698	207987	118041	32877	73467	0.4	13
FB14_29	1045	414029	307004	224639	106689	16943	58960	0.2	13
FB14_3	454	353344	288147	226674	146689	14845	82663	0.1	18
FB14_4	454	376346	294289	223895	130338	43162	68543	0.5	3
FB14_5	461	384339	279095	205864	107162	10710	60975	0.1	12
FB14_6	454	352692	274030	213239	123514	28277	77789	0.3	4
FB14_7	456	364600	285560	220000	116081	21794	65075	0.3	33
FB14_8	454	369657	284052	206630	111351	34583	71055	0.4	3
FB14_9	457	337520	257220	196149	129932	13742	82412	0.1	12
FB15_1	463	340294	271875	206586	121081	32860	79196	0.3	6
FB15_10	468	347308	269935	202319	121486	34085	76784	0.4	4
FB15_11	463	373736	284806	207856	113716	38064	69648	0.4	3
FB15_12	466	362643	290841	219037	129797	41492	80251	0.4	3
FB15_13	464	350897	298276	233479	140878	56234	83317	0.5	4
FB15_14	458	341436	270797	210197	125811	22504	79045	0.2	18
FB15_15	456	352039	271013	209694	125608	36448	83417	0.4	4
FB15_16	460	377488	296336	223632	125068	15705	72965	0.2	8
FB15_17	341	352365	257651	188534	92568	5462	52698	0.1	35
FB15_18	459	366232	289116	218074	126351	30995	79648	0.3	5
FB15_19	472	277325	213147	154048	83986	35933	53166	0.5	7
FB15_20	463	356444	286315	216193	127027	55506	76181	0.6	3
FB15_21	464	366884	278772	213567	127568	14584	79548	0.1	5

Table S1. Detrital monazite U-Th-Pb data LASS-ICP-MS
Table S2. Detrital monazite Nd isotopic data LASS-ICP-MS
Table S3. Detrital monazite REE data LASS-ICP-MS

FB15_22	469	361175	290086	215755	123581	52931	76030	0.5	3
FB15_23	469	343393	271228	208381	119865	15275	75879	0.2	20
FB15_24	458	320392	257004	204179	147703	40906	111859	0.3	4
FB15_25	460	366232	283836	216477	119459	23250	67588	0.3	14
FB15_26	456	363132	276832	209322	117162	16064	69749	0.2	10
FB15_29	471	375530	297091	227133	134122	38845	82060	0.4	4
FB15_3	455	356281	278233	212560	117635	58508	69095	0.6	8
FB15_30	464	379282	298491	224289	127162	18020	74271	0.2	6
FB15_31	467	348940	273922	214070	131959	73321	85528	0.7	18
FB15_32	458	387602	311099	238293	124730	16599	70854	0.2	10
FB15_4	463	363622	276509	211663	122568	20178	73367	0.2	10
FB15_5	461	364600	281466	216937	134662	31030	92362	0.3	4
FB15_6	465	365905	277586	209803	115338	8174	67236	0.1	14
FB15_7	467	368679	284698	212932	118378	30710	72010	0.3	4
FB15_8	471	373409	283944	209650	100000	24885	57688	0.3	11
FB15_9	472	342251	281681	213786	124865	39627	78593	0.4	5
FB1SR-AsheSchist_1	457	283850	222629	169606	97162	12265	60050	0.2	7
FB1SR-AsheSchist_10	473	295269	228448	174026	99257	43179	58543	0.6	5
FB1SR-AsheSchist_11	474	271778	209052	159891	90608	38579	53216	0.6	5
FB1SR-AsheSchist_12	453	300000	234052	178928	102297	14078	62965	0.2	8
FB1SR-AsheSchist_13	461	309788	241810	184486	104662	43854	59447	0.6	5
FB1SR-AsheSchist_2	458	289233	223599	169212	92297	20782	55075	0.3	9
FB1SR-AsheSchist_3	451	289560	223922	171028	97905	41279	58543	0.5	5
FB1SR-AsheSchist_4	465	269494	212716	163545	94730	18597	55980	0.3	12
FB1SR-AsheSchist_5	456	271289	214440	170832	99932	24387	59497	0.3	12
FB1SR-AsheSchist_6	455	285971	226616	172319	96824	14419	59698	0.2	8
FB1SR-AsheSchist_8	462	294617	231034	176149	99459	25915	58995	0.3	7
FB1SR-AsheSchist_9	470	292007	225323	170897	97838	42167	56683	0.6	6
FB2_1	452	348124	276509	207856	126554	64618	78191	0.6	2

Table S1. Detrital monazite U-Th-Pb data LASS-ICP-MS
Table S2. Detrital monazite Nd isotopic data LASS-ICP-MS
Table S3. Detrital monazite REE data LASS-ICP-MS

FB2_10	457	381077	283190	209606	114054	13805	66332	0.2	5
FB2_11	463	373083	274461	201707	105743	12115	63819	0.1	12
FB2_12	455	353670	282220	220569	134459	29325	83467	0.3	9
FB2_13	455	363458	289547	217702	127297	37460	78442	0.4	3
FB2_15	457	366884	288362	209103	120473	45258	74874	0.5	4
FB2_16	457	376509	290733	220197	126892	16421	76583	0.2	6
FB2_17	464	397064	305172	225602	123716	42487	74523	0.4	5
FB2_18	475	375856	295366	229978	129595	18579	74774	0.2	12
FB2_19	459	373736	283728	218512	125338	39787	79447	0.4	8
FB2_2	462	352692	272198	208972	122162	12149	74070	0.1	9
FB2_20	463	355139	279095	215011	126486	35169	82864	0.3	4
FB2_21	461	362969	286422	215558	125541	59982	78794	0.6	4
FB2_24	467	354323	276185	211225	121824	18686	74422	0.2	10
FB2_25	471	359706	297091	223851	127905	39449	78995	0.4	7
FB2_26	457	360359	292134	221291	133378	33428	85779	0.3	4
FB2_27	453	390538	304634	233742	123919	21853	68799	0.2	42
FB2_3	458	372268	286099	210394	113243	55417	65226	0.6	4
FB2_4	457	351550	287500	221597	134257	47762	90503	0.4	4
FB2_5	462	359543	263685	193260	97905	14586	59648	0.2	13
FB2_6	328	340620	254203	186565	128581	7750	77588	0.1	9
FB2_7	457	352692	264978	195952	120811	58561	77889	0.6	8
FB2_8	458	327406	255065	200263	122162	16607	78492	0.2	11
FB2_9	451	366558	284698	218578	117500	13412	63467	0.2	49
FB2lowrow_1	331	340457	244181	186805	109459	64440	66985	0.8	7
FB2lowrow_10	414	330669	261638	205514	124324	41012	76231	0.4	5
FB2lowrow_11	463	349918	255711	188315	112770	17371	73367	0.2	3
FB2lowrow_12	463	361338	283728	209212	110676	19503	66382	0.2	10
FB2lowrow_13	354	358564	264116	194223	108378	66607	63819	0.8	9
FB2lowrow_14	463	354160	282543	210897	121014	46927	73869	0.5	4

Table S1. Detrital monazite U-Th-Pb data LASS-ICP-MS
Table S2. Detrital monazite Nd isotopic data LASS-ICP-MS
Table S3. Detrital monazite REE data LASS-ICP-MS

FB2lowrow_15	388	335073	246983	183698	103649	64849	65176	0.8	6
FB2lowrow_16	340	332463	253017	194989	115811	71243	73367	0.8	16
FB2lowrow_17	464	366069	271228	198534	102635	11016	61106	0.1	12
FB2lowrow_18	462	364927	267457	188031	99324	36004	63447	0.5	4
FB2lowrow_19	451	343719	265841	200941	119595	20107	70302	0.2	5
FB2lowrow_2	460	346819	275539	204748	115743	40089	70653	0.4	4
FB2lowrow_20	466	389886	283944	205230	95946	5448	41347	0.1	13
FB2lowrow_21	461	387113	280172	200919	91824	5245	39874	0.1	15
FB2lowrow_22	450	351223	263685	193392	102432	38401	67940	0.5	14
FB2lowrow_24	463	383524	276078	201379	94662	9421	50357	0.1	15
FB2lowrow_25	462	379445	276401	203392	100676	9520	53402	0.1	14
FB2lowrow_28	653	313866	241272	181182	100000	9201	61307	0.1	16
FB2lowrow_29	460	322349	247522	186193	107568	20551	65784	0.2	16
FB2lowrow_3	375	336705	261422	207615	128851	73872	77638	0.7	8
FB2lowrow_30	370	375530	299569	228731	124527	54352	72010	0.6	20
FB2lowrow_31	466	386623	290409	219912	117500	12554	68342	0.1	12
FB2lowrow_4	468	363458	267026	193063	101014	18632	60603	0.2	8
FB2lowrow_5	344	363948	286315	225317	116486	13551	63719	0.2	6
FB2lowrow_6	341	341925	251185	184770	101081	61456	61910	0.8	5
FB2lowrow_7	334	356607	257220	185514	104662	62700	63216	0.8	5
FB2lowrow_8	330	370636	277802	205252	119527	62504	67638	0.7	4
FB2lowrow_9	357	348124	272845	215252	139392	13535	80151	0.1	16
FB3_10	450	355302	267996	202188	123378	33730	74774	0.4	7
FB3_11	458	326101	260345	207790	138581	39236	89648	0.4	4
FB3_12	460	365742	280065	214486	132365	14222	77236	0.1	5
FB3_13	447	361338	271013	197899	110743	53393	67387	0.6	5
FB3_14	462	362316	270690	202604	99189	20142	55553	0.3	41
FB3_16	464	370962	277155	202013	108851	63925	64673	0.8	6
FB3_18	331	367374	287069	218074	128378	39520	69146	0.4	6

Table S1. Detrital monazite U-Th-Pb data LASS-ICP-MS
Table S2. Detrital monazite Nd isotopic data LASS-ICP-MS
Table S3. Detrital monazite REE data LASS-ICP-MS

FB3_19	458	383524	243319	156280	69459	11448	46508	0.2	13
FB3_20	338	221044	163685	121882	71892	44494	42010	0.8	3
FB3_21	462	376346	298168	229322	135743	65329	76432	0.6	3
FB3_22	382	358401	273599	208031	127432	79982	77739	0.8	4
FB3_23	455	386134	267565	193239	97162	16892	56146	0.2	10
FB3_24	456	357096	285560	224442	143581	15583	87688	0.1	5
FB3_25	459	357912	286638	225339	145000	15716	89146	0.1	4
FB3_26	374	372431	273168	208315	117905	71705	73518	0.8	8
FB3_27	380	377325	275539	206565	120541	78721	74623	0.8	3
FB3_28	461	383850	287716	216630	123176	16163	73116	0.2	6
FB3_29	460	343067	278987	225383	141959	82149	87387	0.7	5
FB3_3	466	358401	278017	208271	116351	46075	71307	0.5	4
FB3_30	335	336542	287069	217068	218176	31883	107588	0.2	2
FB3_33	443	430832	294289	191904	71851	7373	40492	0.1	31
FB3_34	328	369657	273276	199781	110946	56963	66080	0.7	7
FB3_35	336	352202	313039	235230	211486	2268	89347	0.0	31
FB3_36	454	378793	283728	215624	121689	19700	70101	0.2	13
FB3_4	461	360196	270043	194201	102568	26110	63367	0.3	6
FB3_5	368	355954	266595	198862	114730	75204	68744	0.8	5
FB3_6	456	338989	265841	203567	123243	20746	78040	0.2	5
FB3_7	458	330995	262931	203676	124122	21226	78844	0.2	5
FB3_9	456	367047	262823	191794	105676	21936	65477	0.3	8
FB4_1	485	349918	298060	217002	188581	1593	82412	0.0	52
FB4_10	429	346003	266379	205252	108581	49520	61508	0.6	14
FB4_11	446	365905	277586	206893	113311	58295	67276	0.7	5
FB4_12	457	373409	287177	217418	128108	47886	83668	0.5	3
FB4_13	458	360196	271336	200438	105203	7551	60352	0.1	23
FB4_14	458	353018	272198	209409	128649	26270	80000	0.3	4
FB4_15	451	373899	287500	214726	124662	15087	73467	0.2	4

Table S1. Detrital monazite U-Th-Pb data LASS-ICP-MS
Table S2. Detrital monazite Nd isotopic data LASS-ICP-MS
Table S3. Detrital monazite REE data LASS-ICP-MS

FB4_16	461	378467	275539	203173	104865	17105	60955	0.2	13
FB4_17	463	328385	252263	195667	111554	30053	69950	0.3	16
FB4_18	328	361827	255065	192385	114662	71829	73869	0.8	8
FB4_2	491	359543	306573	223195	194189	1629	84724	0.0	52
FB4_20	332	442904	273491	161488	61007	8451	42377	0.2	8
FB4_21	339	372268	277802	204070	112500	62984	67839	0.7	8
FB4_22	460	394454	281897	196652	93311	41119	53553	0.6	11
FB4_23	326	368189	282220	214223	126959	68863	84372	0.7	12
FB4_24	453	352039	267026	203786	131351	17318	86432	0.2	4
FB4_25	432	363948	276401	210066	121351	61314	74020	0.6	16
FB4_26	454	353507	279203	214661	127770	66572	77538	0.7	5
FB4_27	411	211093	165194	120394	64189	5892	35613	0.1	27
FB4_28	450	387765	292026	219300	127905	18130	77236	0.2	9
FB4_29	326	380914	272737	202626	122635	77638	77286	0.8	6
FB4_30	456	382219	277909	200109	107500	39023	68492	0.5	5
FB4_31	457	406362	276078	193020	98378	10547	60000	0.1	4
FB4_32	450	355791	295474	233917	169054	16512	89799	0.1	4
FB4_4	466	414845	275754	179103	68791	5028	42930	0.1	34
FB4_6	475	340783	262284	206761	113514	64600	67538	0.7	82
FB4_7	326	351876	263254	197877	111216	63783	68241	0.7	7
FB4_8	458	372920	280388	211182	116149	10551	65829	0.1	13
FB4_9	453	373899	289332	216105	122905	46217	73970	0.5	9
FB5_1	445	350571	281573	217352	140878	20863	86231	0.2	7
FB5_10	440	360359	261315	202276	119257	62398	76683	0.7	12
FB5_11	451	351387	276940	205208	116824	65417	74472	0.7	6
FB5_12	456	379119	277263	204223	107973	19105	68342	0.2	8
FB5_13	448	357259	258728	188490	104257	15563	68342	0.2	24
FB5_14	452	365253	256466	175317	84223	4700	54206	0.1	18
FB5_15	449	376020	286853	216389	113176	12256	65879	0.1	11

Table S1. Detrital monazite U-Th-Pb data LASS-ICP-MS
Table S2. Detrital monazite Nd isotopic data LASS-ICP-MS
Table S3. Detrital monazite REE data LASS-ICP-MS

FB5_16	458	372104	278341	205667	115135	29218	74221	0.3	4
FB5_17	447	368842	287931	219168	124324	26501	77638	0.3	11
FB5_18	447	332300	256358	200131	135676	34174	89196	0.3	5
FB5_19	460	382545	303017	230000	132432	43304	82764	0.4	4
FB5_2	452	364600	284267	221138	127027	18224	74623	0.2	7
FB5_20	453	372104	294935	226018	133378	22096	84774	0.2	3
FB5_21	456	369168	289009	215427	120608	36288	77538	0.4	5
FB5_22	449	397553	300862	228403	103649	16535	59593	0.2	38
FB5_23	456	370799	290302	217987	122297	27371	77136	0.3	5
FB5_25	457	346982	265086	197024	119797	66607	76080	0.7	14
FB5_26	450	383850	291056	220197	111419	14588	66080	0.2	39
FB5_27	448	381240	292672	221379	128311	20059	80955	0.2	9
FB5_28	456	367537	287716	221575	135608	23659	85980	0.2	19
FB5_29	454	388418	296228	221532	125000	16842	77085	0.2	6
FB5_3	455	360196	284159	217834	125135	66767	74975	0.7	6
FB5_30	443	393475	307004	230963	133986	41474	82412	0.4	4
FB5_31	469	370799	286961	216018	125608	29414	80251	0.3	6
FB5_32	468	341925	273384	204814	116892	60817	71759	0.7	2
FB5_33	447	364111	279849	215120	129459	18176	82060	0.2	6
FB5_34	479	383850	280172	200394	102635	39432	63492	0.5	17
FB5_35	464	370473	298707	224070	129865	44618	82714	0.4	3
FB5_36	461	305710	233190	179650	103311	15536	68141	0.2	18
FB5_37	457	355954	273815	208031	120608	13016	77940	0.1	9
FB5_38	464	370310	286530	223414	130338	16902	79849	0.2	6
FB5_39	470	372594	277263	202626	108378	26039	67286	0.3	10
FB5_4	447	379935	294935	225974	113446	18215	60312	0.2	30
FB5_5	438	378630	293642	222757	115338	18883	61357	0.2	39
FB5_6	452	368679	288039	216608	124865	22185	80302	0.2	7
FB5_7	470	371941	287284	216761	118716	25311	73970	0.3	13

Table S1. Detrital monazite U-Th-Pb data LASS-ICP-MS
Table S2. Detrital monazite Nd isotopic data LASS-ICP-MS
Table S3. Detrital monazite REE data LASS-ICP-MS

FB5_8	445	376835	297091	231466	131486	20632	73668	0.2	33
FB5_9	449	362480	278987	216018	128176	37140	86633	0.4	3
FB6_1	460	346493	273815	209781	122027	34440	76181	0.4	6
FB6_10	452	365253	287823	221597	130000	11078	73216	0.1	10
FB6_11	483	210277	177047	146214	100068	17655	61055	0.2	20
FB6_12	445	352039	272522	207681	120068	27940	71005	0.3	19
FB6_13	466	359543	278987	215580	126554	26377	77739	0.3	6
FB6_14	461	341436	259052	196061	111081	52114	68040	0.6	7
FB6_15	456	354812	284375	216433	125135	30302	77990	0.3	4
FB6_16	458	346330	263470	191444	104797	24067	67286	0.3	10
FB6_17	457	377814	280496	209103	113649	9430	65392	0.1	16
FB6_18	453	355628	276078	214595	127973	27922	80804	0.3	5
FB6_19	458	385155	290086	215295	127297	12881	73417	0.1	5
FB6_2	453	351550	262284	193304	105743	14917	65628	0.2	6
FB6_20	449	371452	291379	227046	139459	21741	80603	0.2	12
FB6_21	451	372757	287069	220810	123581	27602	71085	0.3	15
FB6_22	454	368515	297198	218796	120811	48437	75176	0.5	4
FB6_23	462	352202	281466	218403	133243	21918	84472	0.2	6
FB6_24	456	387439	267565	178293	71824	7536	41899	0.1	39
FB6_25	444	364763	253233	171269	69250	6986	40261	0.1	43
FB6_26	460	355628	280819	215777	128243	66661	73769	0.7	10
FB6_27	453	376835	286746	214376	115878	18709	67593	0.2	12
FB6_28	458	363132	288254	222516	132162	13554	78945	0.1	7
FB6_29	457	401794	282974	202013	73176	11389	40482	0.2	112
FB6_3	455	358891	293103	219716	125405	71758	69095	0.8	4
FB6_30	464	370636	268750	188556	106622	6384	59950	0.1	23
FB6_31	460	380750	295151	222998	125946	13808	73166	0.1	8
FB6_32	447	376020	267888	188840	92973	34760	52487	0.5	44
FB6_33	454	358728	281789	214573	124324	46519	74623	0.5	7

Table S1. Detrital monazite U-Th-Pb data LASS-ICP-MS
Table S2. Detrital monazite Nd isotopic data LASS-ICP-MS
Table S3. Detrital monazite REE data LASS-ICP-MS

FB6_34	445	360196	246983	169278	86014	49041	56281	0.7	16
FB6_35	444	363948	279741	210897	122770	15355	76080	0.2	9
FB6_36	448	363132	281034	213545	126959	14725	79698	0.1	8
FB6_37	454	366558	285991	217615	127635	19467	81106	0.2	8
FB6_38	451	389886	298815	222867	126622	60675	73367	0.6	4
FB6_39	457	370636	291487	218096	125541	46803	76734	0.5	4
FB6_4	453	355791	274246	211904	124392	25933	72362	0.3	7
FB6_40	450	373899	290194	222538	120203	19911	72111	0.2	18
FB6_5	458	367537	281681	213129	104392	18449	52744	0.2	36
FB6_6	452	369984	278233	206937	104730	13101	59709	0.2	17
FB6_7	459	379445	289871	212691	110541	32895	63347	0.4	6
FB6_8	456	366721	292996	220197	119730	55613	73769	0.6	5
FB6_9	455	379445	288362	211947	114662	30764	69497	0.3	4
FB8_11	461	384013	300539	228271	133378	41865	84523	0.4	5
FB8_12	452	367047	271983	194945	104324	12069	64070	0.1	18
FB8_13	454	380914	303556	226258	127027	43641	79950	0.4	5
FB8_14	465	360359	262823	192779	97973	21723	62312	0.3	14
FB8_15	460	355954	282651	211160	118108	26998	74573	0.3	5
FB8_16	463	369331	291703	229322	146284	22558	88342	0.2	3
FB8_2	469	378140	281573	205492	108311	38774	60804	0.5	5
FB8_3	467	358891	296659	240066	151689	15721	84623	0.1	8
FB8_4	458	364927	298815	230197	151081	37726	88744	0.3	5
FB8_5	462	359869	281789	218228	127905	38632	75276	0.4	4
FB8_6	469	379282	298491	223304	126149	34227	77236	0.3	4
FB8_7	454	367537	276509	208884	122568	71012	76884	0.7	6
FB8_8	459	365579	297953	226258	130811	55062	79497	0.5	3
FB8_9	459	388907	292457	218862	105608	19787	60201	0.2	62
FB9_1	465	382545	279741	206214	116486	34085	75829	0.4	3
FB9_11	452	347308	273060	203676	120946	27638	83970	0.3	6

Table S1. Detrital monazite U-Th-Pb data LASS-ICP-MS
Table S2. Detrital monazite Nd isotopic data LASS-ICP-MS
Table S3. Detrital monazite REE data LASS-ICP-MS

FB9_12	443	372594	293319	222298	120946	31918	75276	0.3	18
FB9_13	451	379608	302694	227615	132635	41190	85879	0.4	4
FB9_14	459	381892	299569	224639	129257	45293	84824	0.4	4
FB9_15	452	366721	290194	222188	135203	19858	88543	0.2	4
FB9_16	449	378140	295797	219475	125811	42202	79548	0.4	4
FB9_17	452	371452	295582	223917	128108	25613	76231	0.3	5
FB9_18	446	366395	284375	213632	123716	45506	77337	0.5	4
FB9_19	450	366232	272629	199212	106419	23357	66784	0.3	6
FB9_2	1043	388581	265841	181116	68716	9389	46678	0.2	93
FB9_20	1015	346330	242349	164048	70203	6805	46533	0.1	65
FB9_21	455	363622	286207	217462	126757	43890	81960	0.4	4
FB9_22	457	370799	288793	221729	126689	21883	78392	0.2	7
FB9_23	456	346330	276940	209628	123514	55080	80000	0.6	4
FB9_25	454	354486	291164	220022	137027	48970	105126	0.4	5
FB9_26	445	376998	289871	218118	109865	10883	67940	0.1	27
FB9_27	453	362806	292996	223195	131824	23641	86131	0.2	5
FB9_28	452	392170	314547	236980	130541	19680	70352	0.2	8
FB9_29	448	391354	295905	219694	95676	16485	55106	0.2	38
FB9_3	461	315171	268427	220569	162838	48259	105176	0.4	14
FB9_30	457	387113	305603	234573	134459	29840	86583	0.3	4
FB9_31	448	366069	295690	222123	127838	43801	83618	0.4	4
FB9_32	463	382219	296983	229147	120270	6741	75879	0.1	8
FB9_33	435	361011	277478	208621	121149	63783	80955	0.6	6
FB9_34	455	370310	288362	218600	127095	67815	83166	0.7	5
FB9_35	450	392333	291379	215492	116149	19247	78090	0.2	3
FB9_36	457	342741	276724	209059	125270	52398	85879	0.5	6
FB9_37	453	382708	301078	233020	133243	21883	82412	0.2	12
FB9_38	451	367047	283728	219912	130135	49663	78794	0.5	7
FB9_39	450	385971	299461	228884	123243	18979	71874	0.2	23

Table S1. Detrital monazite U-Th-Pb data LASS-ICP-MS
Table S2. Detrital monazite Nd isotopic data LASS-ICP-MS
Table S3. Detrital monazite REE data LASS-ICP-MS

FB9_4	458	353997	276293	208709	119527	14696	76181	0.2	6
FB9_40	448	373409	289440	218643	123851	24707	81307	0.2	5
FB9_41	445	391191	283190	203260	100743	6535	58849	0.1	28
FB9_42	454	391843	305388	233173	134730	33250	84673	0.3	5
FB9_43	450	387439	301185	230000	133176	21297	84673	0.2	6
FB9_44	449	382382	293858	214464	121351	43481	84221	0.4	4
FB9_46	440	401142	302802	227527	112703	16909	70894	0.2	11
FB9_5	455	324144	273168	215842	141824	14036	106633	0.1	5
FB9_6	465	377488	306358	228884	125135	25187	65276	0.3	9
FB9_7	460	363132	282328	213151	122770	50622	75829	0.5	5
FB9_8	459	359706	277478	216849	127432	14899	78643	0.1	8
FB9_9	452	353670	276832	214398	124257	32895	79899	0.3	3
FinesCreek-Schist_1	451	290375	231358	176586	108378	43925	76583	0.5	5
FinesCreek-Schist_10	447	308646	248060	185602	108243	46732	71256	0.5	3
FinesCreek-Schist_11	444	311093	251616	187790	105946	48348	64030	0.6	3
FinesCreek-Schist_12	448	304241	244828	185930	113108	47158	79598	0.5	3
FinesCreek-Schist_13	443	264111	211961	161269	97973	38863	66382	0.5	4
FinesCreek-Schist_14	445	299021	238147	184639	116959	44050	88794	0.4	4
FinesCreek-Schist_15	443	298206	237177	181379	112703	44956	83719	0.5	4
FinesCreek-Schist_16	444	310277	251832	189409	108108	48828	67286	0.6	3
FinesCreek-Schist_17	447	305873	244289	185864	114527	45968	83266	0.5	4
FinesCreek-Schist_18	443	305873	244289	187877	117905	46057	87286	0.5	5
FinesCreek-Schist_2	447	315008	253772	191182	112095	48064	74975	0.5	3
FinesCreek-Schist_3	444	316476	254418	190394	108176	48419	67538	0.6	3
FinesCreek-Schist_4	448	300000	238793	182385	112297	44707	81508	0.5	4
FinesCreek-Schist_5	442	299511	237177	182976	115473	43588	87085	0.4	5
FinesCreek-Schist_6	456	308972	245259	186608	114932	45222	84121	0.5	5
FinesCreek-Schist_7	454	311419	249569	190306	116892	47336	76935	0.5	3
FinesCreek-Schist_8	452	304078	240841	184508	116284	43286	87437	0.4	5

Table S1. Detrital monazite U-Th-Pb data LASS-ICP-MS
Table S2. Detrital monazite Nd isotopic data LASS-ICP-MS
Table S3. Detrital monazite REE data LASS-ICP-MS

FinesCreek-Schist_9	443	279119	225108	168928	99054	41421	64070	0.5	3
FL7_large_1	1048	351223	317349	264770	170541	7226	93668	0.1	30
FL7_large_10	1027	328059	279310	226039	172095	12425	117136	0.1	5
FL7_large_11	1060	360522	292996	220569	116486	3204	65628	0.0	19
FL7_large_13	1160	353670	280819	208753	127365	7057	82312	0.1	9
FL7_large_14	1166	343556	274784	207440	132230	6899	83568	0.1	11
FL7_large_15	1082	361501	269289	190810	99324	21066	70201	0.3	7
FL7_large_16	1036	372104	273707	193501	103108	26199	71206	0.3	29
FL7_large_17	1054	329527	259159	195842	110135	27673	80000	0.3	12
FL7_large_18	1047	326264	257866	195098	112432	28970	80503	0.3	11
FL7_large_19	1162	341762	266056	195711	124122	2876	84070	0.0	5
FL7_large_2	1045	344209	304634	248906	151149	4101	88040	0.0	47
FL7_large_20	1004	336705	283297	224289	132770	2023	79196	0.0	32
FL7_large_21	1038	325122	303772	255799	184392	1341	90503	0.0	56
FL7_large_22	1053	340457	309591	258425	175203	11794	88894	0.1	39
FL7_large_24	1093	337194	268642	203063	114054	6835	71910	0.1	36
FL7_large_25	1174	327732	264547	202188	117095	4506	73015	0.0	30
FL7_large_26	1043	369331	291595	219387	97095	3607	57487	0.0	19
FL7_large_29	1093	363458	292780	234792	152095	45595	101005	0.4	4
FL7_large_30	1167	343067	273491	210503	135608	32629	84472	0.3	3
FL7_large_34	1003	343883	278448	212910	146959	28988	95477	0.2	5
FL7_large_35	1007	342088	279957	212516	144527	28259	93819	0.2	5
FL7_large_37	1113	349592	288578	226149	138851	19449	88442	0.2	5
FL7_large_5	1135	361175	293534	220963	125270	6629	70603	0.1	50
FL7_large_6	981	329527	271659	207987	137905	7549	77839	0.1	14
FL7_large_8	1161	346493	288254	226039	139932	30195	92764	0.3	4
FL7_large_9	1022	328874	279634	225602	170946	12421	115528	0.1	4
FL7_small_1	1136	342088	289116	237199	165946	12570	113015	0.1	3
FL7_small_10	1139	373246	286638	209847	110743	49165	64171	0.6	4

Table S1. Detrital monazite U-Th-Pb data LASS-ICP-MS
Table S2. Detrital monazite Nd isotopic data LASS-ICP-MS
Table S3. Detrital monazite REE data LASS-ICP-MS

FL7_small_11	1035	326427	282328	219694	176689	1911	100201	0.0	4
FL7_small_13	1148	342741	272522	215098	134122	35098	82814	0.3	7
FL7_small_14	1027	340457	287716	224945	137432	6950	79296	0.1	11
FL7_small_16	1102	357586	298276	241575	159459	46448	90503	0.4	9
FL7_small_17	914	354323	298384	238731	136216	60746	64322	0.6	29
FL7_small_18	1165	310440	232759	180941	98851	23481	50352	0.3	20
FL7_small_21	515	341436	406789	387527	240000	222025	68291	1.7	30
FL7_small_22	1125	334095	268319	202407	112297	34032	65829	0.4	5
FL7_small_24	1049	350897	290517	219475	103851	19165	46231	0.3	73
FL7_small_26	1199	334095	268750	208753	126689	46252	78291	0.5	4
FL7_small_27	1160	328548	280172	219912	149932	3272	97839	0.0	9
FL7_small_28	1093	328222	256681	196105	140135	18171	84171	0.2	2
FL7_small_29	1106	394943	346767	264551	110203	41829	50503	0.6	97
FL7_small_3	1119	332790	281034	226477	164122	6345	104874	0.0	6
FL7_small_30	1048	338010	275862	212473	136149	7531	67940	0.1	7
FL7_small_31	1120	424307	244181	181007	99797	42167	50181	0.6	12
FL7_small_32	1109	307178	298276	269147	181081	18547	81709	0.2	11
FL7_small_34	1108	343556	291164	239825	144054	27744	81809	0.3	3
FL7_small_35	1056	367863	284483	214442	109662	13476	66734	0.2	22
FL7_small_5	1033	400979	282866	192298	108919	18490	65126	0.2	694
FL7_small_7	1026	376183	286638	210941	94459	9236	54136	0.1	26
FL7_small_8	1047	346330	280172	217637	130878	44529	80352	0.4	14
FL7_small_9	1038	365742	288147	218906	126554	33943	67437	0.4	4
KS12-2C_large_1	1061	346003	289224	227790	126149	4458	63518	0.0	56
KS12-2C_large_10	1048	353834	285884	224136	131419	5719	71809	0.1	18
KS12-2C_large_13	1030	357259	300970	237856	132905	5076	65678	0.1	55
KS12-2C_large_14	1031	360522	301293	237418	131351	4877	64724	0.1	56
KS12-2C_large_15	998	337031	287716	219562	199865	7780	118342	0.1	1
KS12-2C_large_16	991	339478	288685	217265	199324	10490	115075	0.1	1

Table S1. Detrital monazite U-Th-Pb data LASS-ICP-MS
Table S2. Detrital monazite Nd isotopic data LASS-ICP-MS
Table S3. Detrital monazite REE data LASS-ICP-MS

KS12-2C_large_2	1043	341599	287177	227790	126554	4945	62965	0.1	57
KS12-2C_large_5	1031	315987	274892	223414	172770	10020	107337	0.1	4
KS12-2C_large_7	1018	388091	262177	160832	61892	4176	57337	0.1	36
KS12-2C_large_8	1044	351387	294289	232385	132432	4938	67487	0.1	38
KS12-2C_large_9	1044	353344	294935	233479	132365	5103	67538	0.1	36
KS12-2C_small_10	1010	297716	257004	206346	164595	6265	103467	0.0	3
KS12-2C_small_11	387	360522	280065	212473	116892	4050	65779	0.0	32
KS12-2C_small_12	370	341925	264871	202713	120811	20977	73769	0.2	25
KS12-2C_small_14	1447	361011	302586	238731	142230	5060	60804	0.1	641
KS12-2C_small_2	1068	326101	276185	228446	165811	36252	90804	0.3	3
KS12-2C_small_3	992	336868	286853	213304	204865	13941	116181	0.1	1
KS12-2C_small_4	996	353181	296552	239387	148986	25577	68784	0.3	13
KS12-2C_small_5	1027	351223	287392	222319	152905	4016	74472	0.0	17
KS12-2C_small_6	1022	384176	276078	208315	122230	38988	77538	0.4	6
KS12-2C_small_7	351	347308	266272	202188	117500	13991	74724	0.1	23
KS12-2C_small_8	1132	388418	277047	206389	122568	89822	75075	0.9	3
LookingGlass-Granite_1	332	277977	234914	182626	155473	21528	80201	0.2	24
LookingGlass-Granite_11	335	266069	221336	174836	147162	24440	79899	0.2	18
LookingGlass-Granite_12	337	280261	238147	188993	164595	21139	83719	0.2	34
LookingGlass-Granite_13	338	269984	225431	177790	147635	21581	76080	0.2	26
LookingGlass-Granite_2	335	235400	200108	157659	132635	14394	66683	0.2	19
LookingGlass-Granite_20	334	271778	225970	180372	151622	26377	82814	0.2	18
LookingGlass-Granite_23	338	276020	231789	184726	154459	24067	81508	0.2	23
LookingGlass-Granite_25	339	256281	217026	166740	172770	17993	81709	0.2	9
LookingGlass-Granite_3	323	304731	251401	192144	164257	20959	85578	0.2	10
LookingGlass-Granite_6	334	260359	216164	170131	139730	26163	77739	0.3	23
LookingGlass-Granite_8	321	289070	235560	175777	150743	29414	78945	0.3	15
PF12-1-Shields_1	974	349103	297737	246171	183243	28224	101859	0.2	7
PF12-1-Shields_10	1044	370147	288254	212691	100000	3254	46794	0.0	60

Table S1. Detrital monazite U-Th-Pb data LASS-ICP-MS
Table S2. Detrital monazite Nd isotopic data LASS-ICP-MS
Table S3. Detrital monazite REE data LASS-ICP-MS

PF12-1-Shields_11	1082	371452	290086	214004	102365	3337	47819	0.0	60
PF12-1-Shields_12	1034	386297	282112	191707	99932	11686	59849	0.2	10
PF12-1-Shields_13	1046	328385	283190	232385	166014	18295	107337	0.1	4
PF12-1-Shields_14	1041	328548	285345	234792	167770	18064	108492	0.1	4
PF12-1-Shields_16	1053	361664	259052	182385	80676	10849	49683	0.2	52
PF12-1-Shields_17	1134	369657	285776	217462	133378	46146	76080	0.5	9
PF12-1-Shields_23	1052	361175	260668	187287	107162	15773	60503	0.2	9
PF12-1-Shields_6	1083	344535	289116	235011	142162	55897	80000	0.5	32
PF12-1-Shields_7	1050	246330	197198	135449	93243	38899	49950	0.6	12
PF12-1-Shields_8	1201	396737	266918	173982	67973	18917	38090	0.4	21
PF12-1-Shields_9	1190	391354	260345	168403	63108	23091	36593	0.5	16
SixmileSchist_1	364	307015	236315	180591	108784	8037	60653	0.1	4
SixmileSchist_10	360	319413	246228	186827	112635	8567	62864	0.1	4
SixmileSchist_11	359	306852	233082	175055	101014	23268	62412	0.3	5
SixmileSchist_12	366	318760	246336	189278	113784	10107	63920	0.1	5
SixmileSchist_13	356	283850	215625	163282	86351	27016	45719	0.4	16
SixmileSchist_14	365	327243	248491	188403	92770	5725	40513	0.1	19
SixmileSchist_15	407	316150	241379	182363	109392	58615	63266	0.7	4
SixmileSchist_16	369	331648	251078	188600	107568	12824	64874	0.2	5
SixmileSchist_17	406	330343	245474	178775	92838	54387	49015	0.8	9
SixmileSchist_18	370	327080	249461	187965	112568	75027	57638	0.9	3
SixmileSchist_19	376	335563	256034	192998	117635	69414	62714	0.8	8
SixmileSchist_2	381	303589	232328	177155	95338	18117	46784	0.3	17
SixmileSchist_20	369	332137	253017	190153	115270	62291	61905	0.7	6
SixmileSchist_3	379	288581	220797	170460	98581	38739	57236	0.5	3
SixmileSchist_4	393	289233	229741	186893	125811	48135	67236	0.5	4
SixmileSchist_5	356	300653	229741	176236	106284	9995	62864	0.1	5
SixmileSchist_6	385	313540	238578	179125	108919	64210	61558	0.8	7
SixmileSchist_7	371	284829	216918	164639	96014	23126	61980	0.3	4

Table S1. Detrital monazite U-Th-Pb data LASS-ICP-MS
Table S2. Detrital monazite Nd isotopic data LASS-ICP-MS
Table S3. Detrital monazite REE data LASS-ICP-MS

SixmileSchist_8	383	306199	233297	177921	94324	21563	48191	0.3	13
SixmileSchist_9	368	300489	229526	172407	108514	39698	62362	0.5	3
WCK12-1-Sandsuck_1	1053	379935	284375	196236	84797	9076	42447	0.2	9
WCK12-1-Sandsuck_2	1071	382871	283190	199037	90676	2401	47186	0.0	41
WCK12-1-Sandsuck_3	1094	359706	266487	187593	98446	3259	55075	0.0	21
WCK12-1-Sandsuck_4	1043	311256	253125	207221	132162	19432	83920	0.2	16
WCK12-1-Sandsuck_5	1039	368026	300000	227790	134662	2135	66930	0.0	39
WCK12-1-Sandsuck_6	1048	367047	277802	197155	96216	1647	48442	0.0	31
WCK12-1-Sandsuck_8	1068	376020	294612	214004	101284	1469	45693	0.0	92

References

Abbott, R.N., and Raymond, L.A., 1984, The Ashe Metamorphic Suite, Northwest North Carolina; metamorphism and observations on geologic history: American Journal of Science, v. 284, p. 350-375.

Aleinikoff, J.N., Southworth, S., Fanning, C.M., and Mazdab, F.K., 2010, Evidence for late Neoproterozoic deposition of the Ocoee Supergroup: SHRIMP U-Pb and trace element analysis of diagenetic xenotime and monazite: Geological Society of America Abstracts with Programs, v. 42, n. 1, p. 59.

Allaz, J., Selleck, B., Williams, M.L., Jercinovic, M.J., 2013, Microprobe analysis and dating of monazite from the Potsdam Formation, New York: A progressive record of chemical reaction and fluid interaction: American Mineralogist, v. 98, n. 7, p. 1106-1119.

Andersen, B.C., Samson, S.D., 1995, Increasing influence of exotic terranes as sources of shales from Sevier and Taconic Foreland basins: Evidence from Nd isotopes: Geology, v. 23, n. 11., p. 983-986.

Bock, B., McLennan, S.M., and Hanson, G.N., 1996, The Taconian orogeny in southern New England: Nd-isotope evidence against addition of juvenile components: Canadian Journal of Earth Science, v. 33, p. 1612-1627.

Bream, B.R., Hatcher, R.D., Miller, C.F., Fullagar, P.D., Tollo, R.P., McLelland, J., Corriveau, L., Bartholomew, M.J., 2004, Detrital zircon ages and Nd isotopic data from the southern Appalachian crystalline core, Georgia, South Carolina, North Carolina, and Tennessee: New provenance contrants for part of the Laurentian margin: Memoirs-Geological Society of America, p. 459-476.

Butler, J. R., 1991. Metamorphism, in Horton, J. W., Jr., and Zullo, V. A., eds., The geology of the Carolinas: Carolina Geological Society Fiftieth Anniversary Volume: Knoxville, University of Tennessee Press, p. 127 - 141.

Carpenter, R.H., 1970, Metamorphic history of the Blue Ridge province of Tennessee and North Carolina: Geological Society of America Bulletin, v. 81, n. 3, p. 749-762.

Carrigan, C.W., Miller, C.F., Fullagar, P.D., Bream, B.R., Hatcher, R.D., Jr., and Coath, C.D., 2003, Ion micro- probe age and geochemistry of southern Appalachian basement, with implications for Proterozoic and Paleo- zoic reconstructions: Precambrian Research, v. 120, p. 1–36, doi: 10.1016/S0301-9268(02)00113-4.

Coler, D.G., Wortman, G.L., Samson, S.D., Hibbard, J.P., and Stern, R., 2000, U-Pb Geochronologic, Nd Isotopic, and Geochemical Evidence for the Correlation of the Chopawamsic and Milton Terranes, Piedmont Zone, Southern Appalachian Orogen: The Journal of Geology, v. 108, n. 4, p. 363-380.

Corrie, S.L. and Kohn, M.J., 2007, Resolving the timing of orogenesis in the Western Blue Ridge, southern Appalachians, via in situ ID-TIMS monazite geochronology: Geology, v. 35, n. 7, p.627-630.

Cottle, J., Kylander-Clark, A., Vrijmoed, J., 2012, U-Th/Pb geochronology of detrital zircon and monazite by single shot laser ablation inductively coupled plasma mass spectrometry (SS-LA-ICPMS), Chemical Geology, v. 332-333, p. 136-147.

Cottle, J., Burrows, A., Kylander-Clark, A., 2013, Enhanced sensitivity in laser ablation multi-collector inductively coupled plasma mass spectrometry, JAAS, v. 28, n. 10, p. 1700-1706.

Dennis, A.J., 2007, Cat Square basin, Catskill clastic wedge: Silurian-Devonian orogenic events in the central Appa- lachians and the crystalline southern Appalachians, in Sears, J.W., et al., eds., Whence the Mountains? Inquires into the evolution of orogenic systems: A vol- ume in honor of Raymond A. Price: Geological Soci- ety of America Special Paper 433, p. 313–329, doi: 10.1130/2007.2433(15).

Dunning, G.R., Macdonald, A.S., and Barr, S.M., 1995, Zircon and monazite U- Pb dating of the Doi Inthanon core complex, northern Thailand: implications for extension within the Indosinian Orogen: Tectonophysics, v. 251, n. 1-4, p.197-213.

Evans, J.A, Chisholm, J.I., and Leng, M.J., 2001, How U-Pb detrital monazite ages contribute to the interpretation of the Pennine Basin infill: Journal of the Geological Society, v. 158, n. 5, p. 741-744.

Fenner, C.N., 1928, The analytical determination of uranium, thorium, and lead as a basis for age calculations, American Journal of Science, v. 26, p. 369-381.

Fisher, C.M., Hanchar, J.M., Miller, C.F., Phillips, S., Vervoort, J.D., and Whitehouse, M.J., 2017, Combining Nd isotopes in monazite and Hf isotopes in zircon to understand complex open-system processes in granitic magmas, Geology, v. 45, no. 3, p. 267-270.

Gehrels, G., Valencia, V., and Ruiz, J., 2008, Enhanced precision, accuracy, efficiency, and spatial resolution of U-Pb ages by laser ablation-multicollector-inductively coupled plasma mass spectrometry: Geochemistry Geophysics Geosystems, v. 9, p. 1–13, doi: 10.1029/2007GC001805.

Goldberg, S.A., and R.D. Dallmeyer. 1997, Chronology of Paleozoic metamorphism and deformation in the Blue Ridge thrust complex, North Carolina and Tennessee: American Jounral of Science, v. 297, n. 5, p. 488-526.

Hacker, B.R., Kylander-Clark, A.R., Holder, R., Andersen, T.B., Peterman, E.M., Walsh, E.O., and Munnikhuis, J.K., 2015, Monazite response to ultrahigh-pressure subduction from U–Pb dating by laser ablation split stream: Chemical Geology, v. 409, p. 28-41.

Hadley, J.B., and Nelson, A.E., 1971, Geologic map of the Knoxville quadrangle, North Carolina, Tennessee, and South Carolina, n. 654.

Harrison, T.M., Catlos, E.J., and Montel, J.-M., 2002, U-Th-Pb Dating of Phosphate Minerals: Reviews in Mineralogy and Geochemistry, v. 48, p. 524–558, doi: 10.2138/rmg.2002.48.14.

Hatcher Jr, R.D., 1987, Tectonics of the southern and central Appalachian internides: Annual Review Earth & Planetary Science, v. 15, p. 337-362.

Hatcher Jr, R.D., 1989, Appalachians introduction: The Appalachian-Ouchita orogen in the United States: Boulder, Colorado, Geological Society of America, Geology of North America 2, p. 1-6.

Hatcher, R.D., Jr., 2002, An Inner Piedmont primer, in Hatcher, R.D., Jr., and Bream, B.R., eds., Inner Piedmont geology in the South Mountains–Blue Ridge Foothills and the southwestern Brushy Mountains, central-western North Carolina: Carolina Geological Society Annual Field Trip Guidebook 2002, p. 1–18.

Hering, O.H., and Zimmerle, W., 1963, Simple method of distinguishing zircon, monazite, and xenotime: Journal of Sedimentary Research, v. 33, n. 2, p. 472-473.

Hietpas, J., Samson, S., Moecher, D., and Schmitt, A.K., 2010, Recovering tectonic events from the sedimentary record: Detrital monazite plays in high fidelity: Geology, v. 38, p. 167–170, doi: 10.1130/g30265.1.

Hietpas, J., Samson, S., and Moecher, D., 2011, A direct comparison of the ages of detrital monazite versus detrital zircon in Appalachian foreland basin sandstones: Searching for the record of Phanerozoic orogenic events: Earth and Planetary Science Letters, v. 310, p. 488–497, doi: 10.1016/j.epsl.2011.08.033.

Hietpas, Jack, "Investigating the Utility of Detrital Mineral Microchemistry and Radiogenic Isotope Compositions as Provenance Discriminators" (2012). Earth Sciences - Dissertations. Paper 29.

Hietpas, J., Samson, S., Speir, J., and Moecher, D., 2013, Assessing detrital garnet chemical composition as a quantitative provenance tool: a multivariate statistical approach: Journal of Sedimentary Research, v. 83, n. 12, p. 1181-1197.

Horstwood, M.S., Foster, G.L., Parrish, R.R., Noble, S.R,. and Nowell, G.M., 2003, Common-Pb corrected in situ U–Pb accessory mineral geochronology by LA-MC-ICP-MS: Journal of Analytical Atomic Spectrometry, v. 18, n. 8, p. 837-846.

Jackson, S.E., Pearson, N.J., Griffin, W.L., Belousova, E.A., 2004, The application of laser ablation-inductively coupled plasma-mass spectrometry to in situ U-Pb zircon geochronology: Chemical Geology, v. 211, n. 1-2, p. 47-69.

Kelly, E., 2014, Age of the Walden Creek Group, western Blue Ridge Province: resolving a decades-old controversy via detrital mineral geochronology and sedimentary provenance analysis, University of Kentucky Thesis.

King, P.B., Hadley, J.B., Neuman, R.B., and Hamilton, W., 1958, Stratigraphy of Ocoee Series, Great Smoky Mountains, Tennessee and North Carolina, Geological Society of America Bulletin, v. 69, p. 947-966.

Kistler, R.W., Wooden, J.L., Premo, W.R., and Morton, D.M., Pb-Sr-Nd-O isotopic characterization of Mesozoic rocks, p. 279, *in* Morton, D.M., and Miller, F.K., 2014, Peninsular Ranges Batholith, Baja and Southern California: Geological Society of America Memoirs, v. 211.

Kylander-Clark, A.R.C., Hacker, B.R., Cottle, J.M., 2013, Laser-ablation split-stream ICP petrochronology: Chemical Geology, v. 345, p. 99-112.

Ludwig, K.R., 2012, Isoplot 3.75: A Geochronological Toolkit for Microsoft *Excel*: Berkeley Geochrnology Center Special Publication No. 5.

Maclure, W., 1809, Observations on the geology of the United States explanatory of a geological map: Transactions of the American Philosophical Society, v. 6, p. 411-428.

McLelland, J., Hamilton, M., Selleck, B., McLelland, J., Walker, D., and Orrell, S., 2001, Zircon U-Pb geochronology of the Ottawan orogeny, Adirondack highlands, New York: regional and tectonic implications: Precambrian Research, v. 109, n. 1-2, p. 39-72.

Merschat, C.E., and Cattanach, B.L., 2008, Bedrock geologic map of the western half of the Asheville 1:100,000-scale quadrangle, North Carolina and Tennessee: North Carolina Geological Survey Geologic Map Series – 13.

Miller, C.F., Hatcher, R.D., Ayers, J.C., Coath, C.D., and Harrison, T.M., 2000, Age and zircon inheritance of eastern Blue Ride plutons, southwestern North Carolina and northeastern Georgia, eith implications for magma history and evolution of the southern Appalachian orogen: American Journal of Science, v. 300, p. 142-172.

Moecher, D.P., Samson, S.D., and Miller, C.F., 2004, Precise time and conditions of peak Taconian granulite facies metamorphism in the Southern Appalachian Orogen, USA, with implications for zircon behavior during crustal melting events: The Journal of geology, v. 112, n. 3, p. 289-304.

Moecher, D., and Samson, S., 2006, Differential zircon fertility of source terranes and natural bias in the detrital zircon record: Implications for sedimentary provenance analysis: Earth and Planetary Science Letters, v. 247, p. 252–266, doi: 10.1016/j.epsl.2006.04.035.

Moecher, D., Hietpas, J., Samson, S., and Chakraborty, S., 2011, Insights into southern Appalachian tectonics from ages of detrital monazite and zircon in modern alluvium: Geosphere, v. 7, p. 494–512, doi: 10.1130/ges00615.1.

Moecher, D., Hietpas, J., Samson, S., and Kelly, E., 2015, Detrital monazite geochronology and textures prove sediment recycling in Appalachian clastic systems: Geological Society of America Abstracts with Programs, v. 47, no. 7, p. 672.

Moecher, D.P., Kelly, E.A., Hietpas, J., and Samson, S.D., 2019, Proof of recycling in clastic sedimentary systems from textural analysis and geochronology of detrital monazite: Implications for detrital mineral provenance analysis: Geological Society of America Bulletin.

Montel, J-M., Foret, S., Veschambre, M., Nicollet, C., and Provost, A., 1996, Electron microprobe dating of monazite: Chemical Geology, v. 131, n. 1-4, p. 37-53.

Morton, A.C., 1991, Geochemical studies of detrital heavy minerals and their application to provenance research: Geological Society, London, Special Publications, v. 57, p. 31-45.

Nier, A.O., Thompson, R.W., and Murphy, B.F., 1941, The isotopic composition of lead and the measurement of geologic time, III. Phys Rev, v. 60, p. 789-793.
O'Sullivan, G.J., Chew, D.M., Samson, S.D., 2016, Detecting magma-poor orogens in the detrital record: Geology, v. 44, n. 10, p. 871-874., doi: 10.1130/G38245.1.
Palin, R.M., Searle, M.P., Waters, D.J., Parrish, R.R., Roberts, N.M.W., Horstwood, M.S.A., Yeh, M.W., Chung, S.L., and Anh, T.T., 2013, A geochronological and petrological study of anatectic paragneiss and associated granite dykes from the D ay N ui C on V oi metamorphic core complex, North Vietnam: constraints on the timing of metamorphism within the Red River shear zone, Journal of Metamorphic Geology, v. 31, n. 4, p. 359-387.
Parrish, R.R., 1990, U-Pb dating of monazite and its application to geological problems: Canadian Journal of Earth Sciences, v. 27, n. 11, p. 1431-1450.
Pe-Piper, G., Piper, D.J., and Triantafyllidis, S., 2014, Detrital monazite geochronology, Upper Jurassic-Lower Cretaceous of the Scotian Basin: significance for tracking first-cycle sources: Geological Society, London, Special Publications, v. 386, n. 1, p. 293-311.
Puetz, S.J., Ganade, C.E., Zimmermann, U., and Borchardt, G., 2018, Statistical analyses of global U-Pb database 2017: Geoscience Frontiers, v. 9, n. 1, p. 121-145.
Rankin, D.W., 1975, The continental margin of eastern North America in the southern Appalachians: The opening and closing of the proto-Atlantic Ocean: American Jounral of Science, v. 275, p. 298-336.
Rasmussen, B., and Muhling, J.R., 2009, Reactions destroying detrital monazite in greenschist-facies sandstones from the Witwatersrand basin, South Africa: Chemical Geology, v. 264, n. 1-4, p. 311-327.
Rivers, T., Ketchum, J., Indares, A., and Hynes, A., 2002, The High Pressure belt in the Grenville Province: architecture, timing, and exhumation: Canadian Journal of Earth Sciences, v. 39, n. 5, p. 867-893.
Rosenblum, S. and Brownfield, I.K., 1999, Magnetic susceptibility of minerals, US Dept. of the Interior, *US Geological Survey, Washington*, p. 10.
Ross, G.M., Patchett, P.J., Hamilton, M., Heaman, L., DeCelles, P.G., Rosenberg, E., and Giovanni, M.K., 2005, Evolution of the Cordilleran orogen (southwestern Alberta, Canada) inferred from detrital mineral geochronology, geochemistry, and Nd isotopes in the foreland basin: GSA Bulletn, v. 117, n. 5-6, p. 747-763.
Samson, S.D., Moecher, D.P., and Satkoski, A.M., 2018, Inherited, enriched, heated, or recycled? Examinging potential causes of Earth's most zircon fertile magmatic episode: Lithos.
Spear, F.S., Pyle, J.M., 2002, Apatite, monazite, and xenotime in metamorphic rocks in phosphates: geochemical, geobiological, and materials importance, Reviews in Mineralogy and Geochemistry, v. 48, p. 293-335.
Su, Q., Goldberg, S.A., and Fullagar, P.D., 1994, Precise U-Pb zircon ages of Neoproterozoic plutons in the southern Appalachian Blue Ridge and their implications for the initial rifting of Laurentia: Precambrian Research, v. 68, n. 1-2, p. 81-95.
Tollo, R.P., Aleinikoff, J.N., Bartholomew, M.J., and Rankin, D.W., 2004, Neoproterozoic A-type granitoids of the central and southern Appalachians: intraplate magmatism associated with episodic rifting of the Rodinian supercontinent: Precambrian Research, v. 128, n. 1-2, p. 3-38.
Tomascak, P.B., Krogstad, E.J., and Walker, R.J., 1996, U-Pb monazite geochronology of granitic rocks from Maine: implications for late Paleozoic tectonics in the Northern Appalachians: The Journal of Geology, v. 104, n. 2, pp. 185-195.
Williams, M., Jercinovic, M., Hetherington, C., 2007, Microprobe monazite geochronology: Understanding geologic processes by integrating composition and chronology, Annual Review Earth Planetary Science, v. 35, p. 137-175.
Woodhead, J.D., Horstwood, M.S., and Cottle, J.M., 2016, Advances in isotope ratio determination by LA-ICP-MS: Elements, v. 12, n. 5, p. 317-322.

Vita

SARAH W. KITTROSS
sarah.kittross@gmail.com
(802)366-0132

EDUCATION

Master of Science, Earth Sciences, Syracuse University, Syracuse, NY
Bachelor of Science, Geology, Union College, Schenectady, NY
Term Abroad 2014, University of Queensland, Brisbane, Australia

AWARDS

Grants-in-Aid-of-Research Award, Sigma Xi, 2019

PROFESSIONAL EXPERIENCE

Teaching/ Research Assistant, Dept. of Earth Sciences, Syracuse University, 2017-2019
AmeriCorps Member, The Collaborative, Londonderry, VT, 2016-2017
External Affairs Intern, UNAVCO, Boulder, CO, 2015
Environmental, Health, & Safety Intern, United Technologies, Farmington, CT, 2014

PRESENTATIONS, ABSTRACTS, POSTERS

Samson, S., **Kittross, S.**, 2019, Beyond detrital zircon: Combining U-Th-Pb dating with Nd isotope composition of detrital monazite to further enhance sediment source identification: GSA Annual Meeting (Session No. 139). (Abstract)

Kittross, S., Samson, S., Moecher, D., Hietpas, J., December 2018, *Insights from combined detrital monazite geochronology and Nd isotopic composition on recording tectonic events and quantifying sedimentary recycling,* Advances and Challenges to Understanding Sedimentary Processes, Dynamics, and the Creation of Stratigraphic Patterns Through Integrated Studies of Sedimentary Deposits from Grain to Basin II, AGU Fall Meeting, Washington DC. (Presentation)

Frey, H., Manon, M., **Kittross, S**., Brehm, S., Babiak, R., Pope, M., 2017, *The zircon record in Dominica: From South America to explosive eruptions*: GSA Annual Meeting (Session No. 48). (Abstract)

Kittross, S., March 2016, *LA ICP-MS U-Pb Analysis of Inherited Zircons from Dominica, Lesser Antilles*, Applications of Geochemistry and Geochronology to Understanding Tectonic Processes, Northeast GSA, Albany, NY. (Poster)

Kittross, S., Rowan, L., Bartel, B., Morris, A., MacPherson-Krutsky, C., December 2015, *Geodesy Brings the Geoscience Community Together as Geophysicists*, What It Means to be a Geoscientist: Defining a Common Identity for the Public and Profession, AGU Fall Meeting, San Francisco, CA. (Presentation)